Coupling of a Multizone Airflow Simulation Program with Computational Fluid Dynamics for Indoor Environmental Analysis

by

Yang Gao

M.S., Environmental Engineering
University of Pittsburgh, 2000

Submitted to Department of Architecture in partial fulfillment of the requirements for the degree of

Master of Science in the field of Building Technology

at the

Massachusetts Institute of Technology

June 2002

Signature of Author _____
Department of Architecture
May 10, 2002

Certified by _____
Qingyan Chen
Associate Professor of Building Technology
Thesis supervisor

Accepted by _____
Stanford Anderson
Head, Department of Architecture
Chairman, Departmental Committee on Graduate Students

Coupling of a Multizone Airflow Simulation Program with Computational Fluid Dynamics for Indoor Environmental Analysis

by
Yang Gao

Submitted to the Department of Architecture
on May 10, 2002 in partial fulfillment of the requirements
for the Degree of Master of Science
in the field of Building Technology

ABSTRACT

Current design of building indoor environment comprises macroscopic approaches, such as CONTAM multizone airflow analysis tool, and microscopic approaches that apply Computational Fluid Dynamics (CFD). Each has certain advantages and shortfalls in terms of indoor airflow simulation. A coupling approach that combines multizone airflow analysis and detailed CFD airflow modeling would provide complementary information of a building and make results more accurate for practical design.

The present study attempted to integrate such building simulation tools in order to better represent the complexity of the real world. The overall objective of this study was to couple an in-house CFD program, MIT-CFD, with a multizone airflow analysis program, CONTAM.

Three coupling strategies were introduced. The virtual coupling makes use of the CFD simulation results in a large scale to provide boundary conditions for CONTAM. The quasi-dynamic strategy assumes that CFD can produce a "true" flow pattern and the CONTAM results should be changed accordingly. The dynamic coupling realizes an active two-way interaction between CFD and CONTAM through a bisection search procedure designed by the author that forces the airflow rates from the two models to converge.

Various case studies were conducted to validate the coupling strategies. Preliminary results show that all three coupling schemes can result in more reliable airflow patterns. Further investigations are needed to improve the coupling procedures and to apply to more generalized and complex real-world cases.

Thesis Supervisor: Qingyan (Yan) Chen
Title: Associate Professor in Building Technology

ACKNOWLEDGEMENTS

I would like to express my sincere thanks to my advisor, Prof. Qingyan (Yan) Chen for offering me the great opportunity to work on this project. My thanks are extended for his tireless support, great advice and consultation throughout the work. He has always given me valuable ideas and encouragement in completion of this thesis. His high standards and deep knowledge in research have provided me the most valuable help in the work.

I would also express my cordial gratitude to the other faculty members in Building Technology program, Professor Leon Glicksman, Professor Les Norford and Professor John Felnandez, for their kindness and support. My sincere thanks extend to Professor Glicksman for his advice and help while I was working as his teaching assistant.

I thank Dr. Yi Jiang and Zhiqiang Zhai for their precious help and generous technical support throughout the research. My special thanks to Dorrit Schuchter and Kathleen Ross for their logistic support. I would also like to thank all my colleagues in the Building Technology Program for their collaboration and friendship.

My sincere love and thanks to my parents, Mei Chen and Zhongshun Gao, my parents-in-law, Aiqing Ye and Zhiming Hu, and my dear sister, Haiyan Gao for their loyal love and support. Finally, I would like to express my deepest love and gratitude to my husband, Dr. Yuanlong Hu, for his love and timeless support.

DEDICATION

To my husband

Table of Contents

Chapter 3 Description and Validation of a CFD Program

Chapter 4 Coupling of CFD and CONTAM

Chapter 5 Conclusions and Future Work

List of Figures

List of Tables

CHAPTER 1

INTRODUCTION

1.1 General Statement of Problem

Since the emergence of the first air-conditioning system designed by W.H. Carrier (1902), people are more and more dependent on indoor climate. At present, people in developed country spend about 90% of their time indoors. Building environmental issues has therefore received more public attentions than ever. "Healthy building" design now becomes the main stream on the verge of a paradigm shift in building ventilation design thinking (Spengler and Chen, 2000).

In the past three decades, the design of indoor environment has undergone several major shifts. In respond to the energy crisis in the 1970s, energy-efficient building concept drove engineers to design more insulated, airtight and less ventilated buildings since building consumed one third of total energy in developed country. Although those energy-efficient measures saved huge amount of energy, the heavy trade-off was insufficient ventilation maintaining a benign indoor environment. Therefore, as a relatively independent ecosystem, indoor environment could not provide well-diluted clean air and desirable thermal comfort level in certain spaces.

On the other hand, many sources of contaminants, such as volatile organic compounds (VOCs) and radon, are introduced to working and living indoor environment. As consequences, indoor air quality (IAQ) becomes impoverished due to inadequate air infiltration or insufficient fresh air supply. Poor IAQ may lead to "Building-Related Illness" and "Sick Building Syndrome", which may have acute or chronic effects on human health. People have growing awareness of health risks from poor IAQ (Molhave 1982, Esmen 1985, Nero 1988). For example, increased cancer risk has been linked to poor IAQ (Spengler and Chen 2000). This leads to an increased minimum fresh air rate for each occupant defined in ASHRAE (American Society of Heating, Refrigerating and Air-Conditioning Engineers, Inc.) Standard 62 (1999) for acceptable indoor air quality.

Moreover, poor IAQ is being blamed for problems of low worker productivity and therefore associated with significant economic loss. According to several studies, impoverished IAQ causes an average 10% loss of productivity, and a widely accepted, conservative value of 6% (Dorgan et al. 1998). The overall economic losses due to poor IAQ in US commercial buildings are estimated to be about $20 to $160 billion per year (Fisk 2000). Although poor IAQ is not a sole contributor to health problems, productivity and economic loss, it declares the fact that "safe" and "benign" interior environment is no longer existing in current modern society. Buildings are now a source of contamination due to the fact that it may actually be more polluted than the surroundings (Spengler and Chen 2000).

Changes in construction, materials, energy cost, and health concerns are shifting ventilation philosophy once again. Health, economics, and aesthetics are becoming more important than comfort in determining the specification for ventilation (Spengler and Chen, 2000). "Healthy" building design requires the consideration of good IAQ and thermal comfort as well as energy-efficiency. This has stimulated the development of new technologies, such as natural ventilation and low energy cooling. The analysis of those new technologies requires tools that can be both sophisticated and simplified as need.

1.2 Current Design Tools and Problems

Modern buildings and their heating, ventilation and air-conditioning (HVAC) systems are required to be both energy- and environmental-conscious. In the last decade, computer design tools have been promoted due to the pressure on designers to perform quick design. Most of computer applications focus only on one or two design aspects, such as load calculations, energy consumption estimation, duct design, pipe design, etc. (Lebrun 1994). However, building indoor air quality and HVAC design is a complex task consisting of various interactive factors that requires experts from different disciplines (Ellis and Mathews, 2002).

The design of acceptable indoor air quality should meet ASHRAE standards 62-1999. Current design simply uses a single value for indoor air parameters, which is a representation often used by multizone or zonal models. In most cases, however, the air within a single room is not well mixed and may have gradient within. Thus, a single value cannot well represent local thermal comfort and air quality. On the other hand, there have been extensive efforts in applying Computational Fluid Dynamics (CFD) to indoor environmental study that may offer detailed IAQ information within a room. This leads to the possibility of integrating these two types of computational tools, i.e., multizone and CFD models, for indoor airflow analysis. In which follows, a brief introduction on each tool categories is given.

1.2.1 Multizone Airflow Analysis Tools

Some indoor air quality problems require the airflow analysis of a whole building driven by pressure difference or temperature difference. Currently, the design of acceptable indoor air quality is according to ASHRAE standard 62-1999 that uses a single value for indoor air quality parameters. Multizone airflow network models become a common tool to provide such indoor air quality information.

Multizone airflow network model calculates air exchange and contaminant migration within the rooms of a building and between a building and outdoors (Schaelin 1993). These models typically represent the rooms of a building as zones with homogeneous air properties and contaminant concentrations. Airflows are described as airflow paths that interconnecting with each other and have user-defined leakage

characteristics (Musser, 2001). By mass balance, the airflow rates through paths and the averaged contaminant concentrations are evaluated. Although a number of assumptions must be made regarding envelope leakage characteristics and weather conditions, multizone models have been used to represent many types of buildings with acceptable accuracy (Furbringer et al. 1996)

1.2.2 CFD Models

In real world, however, the air within a single room is not well mixed but varies spatially. Air temperature and contaminant concentration therefore are distributed with gradient. This is especially true for large spaces, such as atria and lobbies; and for buildings with non-mixing ventilation systems, such as displacement ventilation and natural ventilation. A single value cannot well represent local thermal comfort and air quality. Therefore, multiple values that can reflect non-homogeneous condition in a room is necessary for proper indoor air quality and HVAC design.

Such characteristics can be captured by CFD techniques. In CFD analysis, room is divided into numerous grids, and the nonlinear partial differential equations that govern the airflow, heat and mass transfer in a space are discretized and solved numerically. A detailed description of air velocities, air temperature, and contaminant concentrations is therefore obtained. Theoretically, CFD can be applied to whole building airflow analysis. However, such endeavor is not attempted to achieve due to huge computer resources involved even for a simplified building geometry. Therefore, CFD analysis has historically been limited to flows in single spaces or small sets of rooms where detail information is needed rather than entire buildings (Musser 2001).

1.2.3 Integration of Multizone Model and CFD Models

A modeling approach that combines multizone airflow analysis and detailed CFD airflow modeling would provide complementary information of a building and make results more accurate for practical design. The integration of multizone and CFD models has therefore been investigated in several studies.

A link between multizone models and CFD can be in a two-way sense. One is to supply the calculated airflow information from a CFD model into multizone models. The other is to perform CFD calculation using boundary conditions obtained from a multizone model simulation. Schaelin et al. (1993) demonstrated a method to include the CFD results from detailed single-room calculation into multizone models for a more adequate description of real cases. The method worked for a whole building with one room for CFD calculation. And the interface parameters of this room were transferred between the CFD program and the multizone program with manual iteration. The whole procedure was called a "ping-pong" technique.

More recently, Musser (2001) investigated the impact of room representation and boundary conditions on predicted contaminant concentrations and airflow profiles in a set of two isothermal rooms connected by an opening with varying sizes. The study compared four possible combinations of the multizone and CFD model assembly: multizone only, CFD only, CFD for the first room and multizone for the second room, and multizone for the first room and CFD for the second room. Although this investigation confirmed that the multizone models could not accurately predict the airflow and contaminant level in a poorly mixed room, the two programs were just manually combined. Nevertheless, this study suggests the combination of CFD and multizone models is desirable when a critical room is poorly mixed.

One attempt in dynamically coupling CFD with multizone network model was conducted by Negrao (1995). He implemented a CFD algorithm within the ESP-r module that is a building energy modeling system. Both ESP-r system and the CFD program that he used employed finite volume method. The conflation technique essentially treated the airflows across the openings as sources. The information exchange of such sources was conducted at every sweep of CFD solver iteration until the CFD convergence criterion was met. However, other multizone airflow network programs, such as COMIS and CONTAM, do not consider the source term in mass balance equation. Therefore, the coupling method developed in ESP-r may not applicable to other multizone programs if their original algorithm and data structure are to be maintained.

1.3 Objective of the Present Study

The discussion in the previous sections indicates the importance of integrating multizone airflow models and CFD models. Preliminary studies conducted by other researchers have also been briefly discussed. However, it suggests that different approach should be investigated in order to fully couple a CFD program with the most common multizone airflow analysis programs, such as CONTAM and COMIS. The present work will focus on the coupling of CFD with one of such multizone programs, in this case, CONTAM, because it has received more attention for its validity and application.

CONTAM is a multizone airflow analysis program developed by National Institute of Standard and Testing (NIST) (Stuart Dols 2000). It is an object-oriented program written in C language with user-friendly interface, which becomes increasingly popular recently. Although the impact of combining CONTAM and CFD program was mentioned by Musser (2001), the real implementation of coupling a CFD program and CONTAM has never been realized.

Building Technology Program at the Massachusetts Institute of Technology has developed an in-house CFD program, called MIT-CFD. This program can solve a variety of three-dimensional airflow problems within a specific space, whether turbulent or laminar. The program has been developed to be user-friendly and it allows user to make changes for specific purpose. MIT-CFD is therefore chosen for the present study.

The overall objective of this investigation is to couple MIT-CFD with CONTAM and study the impact of the coupled program on airflow analysis. More specifically, the present study aims to:

- Validate MIT-CFD program for coupling needs.
- Apply CONTAM into indoor airflow and IAQ analysis.
- Develop a coupling procedure by MIT-CFD and CONTAM, and verify the techniques employed.
- Apply the coupled program for indoor airflow and IAQ studies.

1.4 Thesis Outline

The thesis can be outlined into the following chapters:

Chapter 2 introduces a multizone airflow analysis program—CONTAM and its theoretical background. The application of CONTAM is then discussed using case study approach. The limitation of CONTAM is therefore identified.

Chapter 3 reviews the fundamentals of MIT-CFD program followed by validating this program with experimental data.

Chapter 4 introduces three coupling strategies conforming to different research objectives and details; these include virtual coupling, quasi-dynamic coupling, and dynamic coupling. In virtual coupling, CFD simulation provides CONTAM pressure boundary information for the whole building simulation. Quasi-dynamic coupling focuses on the cases in which CFD simulation results is presumably correct and can fully impact the CONTAM simulation results. Dynamic coupling deals with the cases when CFD and CONTAM can communicate with each other during the simulation. After discussions on each coupling strategies, verifications are conducted to examine the coupling strategies. The applications of the coupled program for building airflow simulation are discussed and the engineering significance of the coupling between CFD and CONTAM is highlighted.

Chapter 5 summarizes the work presented in this thesis, and provides recommendations for future research.

CHAPTER 2

MULTIZONE AIRFLOW ANALYSIS PROGRAM—CONTAM

2.1 Introduction

The design to prevent indoor air quality problem and to meet space-conditioning loads for energy consumption requires the understandings of airflow pattern and the mechanisms of contaminant migration in an entire building. Traditionally, three hierarchical types of simulation tools are available for research purposes and engineering applications: multizone models, zonal models, and CFD models.

Multizone IAQ modeling has been available as a research and analysis tool for over 20 years (Emmerich, 2001). The multizone models simulate airflow pattern from one zone to another in an entire building with only coarse structure information and assume uniform air parameters in a zone. The multizone models can provide designers gross information regarding indoor air quality in a building. Typical multizone models include CONTAM (Stuart Dols, et al. 2000) and COMIS (Pelletret and Keilholz 1997). Such models take a macroscopic view of air motion and contaminant dispersion, which enable the analysis of whole building airflow pattern and airborne contamination levels. Unfortunately, these models have great uncertainties when they are used to simulate large spaces, such as atria. This is because the air distribution in large spaces is not uniform.

CFD simulation divides a single zone into numerous small cells. By solving discretized mass, momentum, energy and species conservation equations, CFD generates detailed temperature, concentration and airflow field in a zone. The CFD approach is very powerful, but it would cost too much computing time if it were used to simulate indoor air quality problem within an entire building.

The zonal modeling acts as a bridge between the multizone macroscopic modeling and CFD microscopic modeling. The zonal model calculates the airflow pattern in a zone with limited subzones/nodes over which mass and energy conservation based on a number of approximations must be satisfied. Some of typical models are from Lebrun (1970), Inard et al. (1996), Howarth (1985), Togari et al. (1993), Rodriguez et al. (1994), Inard and Buty (1991), Wurtz et al. (1999), Haghighat et al. (2001), and Musy et al. (2001). For all the zonal models at present, assumptions must be made on inter-zonal airflow patterns. The use of zonal models thus requires a large competence in modeling and experimenting in buildings. Morover, for each different problem, a particular analysis is necessary to build a new cell arrangement and the whole set of equations have to been solved repeatedly. A recent review by Griffith (2002) found that most of the zonal models are unstable and need extensive prior knowledge of airflow pattern. It is very difficult to use zonal models for studying indoor air quality problem in an entire building.

Therefore, the integration of CFD into a multizone model would be ideal, since the CFD can provide accurate and detailed information for large spaces and the multizone model can simulate quickly on indoor air quality problem for an entire building. The following section will give an introduction and description of a specific multizone model program – CONTAM. Several applications of CONTAM will be discussed in section 2.3.

2.2 A Multizone Model – CONTAM

2.2.1 Overview

A 1992 survey reported that nearly fifty multizone network airflow models are used in industry and academic communities (Feustel and Dieris 1992). However, many of these were developed as in-house research tools, and only a few have been made available to the public. CONTAM is among these that are available to for public access and becomes increasingly popular recently. CONTAM includes graphical input and output interfaces, which is user-friendly. It also has the capacity to allow the user to specify schedules for occupants, contaminants, weather conditions, and HVAC system operation (Musser 2001). Therefore, it has been received more public attentions and is chosen for this study.

CONTAM is a multizone indoor air quality and ventilation analysis computer program designed to determine general airflow pattern, contaminant concentrations and personal exposure if needed. The model can be applied to a variety of applications, such as assessing the adequacy of ventilation rates in a building and obtaining the distribution of ventilated air throughout a building. It can also be used to predict contaminant concentrations so as to determine the indoor air quality performance for a building in its design stage or for an existing building, and to evaluate the impacts of various design decisions related to the ventilation system construction. Predicted contaminant concentration can also be used to estimate personal exposure based on occupancy patterns within the building.

The multizone network airflow model approach has been extensively evaluated using both analytical solutions and experimental data (Furbringer et al. 1996). Upham (1997) also reviewed past validation work and compared model predictions with tracer gas measurements taken in a five-story building. In her study, the predicted tracer gas concentrations by CONTAM were shown to within approximately 20% of true values. Deviations of this order of magnitude are commonplace in infiltration and contaminant prediction and have been deemed acceptable for many types of analysis (Persily and Linteris 1983).

2.2.2 Building Representation in CONTAM

To represent a building using the CONTAM model, the building must be simplified into a set of zones that represent individual rooms and spaces. CONTAM provides a macroscopic model for a building, that is, zones are treated as perfectly mixed volumes in the simulation. Figure 2.1 illustrates the process of building idealization that is presented by NIST in its CONTAM website in the division of building technology (http://www.bfrl.nist.gov/IAQanalysis/default.htm). In many applications, each room of a building can be represented as a single zone. These zones are connected to one another or to ambient by airflow paths that represent the cracks, openings, fans, etc. The temperature of each zone and weather condition need to be specified in order to perform simulation. Optional inputs include contaminant sources and sinks, occupant schedules, and HVAC systems with ducts, filters, and recirculation.

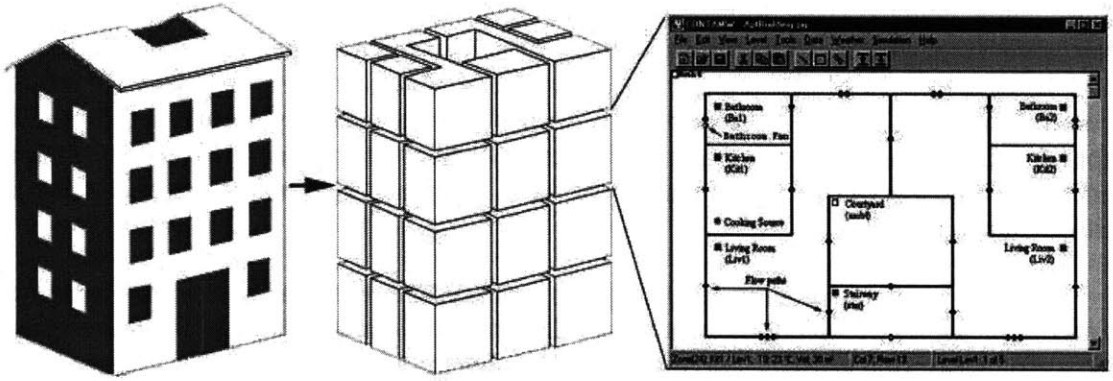

Figure 2.1. Illustration of building idealization in CONTAM (NIST).

2.2.3 Theoretical Background

CONTAM requires the use of various assumptions in order to implement mathematical relationships to model airflow and contaminant dispersion. Firstly, each zone representing certain building space is treated as a single node, where the assumption of uniform (well-mixed) condition is employed. The uniform assumption treats zone temperature, pressure and contaminant concentrations as single values whereas the localized effects within a given zone are overlooked. Secondly, CONTAM does not treat heat transfer automatically. Users are responsible to manually set the temperatures in all zones. The model can only determine airflows induced by temperature differences between zones including ambient caused by stack effect. Moreover, empirical nonlinear mathematical models are utilized to represent the airflow paths to which the pressure drop relates. Other major assumptions include quasi-steady airflows, trace contaminants and source/sink models, etc.

A variety of air movement models have been developed for estimating airflows in buildings. These flows include infiltration, natural ventilation, inter-room airflows

through various openings including doorways and flows through the HVAC system (Walton, 1989). Infiltration is the result of air flowing through openings. These opening could be large or small, intentional or accidental in the building envelope. Infiltration is driven by pressure difference, Δp, across the opening. The relationship between the airflow through an opening in the building envelope and the pressure difference across it can be modeled in several ways in CONTAM.

It is assumed that Bernoulli's equation governs the flow within each airflow element.

$$\Delta P = \left(P_1 + \frac{\rho V_1^2}{2}\right) - \left(P_2 + \frac{\rho V_2^2}{2}\right) + \rho g(z_1 - z_2) \tag{2.1}$$

where,

ΔP = total pressure drop between points 1 and 2
P_1, P_2 = entry and exit static pressures
V_1, V_2 = entry and exit velocities
ρ = air density
g = acceleration of gravity (9.81 m/s^2)
z_1, z_2 = entry and exit elevations

In CONTAM, the pressure terms are rearranged and a possible wind pressure term for a building envelope opening is added:

$$\Delta P = P_j - P_i + P_s + P_w \tag{2.2}$$

where,

P_i, P_j = total pressure at zones i and j
P_s = pressure difference due to density and elevation differences, and
P_w = pressure difference due to wind.

P_w is defined as Equation 2.3:

$$P_w = \frac{\rho V_H^2}{2} C_p \tag{2.3}$$

where

ρ =ambient air density
V_H = approach wind speed at the upwind wall height
C_p = wind pressure coefficient

P_s is defined as Equation 2.4:

$$P_s = \frac{\rho_n + \rho_m}{2} g\Delta h \tag{2.4}$$

where

ρ_n, ρ_m = air density in zone n and m
g = gravitational acceleration, 9.80 m^2/s
Δh = elevation difference

Most infiltration models are based on the powerlaw relationship between the flow and the pressure difference across a crack or an opening in the building envelope. In CONTAM, three basic variations of power law relationship for turbulent flow are included:

$$Q = C(\Delta P)^n \tag{2.5}$$

$$F = C(\Delta P)^n \tag{2.6}$$

$$Q = C_d A \sqrt{\frac{2\Delta P}{\rho}} \tag{2.7}$$

Where,

Q = volumetric flow rate [m^3/s]
F = Mass flow rate [kg/s]
ΔP = the pressure drop
C_d = discharge coefficient, and
A = orifice opening area
n = exponent constant

Theoretically, the value of the flow exponent constant should lie between 0.5 and 1.0. A variety of research indicates that n=0.5 characterizes large openings well, while n=0.65 can be used to describe crack-like openings.

Besides the powerlaw flow elements, CONTAM also enables calculation based on quadratic relationship($\Delta P = AQ + BQ^2, for Q, \Delta P > 0$ $\Delta P = AQ - BQ^2, for Q, \Delta P < 0$). Baker et al. (1987) indicated that infiltration openings could be more accurately modeled by a quadratic relationship. Duct flow is treated based on 1997 ASHRAE Handbook of Fundamentals (1997), and CONTAM also includes special treatment of large openings

for possible two-way flow. In the present study, we only consider one-way flow through the openings, most of which can be represented by powerlaw relationship. Therefore, for the current stage of the coupling, only powerlaw airflow paths are considered.

To account temperature dependence in CONTAM, a correction factor to the base condition is used, according to the following formulae for computing air density, ρ, and dynamic viscosity, v:

$$\rho = P / (287.005T) \tag{2.8}$$

$$\mu = 3.7143\times10^{-6} + 4.9286\times10^{-8}T \tag{2.9}$$

$$v=\mu / \rho \tag{2.10}$$

The base conditions refers to standard atmospheric pressure and 20°C, where $\rho_0 =$ 1.2041 kg/m^3 and $v_0 = 1.5083\times10^{-5}$ m^2/s.

2.2.4 Solution Methods

CONTAM calculates the infiltration and ventilation rates in a building by solving a non-linear system of equations (2.14) for all zones. An iterative method can be used in which a linear system of equation is solved in each step of the process. The Newton-Raphson method is often used for this kind of problem, which will be detailed later.

An airflow network consists basically of a set of pressure nodes (zones) connected by links, which are called airflow elements in CONTAM. The zones may represent rooms, connection points in ductwork, or the ambient environment. The airflow elements correspond to discrete airflow passages such as doorways, construction cracks, ducts, fans, and other openings. The airflow rate from zone j to zone i, $F_{j,i}$ [kg/s], is some function (f) of the pressure drop along the flow path, $P_j - P_i$:

$$F_{i,j} = f(P_j - P_i) \tag{2.11}$$

The mass of air, m_i [kg], in zone i is given by the ideal gas law:

$$m_i = \rho_i V_i = P_i V_i / RT_i \tag{2.12}$$

where

ρ_i = air density in zone i [kg/m^3],
V_i = zone volume [m^3],
P_i = zone pressure [Pa],
T_i = zone temperature [K], and
R = 287.055 [J/kg·K] (gas constant of air).

For a transient solution the principle of conservation of mass states that

$$\frac{dm_i}{dt} = \sum_j F_{j,i} + F_i \tag{2.13}$$

where

m_i = mass of air in zone i,
$F_{j,i}$ = airflow rate [kg/s] between zones j and zone i: positive values indicate flows from j to i and negative values indicate flows from i to j, and
F_i = non-flow processes (sources or sinks) that could add or remove significant quantities of air from the zone.

Sources and sinks are not considered in CONTAM and flows are evaluated by assuming quasi-steady conditions, $dm_i/dt = 0$, which leads to:

$$\sum_j F_{j,i} = 0 \tag{2.14}$$

The steady-state airflow analysis of multiple zones requires simultaneous solution of equation (2.12) for all zones. Since the function in equation (2.9) is usually nonlinear, a method is needed to obtain the solution of simultaneous nonlinear algebraic equations. The Newton-Raphson (N-R) method (Conte, and de Boor 1972) is chosen in CONTAM to solve the nonlinear problem by iteration. In the N-R method a new estimation of the vector for all zone pressures, $\{\mathbf{P}\}^*$, is computed from the current estimate of pressures, $\{\mathbf{P}\}$, by

$$\{\mathbf{P}\}^* = \{\mathbf{P}\} - \{\mathbf{C}\} \tag{2.15}$$

where the correction vector, $\{\mathbf{C}\}$, is computed by the matrix relationship

$$[\mathbf{J}]\ \{\mathbf{C}\} = \{\mathbf{B}\} \tag{2.16}$$

where $\{\mathbf{B}\}$ is a column vector with each element given by

$$\mathbf{B}_i = \sum_j F_{j,i} \tag{2.17}$$

And $[\mathbf{J}]$ is the square Jacobian matrix whose elements are given by

$$\mathbf{J}_{i,j} = \sum_i \frac{\partial F_{j,i}}{\partial P_j} \tag{2.18}$$

In equations (2.15) and (2.16), $F_{j,i}$ and $\partial F_{j,i}/\partial P_j$ are evaluated using the current estimate of pressure $\{\mathbf{P}\}$. The CONTAM program contains subroutines for each airflow element,

which returns the mass flow rates and the partial derivative values for a given pressure difference input.

Equation (2.16) represents a set of linear equations, which must be set up and solved for each iteration until a convergent solution of the set of zone pressures is achieved. In its full form [**J**] requires computer memory for N^2 values, and a standard Gauss elimination solution has execution time proportional to N^3. Sparse matrix methods can be used to reduce both the storage and execution time requirements. A skyline solution process following the method presented by Dhatt (1984) was utilized. This method can be applied to solve equations with symmetric or nonsymmetrical matrices. In this case, the Jacobian matrix is symmetric.

Analysis of the element model will show that

$$|\mathbf{J}_{i,I}| = \sum_{j+i} |\mathbf{J}_{i,j}| \tag{2.19}$$

This condition allows a solution without pivoting, although scaling may be useful. Note that the degree of sparsity of the Jacobian matrix after factoring is dependent on the arrangement of the zones. The CONTAM user interface ensures the correct interconnection the airflow elements in the network.

CONTAM allows zones with either known or unknown pressures. The constant pressure zones are included in the system of equation (2.14), which is processed so as not to change the pressure of the chosen zone. This gives flexibility in defining the airflow network while maintaining the symmetric set of equations. A sufficient condition for the Jacobian to be nonsingular is that the entire unknown pressure zones being linked, either directly or indirectly, by pressure dependent flow paths to a constant pressure zone. In CONTAM, the ambient (or outdoor) air is treated as a constant pressure zone (Axley, 1987). The pressure difference due to wind effect is considered in Equation 2.2 separately. The ambient zone pressure is assumed to be zero for the flow calculation causing the computed zone pressures to be values relative to the true ambient pressure and helping to maintain numerical significance in calculating ΔP.

Conservation of mass at each zone provides convergence criterion for the N-R iterations. That is, when equation (2.12) is satisfied for all zones for the current system pressure estimate, the solution has converged. Testing for relative convergence at each zone attains sufficient accuracy:

$$\frac{|\sum_j F_{j,i}|}{\sum_j |F_{j,i}|} < \varepsilon \tag{2.20}$$

with a test of $\sum|F_{j,i}| < \varepsilon_1$ to prevent division by zero. The magnitude of ε can be established by considering the use of the calculated airflows, such as in the situation of an energy balance. In any case, round-off errors may prevent perfect convergence ($\varepsilon = 0$).

To achieve faster and reliable convergence, a simple constant under-relaxation coefficient suggested by Walton (2000) and Wray (1993) is used. Equation (2.13) for the iteration becomes

$$\{\mathbf{P}\}^* = \{\mathbf{P}\} - \omega\{\mathbf{C}\} \tag{2.21}$$

where ω is the relaxation coefficient. A relaxation coefficient of 0.75 has been found to be usable for a broad range of airflow networks. This value is not a true optimum but appears to work quite well without the computational cost of finding the theoretically optimum value.

When Convergence is progressing rapidly, under-relaxation ($\omega < 1$) slows convergence compared to no relaxation. To prevent this, a global convergence value is computed:

$$\gamma = \frac{\sum_i |\sum_j F_{j,i}|}{\sum_i \sum_j |F_{j,i}|} \tag{2.22}$$

when $\gamma^* < \alpha\gamma$, ω is set to 1. Currently, CONTAM uses α = 30%. This often reduces the number of iterations.

Newton-Raphson's method requires an initial set of values for the zone pressures. These may be obtained by including in each airflow element model a linear approximation relating the flow to the pressure drop:

$$F_{j,i} = c_{j,i} + b_{j,i}(P_j - P_i) \tag{2.23}$$

Conservation of mass at each zone leads to a set of linear equations of the form

$$[\mathbf{A}]\ \{\mathbf{P}\} = \{\mathbf{B}\} \tag{2.24}$$

Matrix [**A**] in equation (2.22) has the same sparsity pattern as [**J**] in equation (2.14) allowing use of the same sparse matrix solution process for both equations. This initialization handles stack effects very well and tends to establish the proper directions of the element models used by CONTAM. When solving a set of similar problems, such as when approximating a transient solution by successive steady-state solutions, it tends to be preferable to use the previous solution for the zone pressure as the initial values for the new problem.

2.2.5 Boundary Conditions

The determination of airflow pattern and contaminant dispersion in an entire building requires boundary conditions to be provided. The boundary conditions of

CONTAM include the weather data and wind pressure information on the building envelope.

CONTAM enables the user to incorporate the effects of weather on a building. Weather parameters include ambient temperature, barometric pressure, wind speed, wind direction and outdoor contaminant concentrations. Depending on different simulation purposes different boundary conditions are needed. Steady state weather information is provided to CONTAM if only steady state simulation is used. During the simulation, CONTAM keeps the ambient temperature, wind speed and direction, and ambient contaminant concentration unchanged. Transient weather data is used to simulate the changing outdoor weather and wind conditions when performing a transient simulation. Such data are stored in a weather file that has a special format.

Wind pressure can be a significant driving force for air infiltration through a building envelope. It is a function of wind speed, wind direction, building configuration, and local terrain effects. CONTAM enables the user to account for the effects of wind pressure on the flow paths across the building envelope (external airflow paths). It also provides general approaches to handle the variable effects of wind on the building envelope, through which the local wind pressure coefficient for the building surface is determined. The detailed information can be found in the user manual of CONTAMW1.0, which is the latest windows version of CONTAM.

2.3 Applications of CONTAM

In order to use CONTAM to simulate airflow and contaminant dispersion in a building, it is necessary to validate the multizone model. The validation process is to ensure that the user is able to use the program correctly and the program is free from serious bugs. Herrlin (1992) made a critical point in a general discussion that an absolute validation is impossible because the numbers of cases that a complex multizone model can simulate are unlimited. However, validation efforts are still important to identify and eliminate large errors and to establish the range of applicability of the multizone model. Therefore, a model's performance should be evaluated under various situations. Herrlin also addressed the importance for the user to recognize that the prediction of a model will always have a degree of uncertainty. He listed three techniques for the model validation:

1. Analytical verification — comparison to simple, analytically solved cases
2. Inter-model comparison — comparison of one model to another
3. Empirical validation — comparison to experimental tests

There exist some special difficulties in validating multizone airflow models. These include input uncertainty (particularly the air leakage distribution) and the attempts to simulate processes that cannot be modeled (e.g., using a steady-state airflow model to simulate dynamic airflow process). To ensure the quality of our present investigation,

CONTAM is verified for its applicability by inter-model comparison with other multizone models or CFD simulation results.

Three cases will be examined to verify the applicability of CONTAM. The first case – AIVC three-story building uses inter-model comparison with other multizone models, in this case, COMIS and the previous version of CONTAM93. The second case – French house case is to predict personal exposure within a residential house. The results will be compared to those from CFD studies. In the end, a 90-degree planar branch case will be used to testify the limitation of CONTAM multizone model in predicting correct airflow pattern.

2.3.1 AIVC Three-Story Building Case

The AIVC building has three stories with a connecting enclosed stairwell. A vertical cross-section is shown in Figure 2.2. Each floor has a volume of 150 m^3 excluding the stairwell (zones A, B, and C in Figure 2.2) and the stairwell is 135 m^3 (zone D in Figure 3.1). The total building volume is therefore 585 m^3. The flow characteristics of the leakage paths have been represented using power law expressions (i.e. $F=C(\Delta p)^n$, where C is the mass flow coefficient, and n is the flow exponent). Wind pressure coefficients C_p are given for the external openings.

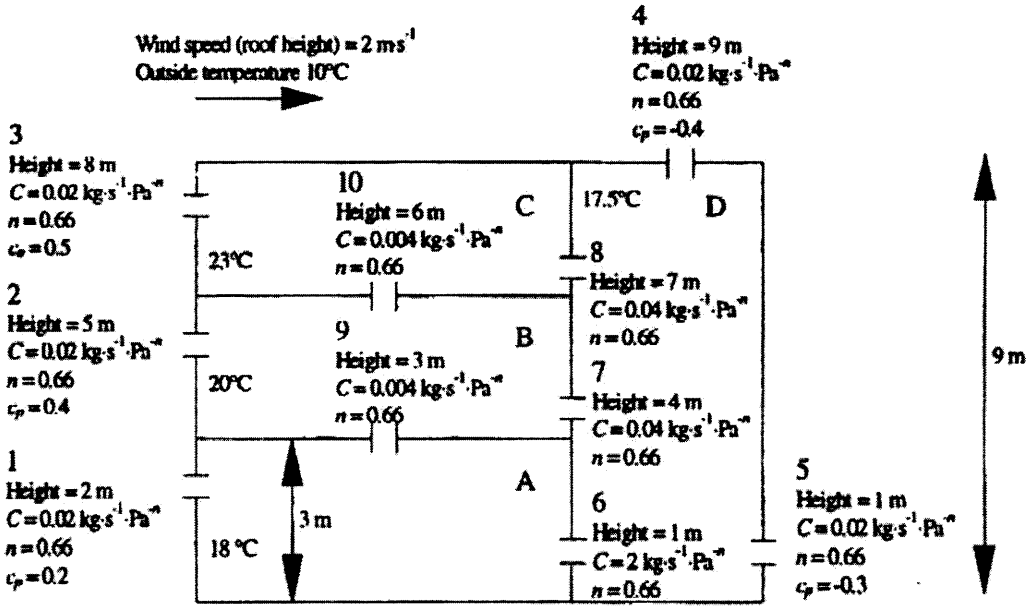

Figure 2.2. Cross-section of the AIVC three-story building.

Atmospheric pressure is taken to be equal to 101.325 kPa, with an outdoor air temperature of 10 °C. The wind speed at the roof height of the building (9m), at the building location, is 2m/s. Both the indoor and outdoor humidity ratio was assumed to be equal to 0.0 $g \cdot kg^{-1}$(dry air). The reason for this is to use identical air density profiles in all of the models, although such scenario would be extreme unlikely to occur in the real world. The physical arrangement of the leakage paths in the building structure is also shown in Figure 2.2.

Comparison was initially conducted among COMIS, CONTAM93 (an earlier version of CONTAMW1.0), and BREEZE by other researchers. In the present study, a verification of CONTAMW1.0 is performed and the results are compared to those published. The plane view of each floor in the AIVC building and the CONTAM simulation results are shown in Figure 2.3. It also exhibits the visualized magnitudes of the mass flow rates (blue bars) and the relative pressure differences (red bars) in CONTAMW1.0. The air flows to the direction to which the blue bar points. Though highly idealized, one can easily obtain a general impression of the airflow pattern within the building. More detailed information such as zone temperature, pressure, contaminant concentrations (if applicable) are also computed.

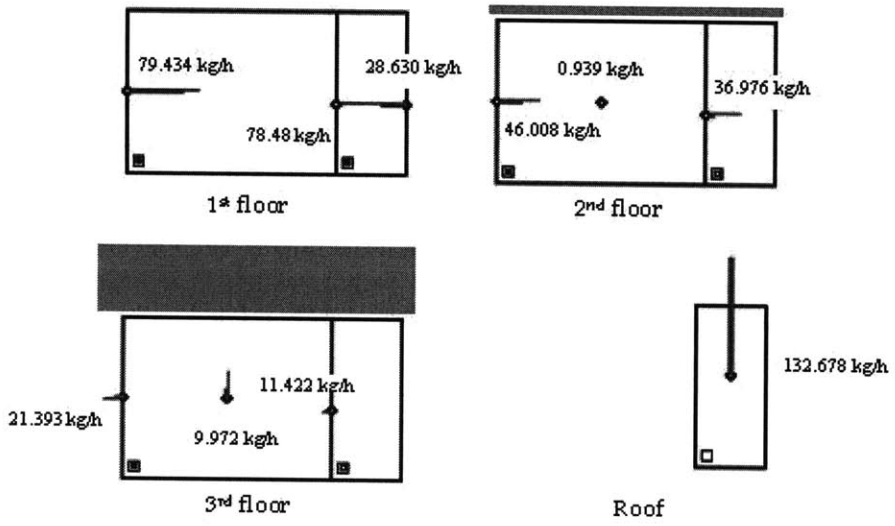

Figure 2.3. Plane view of each floor of the AIVC building and CONTAM simulation results. Blue bars represent airflow rates, and red bars denote pressure.

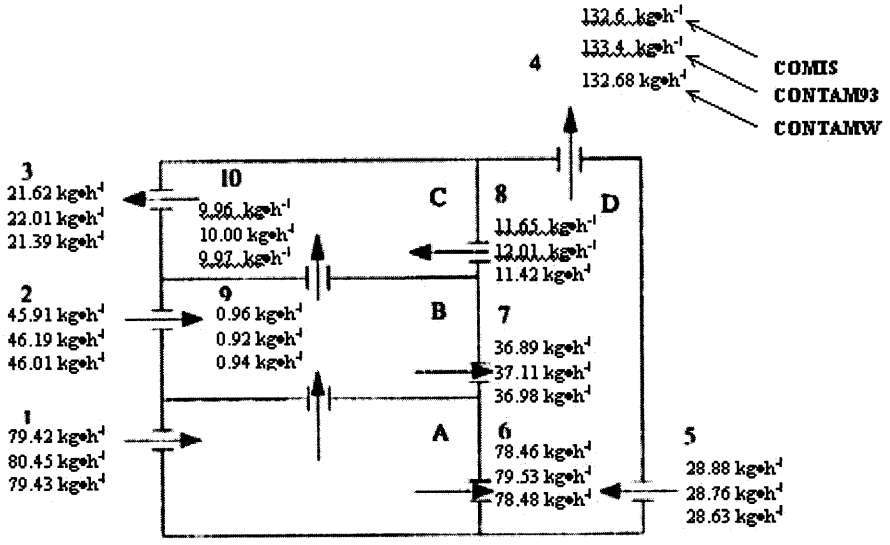

Figure 2.4. Simulation results – mass flow rates through the leakage paths.

The results simulated by CONTAMW1.0 and the simulation data by COMIS and CONTAM93 published in AIVC Technical Note 51 (1999) are co-presented in Figure 2.4. In this figure, the mass flow rates are listed for each leakage opening in the order of COMIS, CONTAM93, and CONTAMW1.0. The results obtained from the three programs are in general agreement with each other. However, the results from CONTAMW1.0 are closer to those from COMIS for this well-defined problem. For example, the airflow direction through each path simulated by different models is exactly the same, although small variations in the magnitudes (between ~0.15% and ~ 5.2%) are detectable. The airflow rates in the figure also indicate that the results of CONTAMW1.0 appear to be closer to those of COMIS (9 out of 10 paths), which is a little out of expectation since CONTAM1.0 and CONTAM93 are more closely related.

2.3.2 French House Case

To study ventilation and contaminant exposure, a more accurate modeling technique is required. Since the indoor airflow is quite complicated and the transport of contaminants is highly dependent on the room airflow, often a perfect mixing model is used to determine an average airflow rate and contaminant concentration level in a room. This is the basic assumption for the multizone models. A clear advantage of such model settings is its simplicity, in which the results could be validated by hand calculation for some simple problems. The major tradeoff stems quite clearly from those assumptions of instantaneous and complete mixing condition within a room, which effectively averages a value throughout the whole room.

In this section, a case study was conducted based on a house plan transcribed directly from the Mozart House from "Catalogue de Logements-Types (de Montureux 1996)" that is illustrated in Figure 2.5. The Mozart House has a floor area of 99.6 m^2 and is considered to be a typical French dwelling, to which the greatest universality may be applied. The single-family house displayed in Figure 2.6 is from a CFD model without the garage, which consists of a dining/living room (36.5m^2), a kitchen (9.5 m^2), two childrens' bedrooms (10.9m^2 and 11.1m^2), a bathroom with a shower (3.2m^2), a WC (1.7 m^2), and a master bedroom (10.1m^2), each containing a variety of everyday furniture. Furniture is included as it normally affects the airflow throughout the house (Etheridge 1996) as well as changes the location of a person relative to the room (e.g. sleeping on a bed elevates the body). These factors are included to model the real world as close as possible. Figure 2.7 is the CONTAM idealization of this single-family house based on the CFD model adaptation. However, CONTAM does not have the functionality to consider the detailed furniture effect.

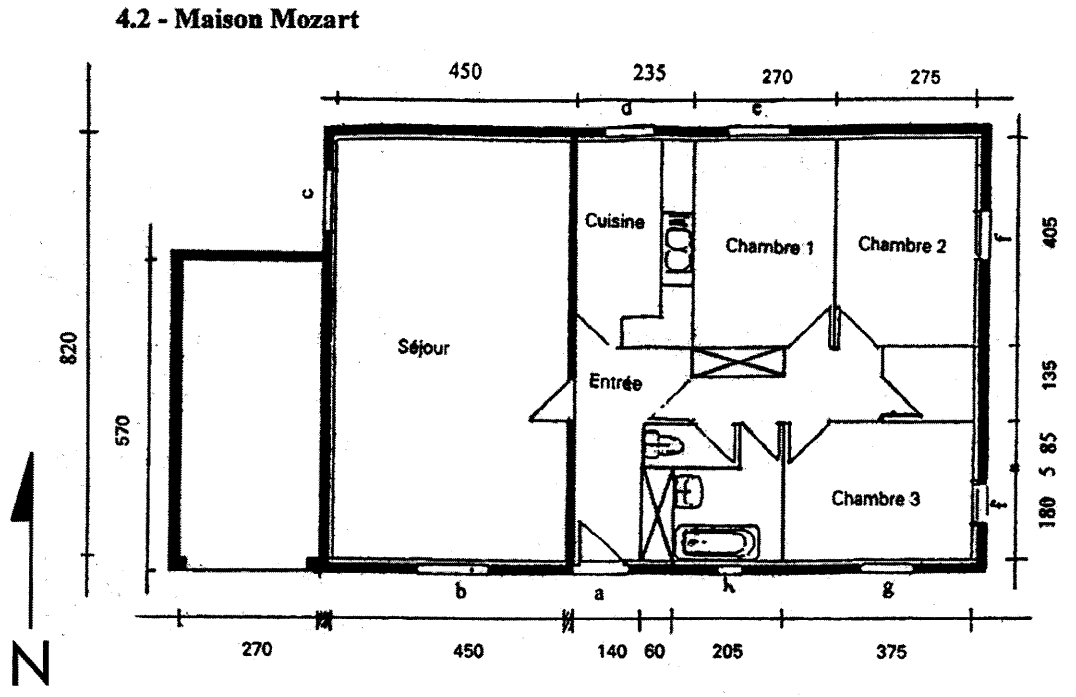

Figure 2.5. Mozart House floor plan from "Catalogue de Logements-Types" (de Montureux 1996) used in the case study.

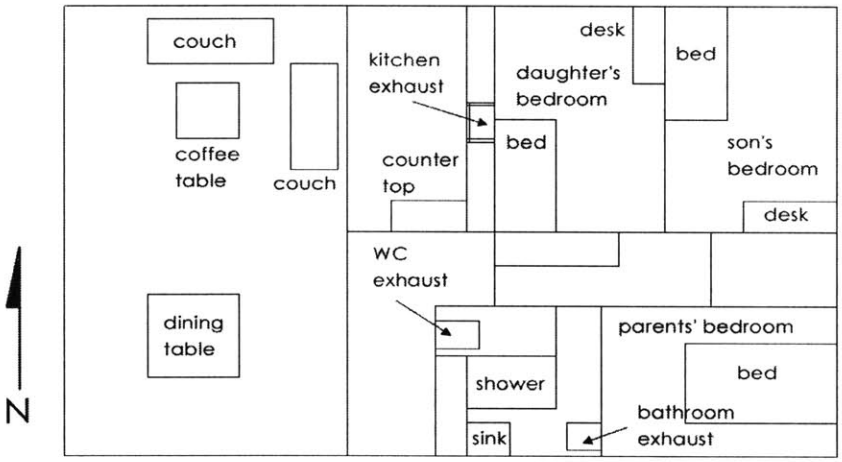

Figure 2.6. CFD model adaptation of the Mozart House including furniture types.

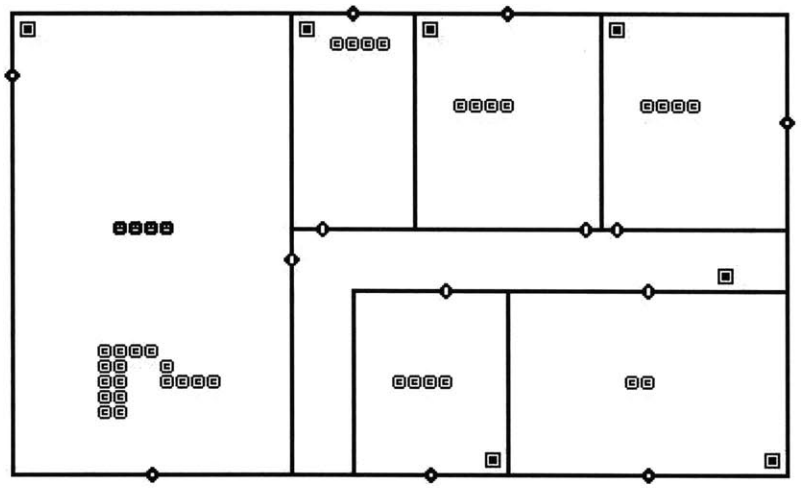

Figure 2.7. CONTAM idealization of Mozart House based on adapted CFD model.

Considering a typical family of four, including the parents, a son, and a daughter, the house is occupied for about fifteen hours of a day. The location of each person in the house throughout the day is shown in Figure 2.8. Between 09:00-18:00h, the parents are working outside and the children are attending school, so nobody is at home during this period. Each person's activity throughout the day is shown in Table 2.1.

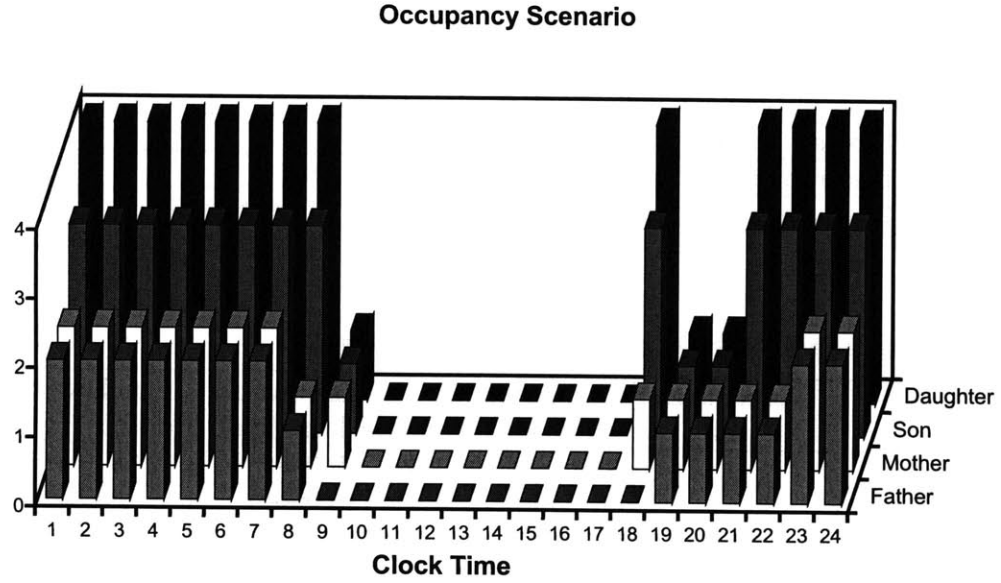

Figure 2.8. Occupancy scenario for each person spent at home: (0) not at home (1) dining/living room (2) parents' bedroom (3) son's bedroom (4) daughter's bedroom.

Table 2.1. Daily activity of occupancy.

Hour	Mother	Father	Son	Daughter
18.00-19.00	Cooking	Not home	Studying	Studying
19.00-21.00	Eating Dinner	Eating Dinner	Eating Dinner	Eating Dinner
21.00-22.00	Reading	Reading (Smoking)	Studying	Studying
22.00-23.00			Sleeping	Sleeping
23.00-07.00	Sleeping	Sleeping		
07.00-07.15	Cooking	Showering		
07.15-07.30	Showering	Eating Breakfast		
07.30-07.45	Eating Breakfast			
07.45-08.00		Not home		
08.00-08.15	Cooking		Sleeping	Showering
08.15-08.30			Showering	Eating Breakfast
08.30-09.00	Reading		Eating Breakfast	

Some characteristics of residential indoor environments and a variety of pollutant sources are placed within the house based on the type and level of activity. These include CO_2, CO, HCHO (formaldehyde), NO_2, and water vapor (H_2O). The characteristics of the pollutants are listed in Table 2.2, and the strengths of the pollutant sources used in the simulations are given in Tables 2.3 and 2.4.

Table 2.2. Description of indoor contaminants used.

Pollutant	Description
CO_2	Typical metabolic bioeffluent that changes based on type of activity
CO	Typical cooking pollutant
NO_2	Typical cooking pollutant
HCHO	Tracer for contaminants associated with smoking
Vapor (H_2O)	Typical metabolic bioeffluent and tracks the influence of the shower

Table 2.3. Strengths of pollutant sources used in the simulations.

	Outside [ppm]	Gas cooking [g/kJ]	Cigarette Smoking [g/s]	Adult awake (asleep) [g/s]	Child awake (asleep) [g/s]
CO_2	307.4	0.045	0.00065	0.0099 (0.0066)	0.0066 (0.0022)
CO	0.116	0.00005	0.00011	0	0
NO_2	0.064	0.000011	0.0000018	0	0
HCHO	0.00896	0	0.0000037	0	0

Table 2.4. Strengths of vapor source used in the simulations.

	Adult awake (asleep) [g/h]	Child awake (asleep) [g/h]	Breakfast [g/person]	Dinner [g/person]	Shower [g/person]
Vapor	55 (30)	45 (15)	50	300	300

Two ventilation systems working in summer condition without cooling device will be evaluated in this case. In summer, the outdoor air comes in at 25°C with a humidity ratio of 15.5 $g_{water}/kg_{dry\text{-}air}$, which corresponds to a relative humidity of 78%. No convectors or other heating device is used in the summer. The two ventilation systems are:

1. Bimodal exhaust: ventilation rate varies between the base rate and a rate that is elevated only when someone in cooking;

2. Relative humidity controlled exhaust (RHC): ventilation rate varies between a minimum and a maximum exhausting values based on the relative humidity at the exhaust.

The bimodal ventilation system has a constant exhaust at the bathroom and WC, with a kitchen range hood exhaust fan that increases its flow rate during the cooking period. At all other time, it exhausts at the base rate. Table 2.5 outlines the exhaust rates used for the bimodal ventilation system, and Figure 2.9 shows the exhaust rate visually.

Table 2.5. Exhaust flow rate for bimodal ventilation.

	Kitchen	Bathroom	WC
Normal flow rate [m^3/h]	45	30	15
Cooking flow rate [m^3/h]	120		

In addition to a bimodal ventilation system, a relative humidity controlled (RHC) system will be simulated to see the difference in performance on personal exposure. Tables 2.6 and 2.7 describe the variation of the ventilation rate based on the relative humidity recorded at the exhaust, and Figure 2.10 shows the exhaust rate visually.

Table 2.6. Minimum and maximum flow rates of the humidity controlled ventilation system (RHC).

	Kitchen	Bathroom	WC
Minimum flow rate [m^3/h]	45	30	15
Maximum flow rate [m^3/h]	120	65	30

Table 2.7. Ventilation rate changes by controlled humidity.

	RH < 30%	30% < RH < 70%	70% < RH
Exhaust ventilation rate	Minimum value	Linear variation between min and max	Maximum value

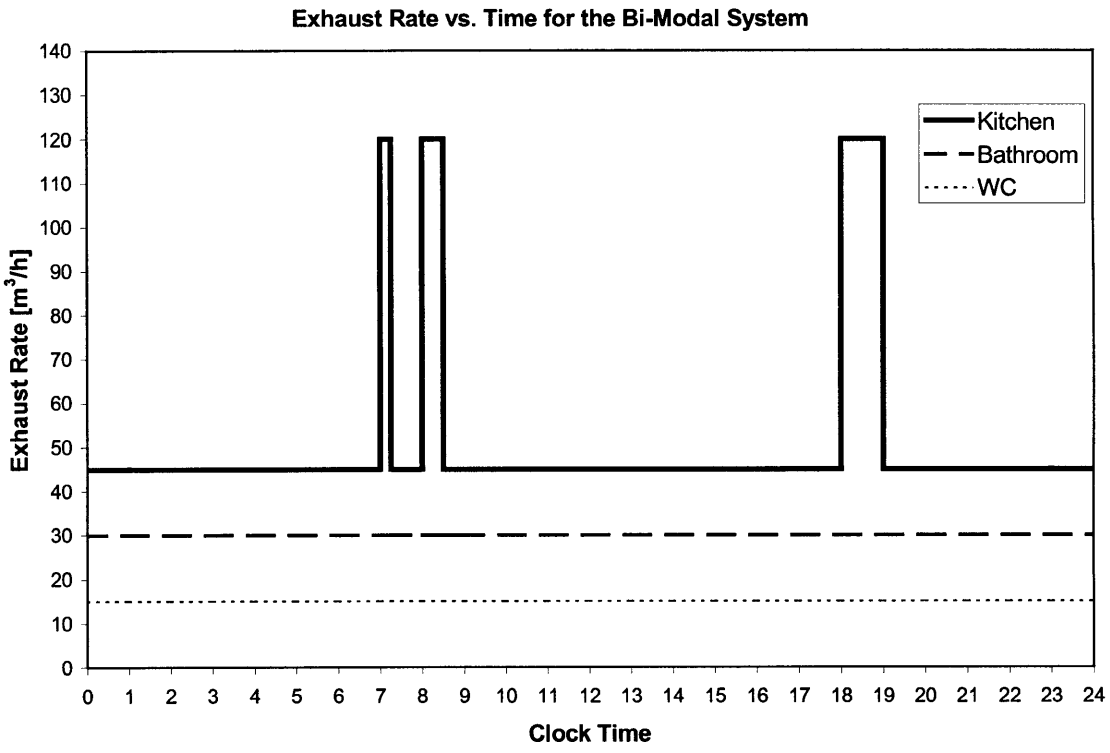

Figure 2.9. Exhaust rates for the bimodal system showing an increase of the kitchen exhaust rate during cooking; and constant bathroom and WC exhaust in summer.

Huang (2001) conducted a CFD study of this French house case and assumed the inlet mass flow rate of each room is proportional to its window area. To make the CONTAM simulation results and those from CFD computation comparable, the actual window leakage areas, which must be provided in CONTAM, were computed directly from the results obtained by Huang. The effective air leakage of unweatherstripped awning windows (1.6 cm^2/m^2) was chosen for the calculation of the actual window leakage area (ASHRAE 1997). The calculated effective leakage areas are given in Table 2.8.

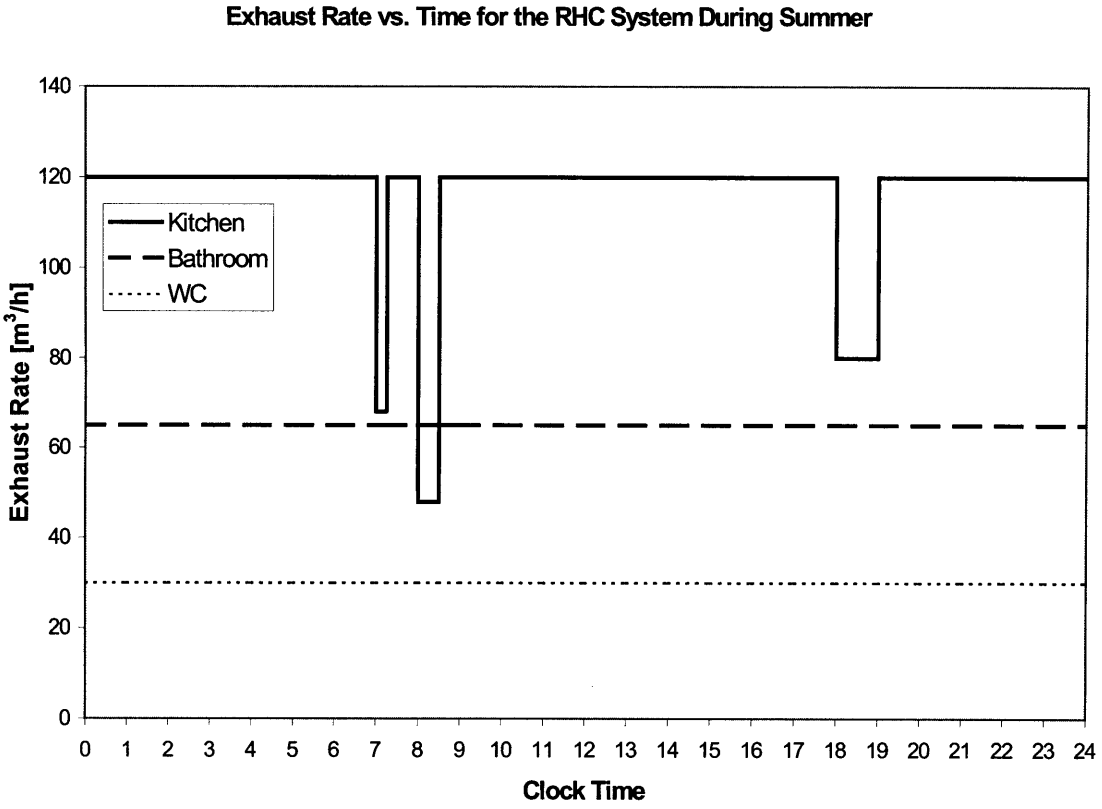

Figure 2.10. Exhaust rates for the RHC case in summer.

Based on the actual window leakage area and the empirical leakage area equation (Equation 2.5), the air change rate (ACH) of each room is computed by CONTAM. Tables 2.9 and 2.10 give the air change rates in the rooms computed by the CFD and CONTAM during 18:00 – 19:00 and 19:00 – 21:00, respectively. The two tables show significant differences in the air change rates between CFD and CONTAM. Although the airflow direction through each path is the same from the two models, significant differences can be found in their magnitudes. For both periods, there exist systematic positive changes. The ACH of CONTAM is greater than that of CFD for the kitchen, daughter and son's bedrooms and bathroom. Negative changes for the living room and the parents' rooms are observed. The most significant changes occurred in daughter's bedroom (~60.7%) for the first episode and in son's bedroom (~39.7%) for the second period. As expected, larger negative changes were also found during the first time interval since the whole house ACH is unchanged for both models.

Large differences in airflow rates may raise questions of which method can provide more reliable results. For this particular case, CFD model has taken into account of the whole house structure and incorporated detailed boundary conditions from Huang (2001), whereas CONTAM model employed empirical formula to calculate the airflow rates that may cause possible systematic biases. Therefore, it appears that the CFD results are more consistent and credible.

Table 2.8. Window leakage area in each room obtained from CFD simulation.

	Window Leakage Area Obtained from CFD Simulation		
	Inlet mass flow rate per window area [$m^3/h/m^2$]	Effective Air Leakage Area (cm^2/m^2)	Actual Window Leakage Area (cm^2)
Living Room	21.48	1.6	4.768
Kitchen	11.84	1.6	1.744
Daughter's Bedroom	6.86	1.6	2.112
Son's Bedroom	10.73	1.6	3.168
Parent's Bedroom	21.50	1.6	2.320
Bathroom	11.46	1.6	1.056

Table 2.9. Comparison of individual room air change rate (ACH) computed by CFD and CONTAM from 18:00 – 19:00.

	Individual Room ACH, 18.00-19.00h		
	CFD	CONTAM	% Difference of Room ACH
Living Room	0.69	0.57	-21%
Kitchen	0.54	0.80	32.5%
Daughter's Bedroom	0.33	0.84	60.7%
Son's Bedroom	0.75	1.24	39.5%
Parents' Bedroom	1.24	1.00	-24%
Bathroom	0.61	0.94	35%
Whole House	0.67	0.67	0%

Table 2.10. Comparison of individual room ACH computed by CFD and CONTAM from 19:00 – 21:00.

	Individual Room ACH, 19.00-21.00h		
	CFD	CONTAM	% Difference of Room ACH
Living Room	0.37	0.31	-19.4%
Kitchen	0.27	0.43	37.2%
Daughter's Bedroom	0.28	0.46	39.1%
Son's Bedroom	0.41	0.68	39.7%
Parents' Bedroom	0.66	0.54	-22.2%
Bathroom	0.32	0.51	37.3%
Whole House	0.36	0.36	0%

Figures 2.11 and 2.12 present the CO_2 exposure by the bimodal and RHC ventilation simulated by CONTAM. The results are compared to those of CFD obtained by Huang (2001), which are shown in Figure 13. Similar trends and patterns can be found for both CONTAM and CFD results. For example, CO_2 concentration accumulates when the occupants are in sleep (around 22:00 p.m. to 7:00 p.m.), or peaks when there are cooking activities (between 18:00 p.m. and 19:00 p.m. or between 8:00 a.m. and 8:30 a.m.). The latter appears clearer for the CONTAM simulation. CO_2 exposure from the different family members (parents and kids) is also modeled well in both CONTAM and CFD simulations. The bimodal ventilation method produces higher exposure of CO_2 for all the family members than that produced by the RHC method within each simulation. However, major discrepancies in the magnitudes of personal exposure are evident between the results calculated from CONTAM and those from CFD (peak value for bimodal ventilation is ~2125 ppm in CONTAM and is ~800 ppm in CFD). The magnitude of CO_2 concentration derived from the bimodal ventilation is nearly 10^6 order larger than that derived from RHC ventilation in CONTAM, whereas these two are within the same magnitude range in CFD). Again, the results obtained by CFD simulation seem to be more reasonable. Similar behavior can also be seen on water vapor exposure for individual person in Figures 14-16.

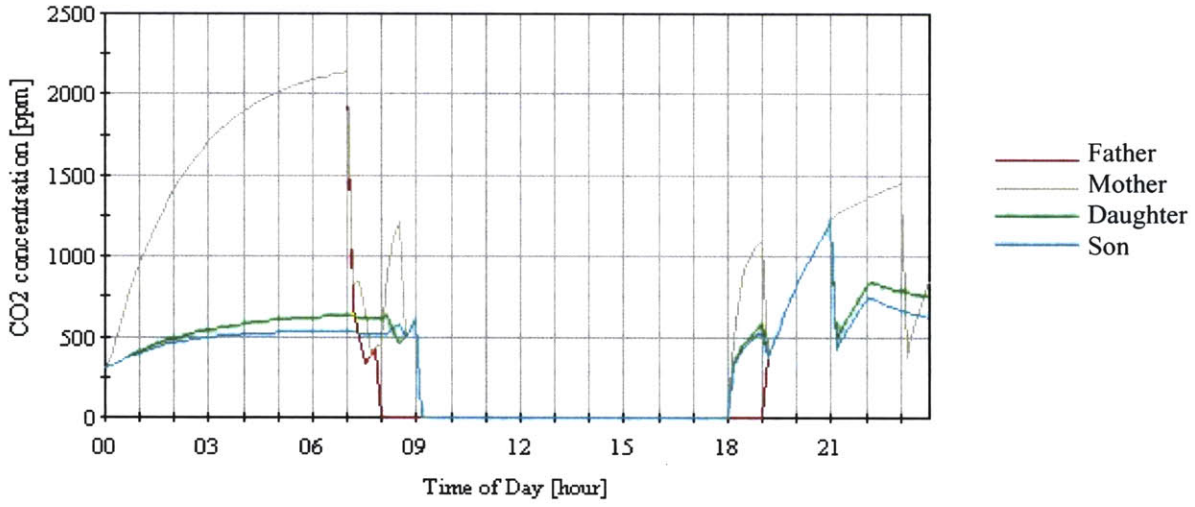

Figure 2.11. CO_2 concentration history for bimodal ventilation in summer.

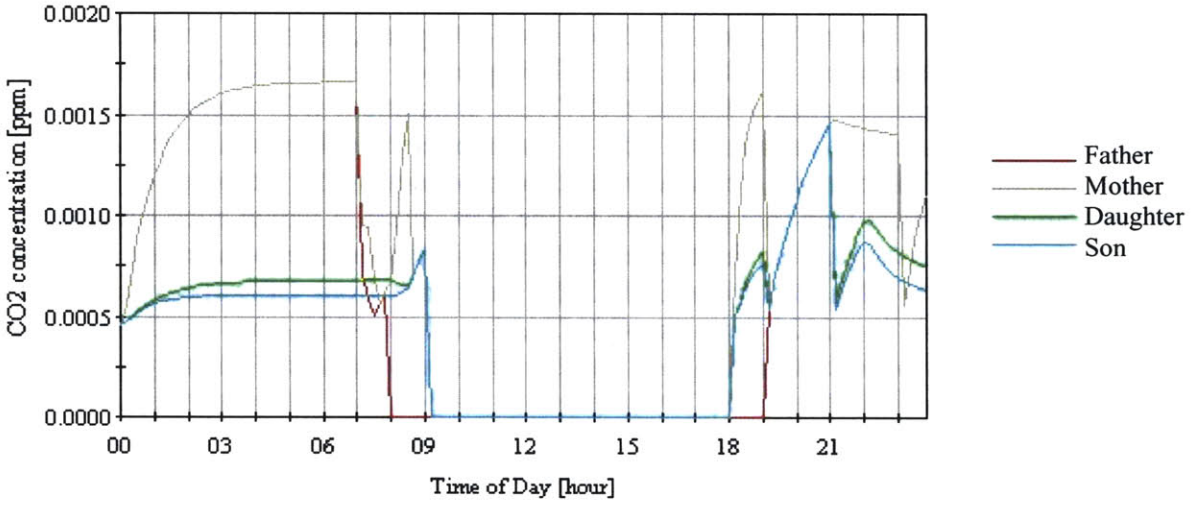

Figure 2.12. CO_2 concentration history for RHC ventilation in summer.

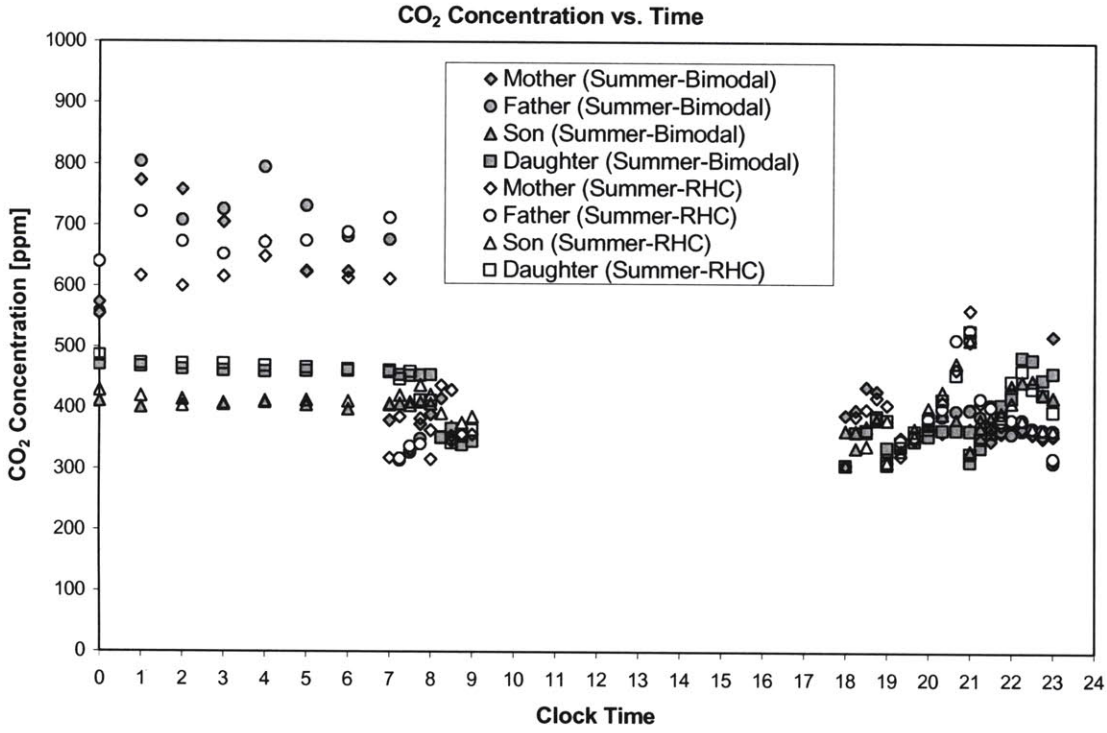

Figure 2.13. CO_2 concentration history of bimodal and RHC ventilation in summer obtained from CFD simulation (Huang 2001).

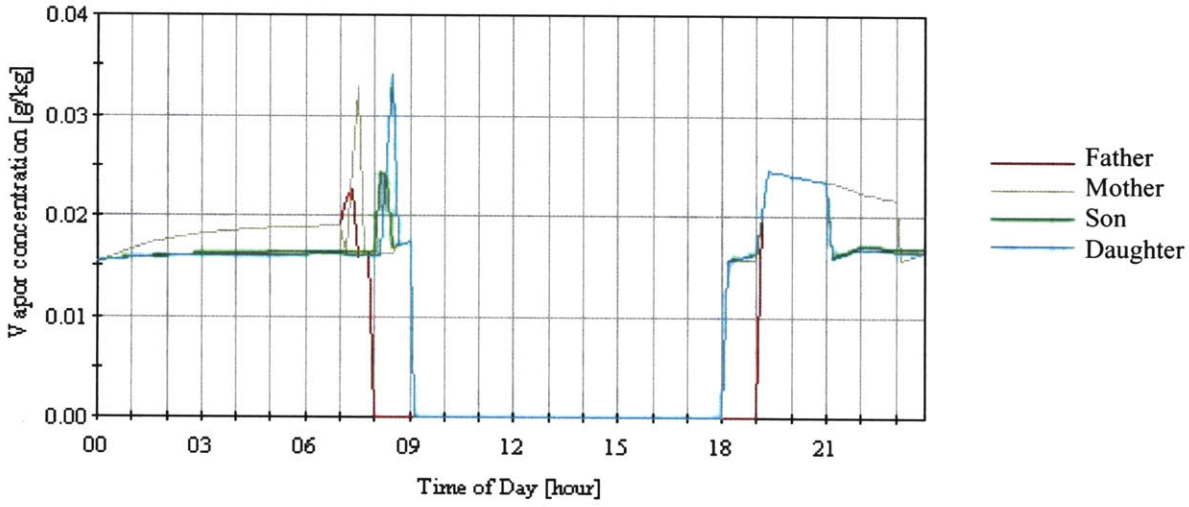

Figure 2.14. Water vapor concentration history for bimodal ventilation in summer.

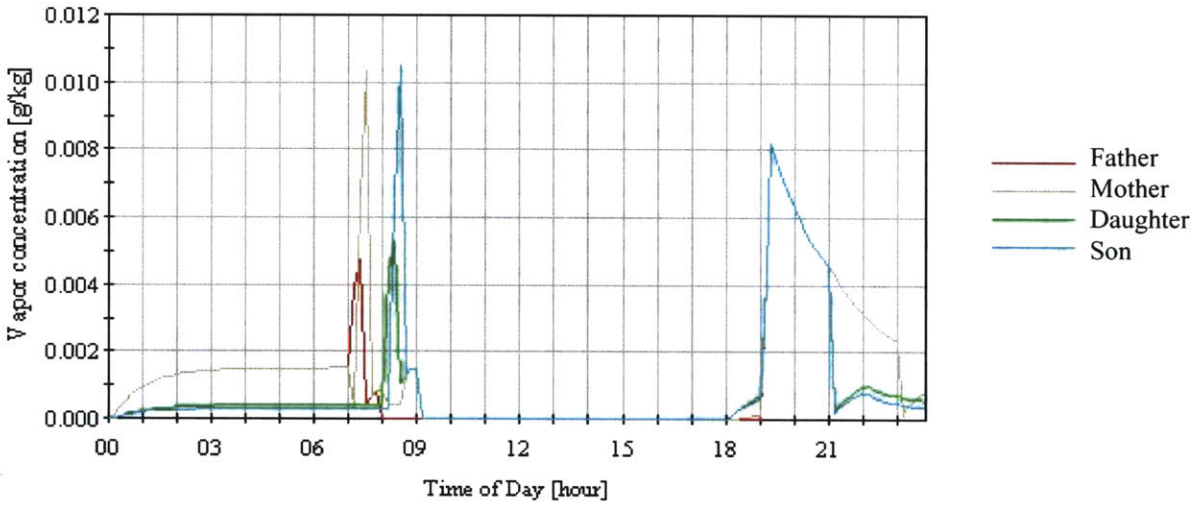

Figure 2.15. Water vapor concentration history for RHC ventilation in summer.

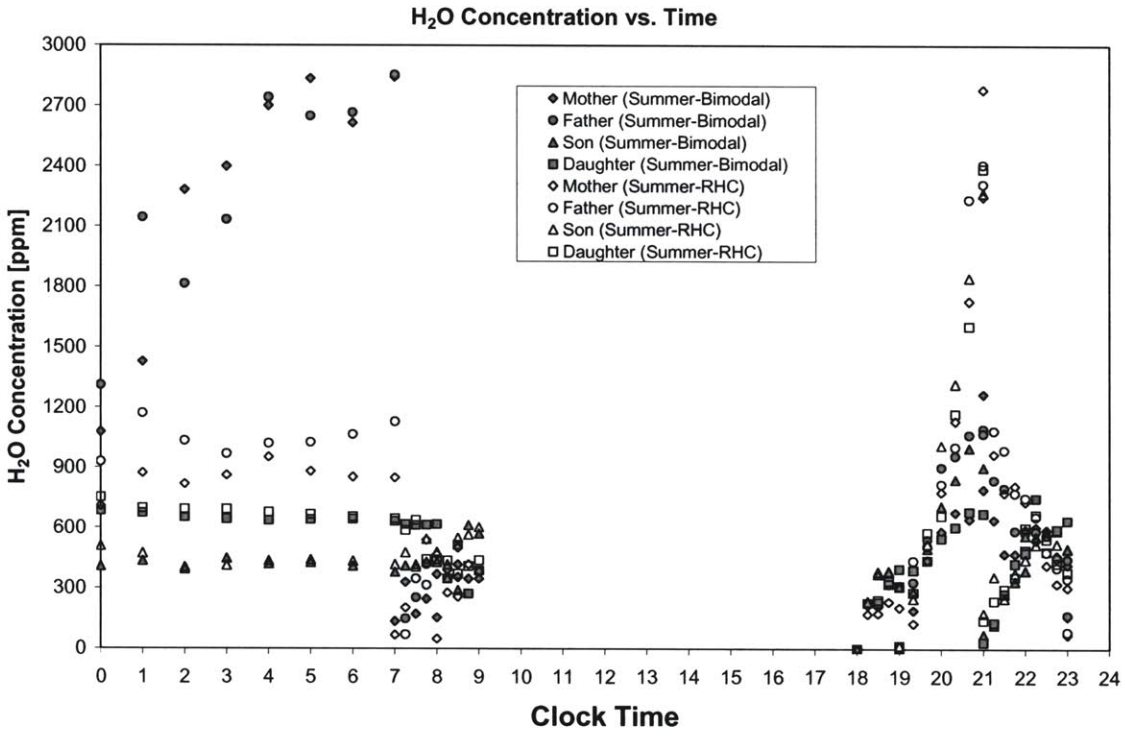

Figure 2.16. Water vapor concentration history of bimodal and RHC ventilation in summer from CFD simulation (Huang 2001).

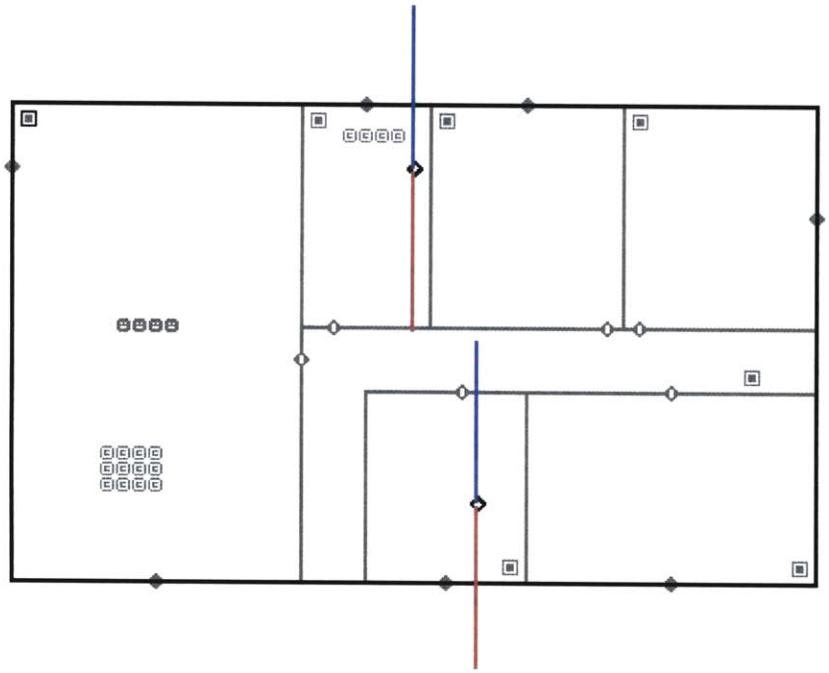

Figure 2.17. CONTAM representation of exhaust systems on the roof of French house.

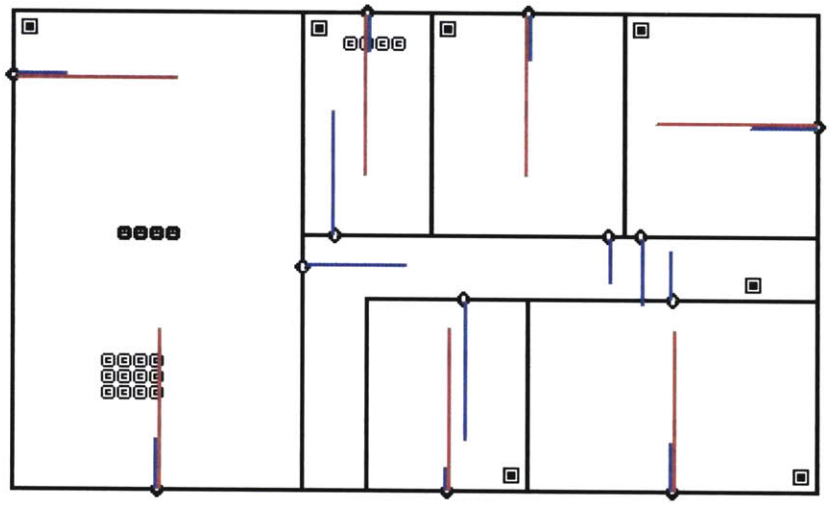

Figure 2.18. Results of general airflow pattern obtained from CONTAM simulation.

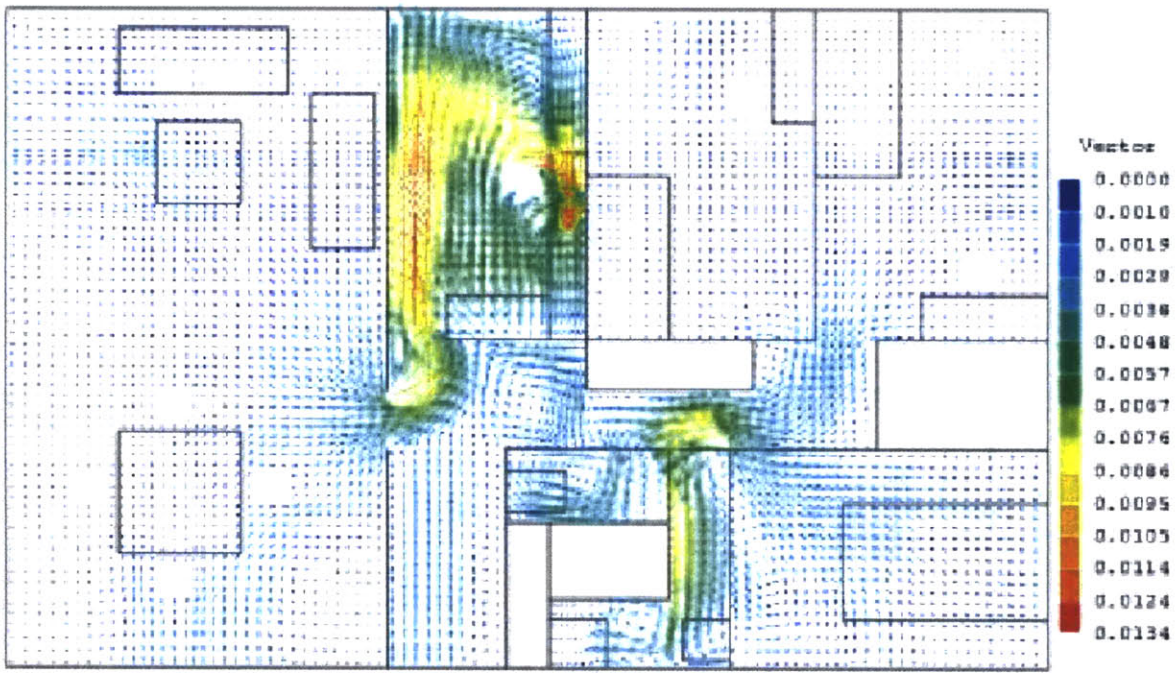

Figure 2.19. Detail airflow pattern obtained from CFD by Huang (2001).

Figure 2.17 shows the CONTAM representation of exhaust systems on the roof of the French house. Figures 2.18 and 2.19 display the general airflow pattern obtained from both CONTAM and CFD simulations. When compared to CFD simulation results, CONTAM appears to be able to present a similar airflow pattern. Simulation applying CFD technique in this particular case require enormous human effort and time, while such simulation, even in unsteady state simulation, only requires one second or two if CONTAM is used. As mentioned earlier, although major difference in the magnitude of contaminant exposure rate does occur using the two techniques, the airflow pattern obtained by CONTAM suggests that it is a valuable tool for general design purpose.

2.3.3 90 Degree Planar Branch Case and Program Limitations

The 90-degree planar branch case has been extensively evaluated by various studies (e.g. Kelkar and Choudhury 2000). There are two ways in representing this Tee branch, either by treating it as room airflow with obstacles inside or by treating it solely as a duct. Once the 90-degree planar branch configuration has been adapted to the CONTAM environment, however, the results obtained from CONTAM simulation are the same regardless of different representation.

The detailed configuration of this branch and its CONTAM representation are shown in Figures 2.20 – 2.22.

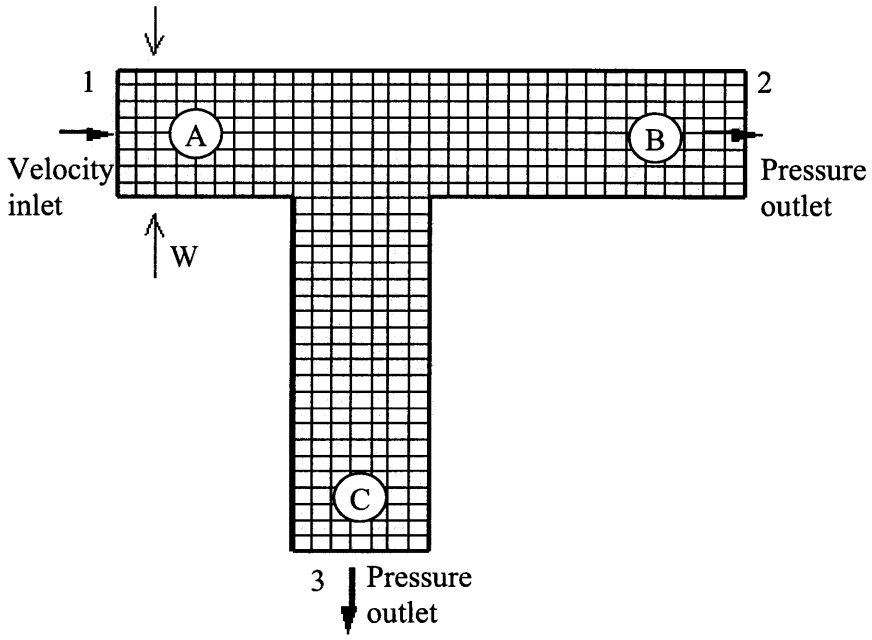

Figure 2.20. 90-degree planar branch configuration.

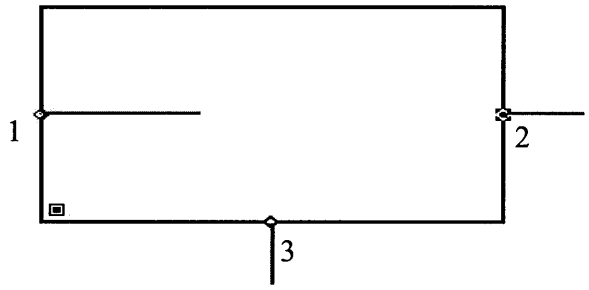

Figure 2.21. 90-degree planar branch represented as airflow paths.

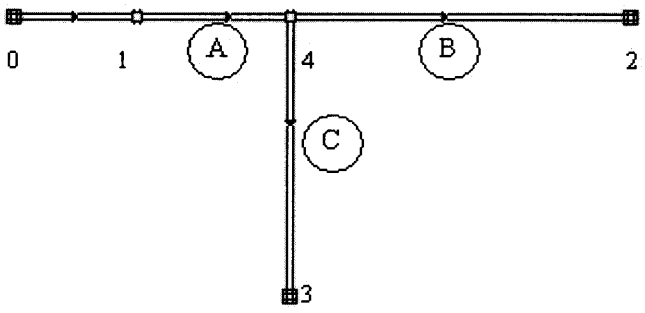

Figure 2.22. 90-degree planar branch represented as ducts.

In both CONTAM and CFD simulations, uniform velocity is exerted at inlet 1 (Figure 2.20). In CONTAM simulation, outflow rates through the main exit branch (outlet 2) and the side exit branch (outlet 3) are the same, which is 0.0235 kg/s for each. However, significant difference exists for these two outflows from the CFD simulation (more detail results will be given in Chapter 3). Hence, the integration of CFD and CONTAM would be desirable to provide more realistic prediction of room airflow by taking advantages of their different modeling philosophies.

2.4 Conclusion Remarks

In this chapter, the fundamentals of CONTAM program has been discussed followed by three application cases. CONTAM is among one of the best multizone models that are available to the public, and becomes increasingly popular recently. The model has undergone constant development and its application appears promising. This provides us with confidence to couple a CFD program into it.

Comparison among three multizone models (CONTAM, COMIS and CONTAM93) was conducted for an AIVC three-story building. The results show that multizone models can simulate the airflow rates with reasonable direction and magnitude.

Simulations of a typical, detached French house on IAQ using both CONTAM and CFD show a general agreement on trends and patterns of CO_2 and H_2O concentrations as well as airflow directions. However, there exist significant magnitude differences in room ventilation rates and contaminant exposure rates between CONTAM and CFD simulations. Huge magnitude differences for CO_2 and H_2O concentrations under different ventilation methods (bimodal or RHC) were also observed. Which one provides more reliable prediction? The answer is unclear since both programs have their own assumptions and configurations on flow characteristics and boundary conditions. Generally speaking, CONTAM may provide reasonable results for a quick time check, while CFD can provide reliable results for certain critical area once the boundary conditions are well specified.

In the last application example of a 90-degree planar branch case, CFD generates reasonable airflow field and predicts the flow partition well. However, CONTAM provides user with erroneous flow partition information. This testifies the need of coupling a CFD program into CONTAM for the purpose of better airflow analysis and IAQ study.

CHAPTER 3

DESCRIPTION AND VALIDATION OF A CFD PROGRAM

3.1 Introduction

Proper design of indoor environment requires detailed information of indoor air distribution, such as airflow pattern, velocity, temperature, and contaminant concentrations. Both experimental measurements and computational simulation can provide such information. Although experimental measurements are reliable, they require tedious labor-effort and considerable time. Computational simulations, such as multizone modeling and computational-fluid-dynamics (CFD) techniques, have received much more attention over experimental approaches recently, because they are timesaving tools and can render reasonable results for design purpose.

As illustrated in Chapter 2, many different types of indoor airflows can be modeled as uniform mixtures, when the air properties such as temperature and contaminant concentration inside rooms are well mixed or nearly so. This is the basic assumption employed in multizone airflow analysis models. Clear advantage of a multizone zone model is its simplicity. However, the heavy tradeoff stems also from this well-mixed assumption of the properties inside a zone, usually a room. The temperature and contaminant distributions are very often not homogenous, and indeed stratified. In some cases, such air property gradients play major roles in indoor quality, building energy consumption and human comfort. Therefore, the CFD method has the advantages over both experimental measurement and multizone airflow models in capturing such detailed airflow characteristics.

This chapter describes the fundamentals of a CFD program—MIT-CFD that is used for the present study. MIT-CFD is a MIT-CFD program developed by the Building Technology Program at the Massachusetts Institute of Technology. It is written in FORTRAN with an easy-to-use input interface. The program is divided into problem-independent part and problem-dependent part. User can modify the problem-dependent part of the program as necessary. MIT-CFD has been applied to study a number of building simulation problems. The description of MIT-CFD starts from the governing flow equations and mathematical models in section 3.2 and 3.3. Numerical methods and boundary conditions used by the program will be introduced in section 3.4 and 3.5. Several cases will be studied for the purpose of verification, and the processes that are important to the future coupling will be addressed in section 3.6. This will be followed by a summary in section 3.7.

3.2 Governing Flow Equations

The nature of turbulence is sophisticated and not yet fully understood. The turbulent flow is three-dimensional and random with many vortices (turbulent eddies) that enhance mixing in the flow field. The mixing decreases velocity gradients and dissipates kinetic energy of the fluid stream. Kinetic energy is finally transformed to the internal energy of the fluid due to irreversible dissipation. In addition, the enhanced mixing increases diffusion of mass, momentum, temperature, and concentration. Therefore, the turbulent indoor airflow can carry on effective mass and heat transfer, which is an important parameter for indoor air quality and thermal comfort. To study the impact of turbulent mixing on indoor air quality and thermal comfort, partial differential transport equations that govern turbulent flow must be solved.

We deem indoor airflow as three dimensional, turbulent, incompressible flow of a Newtonian fluid. In Cartesian coordinates, the transport equations of a flow has the following forms (in tensor notation):

- Mass continuity equation:

$$\frac{\partial \rho}{\partial t} + \frac{\partial \rho \tilde{u}_i}{\partial x_i} = 0 \tag{3.1}$$

where ρ is the air density, $\tilde{u}_i$ is the instantaneous velocity component in x_i-direction, x_i is the coordinate (for i=1, 2, 3, x_i corresponds to three perpendicular coordinate axes), and t denotes the time.

- Momentum conservation equation (Navier-Stokes equation):

$$\frac{\partial \rho \tilde{u}_i}{\partial t} + \frac{\partial \rho \tilde{u}_i \tilde{u}_j}{\partial x_j} = -\frac{\partial \tilde{p}}{\partial x_i} + \frac{\partial}{\partial x_j}\left[\mu\left(\frac{\partial \tilde{u}_i}{\partial x_j} + \frac{\partial \tilde{u}_j}{\partial x_i}\right)\right] + \rho\beta(T_0 - \tilde{T})g_i \tag{3.2}$$

where $\tilde{u}_j$ is the instantaneous velocity component in x_j-direction, $\tilde{p}$ is the instantaneous pressure, μ is the molecular viscosity, β is the thermal expansion coefficient of air, T_0 is the temperature of a reference point, $\tilde{T}$ is the instantaneous temperature, and g_i is the gravity acceleration in i-direction.

- Energy conservation equation:

$$\frac{\partial \rho \tilde{T}}{\partial t} + \frac{\partial \rho \tilde{u}_j \tilde{T}}{\partial x_j} = \frac{\partial}{\partial x_j}\left(\frac{k}{c_p}\frac{\partial \tilde{T}}{\partial x_j}\right) + S_T \tag{3.3}$$

where k is the thermal conductivity of air, S_T is the thermal source, and c_p is the specific heat at constant pressure.

- Species concentration conservation equation:

$$\frac{\partial \rho \tilde{c}}{\partial t} + \frac{\partial \rho \tilde{u}_j \tilde{c}}{\partial x_j} = \frac{\partial}{\partial x_j}\left(\rho D \frac{\partial \tilde{c}}{\partial x_j}\right) + S \tag{3.4}$$

where $\tilde{c}$ is the instantaneous species concentration, D is the molecular diffusion coefficient for the species, and S is the species source.

Indoor airflow calculations use the Boussinesq approximation for thermal buoyancy (see the last term in Equation 3.2), where air density is assumed to be a constant, and the buoyancy influence is considered by temperature difference.

The partial differential equations (3.1) to (3.4) of conservation must be solved numerically, since no analytical solution for the equations is available. The numerical solution is called the CFD technique. There are three CFD techniques: Direct Numerical Simulation (DNS), Large-Eddy Simulation (LES), and Reynolds Averaged Navier-Stokes (RANS) modeling using turbulence models.

DNS solves full time-dependent Navier-Stokes equation without approximation. Hence, DNS requires a fine grid resolution of Kolmogorov micro-scale for small eddies, which is on the order of Kolmogorov length scale (ν^3/ε) about 0.01 to 0.001m. Since the Reynolds number for a typical indoor airflow is approximately 10^5, the total grid number for solving a three-dimensional airflow is approximately 10^{11} to 10^{12}. Current super computers can solve for the grid resolution as high as $1{,}000^3$, which is 10^9. Therefore, they are still incapable of solving such a flow. In addition, the DNS method requires very small time steps, which make the calculation extremely time consuming. In conclusion, it is not realistic to use DNS for indoor environment simulation at present except for handful case studies. However, DNS may be used to develop new turbulent models (Chen and Xu 1998). With the exciting advances in computer architecture and the

emergence of new numerical algorithms, DNS may be possible to tackle engineering flows directly in near future.

LES was developed in the late 1960s by Smagorinsky et al. (1965) and Deardorff (1970) for meteorological applications. Small eddies in flow motion were separated from large eddies by assuming that they would not significantly affect the evolution of large eddies. LES solves large eddies through a set of filtered Navier-Stokes equations governing three dimensional and time dependent motion. Small eddies are treated independently from the flow geometry by turbulent transport approximations using sub-grid scale models. Since the main contribution to turbulent transport comes from large eddy motion, LES has been successfully applied in some airflow problems. LES can be performed on a relative large and fast workstation, so it is more realistic for engineering application. Nevertheless, LES is still too time consuming because it calculates time dependent flow despite of larger time and space steps than those of DNS.

The RANS modeling is the fastest one but also the least accurate method among the three techniques. RANS solves ensemble-averaged Navier-Stokes equations by using turbulent modeling. In RANS, all unsteadiness is averaged and regarded as part of the turbulence (Ferziger and Peric 1996). Simulation performed by RANS uses less grid number compared to those of DNS and LES. Moreover, steady flow can be solved as time-independent. Since less computing cost is associated with RANS, it is superior to DNS and LES in this regard. Although turbulence modeling introduces an additional error into the calculation, RANS can still give reasonable results with an affordable computing effort for most flows in buildings.

Among the three different approaches discussed in the above, RANS models appear to be the most appropriate one for the present work. MIT-CFD is developed based on RANS technique and is therefore chosen.

In MIT-CFD, the averaging over the conservation equations in RANS is to decompose instantaneous variables into mean and fluctuating parts. The mean parts are denoted with capital letters and the fluctuating parts are represented by variables with a prime:

$$\widetilde{u}_i = U_i + u_i' \qquad \widetilde{p} = P + p' \qquad \widetilde{T} = T + T' \qquad \widetilde{c} = C + c' \tag{3.5}$$

Averaging the conservation Equations (3.1) and (3.4) gives a new set of equations called RANS equations:

$$\frac{\partial \rho}{\partial t} + \frac{\partial \rho U_i}{\partial x_i} = 0 \tag{3.6}$$

$$\frac{\partial \rho U_i}{\partial t}+\frac{\partial \rho U_i U_j}{\partial x_j}=-\frac{\partial P}{\partial x_i}+\frac{\partial}{\partial x_j}\left[\mu\left(\frac{\partial U_i}{\partial x_j}+\frac{\partial U_j}{\partial x_i}\right)-\rho\overline{u_i' u_j'}\right]+\rho\beta(T_0-T)g_i \tag{3.7}$$

$$\frac{\partial \rho T}{\partial t}+\frac{\partial \rho U_j T}{\partial x_j}=\frac{\partial}{\partial x_j}\left(\frac{\mu}{Pr_l}\frac{\partial T}{\partial x_j}-\rho\overline{u_j' T'}\right)+S_T \tag{3.8}$$

$$\frac{\partial \rho C}{\partial t}+\frac{\partial \rho U_j C}{\partial x_j}=\frac{\partial}{\partial x_j}\left(\frac{\mu}{Sc_l}\frac{\partial C}{\partial x_j}-\rho\overline{u_j' c'}\right)+S \tag{3.9}$$

where the coefficients for the viscous diffusion terms are rearranged as follows:

$$\frac{k}{c_p}=\frac{1}{k/c_p}=\frac{\mu}{\mu k/c_p}=\frac{\mu}{Pr};\ \rho D=\frac{1}{1/\rho D}=\frac{\mu}{\mu/\rho D}=\frac{\mu}{Sc},$$

Pr is the laminar Prandtl number, and *Sc* is the laminar Schmidt number.

The variable in the equations are the mean values (capital letters). Equations (3.7) through (3.9) contain additional terms, Reynolds stress ($\rho\overline{u_i' u_j'}$) and scalar fluxes ($\rho\overline{u_i'\varphi'}$), which are high-order unknown terms that need to be parameterized. Here, the additional terms resulting from the averaging are moved to the right hand side of the equation and grouped with viscous diffusion terms. This re-arrangement is suitable for eddy-viscosity turbulent modeling.

3.3 Mathematical Models

In order to close the system of equations from (3.6) to (3.9), it is required to model the Reynolds stress and turbulent scalar fluxes. Modeling of these additional transport terms is the main task of turbulent modeling. Eddy-viscosity turbulence models are based on the Boussinesq assumption in which the Reynolds stresses are proportional to the main strain-rate, and the coefficient of the proportionality is the turbulent (eddy) viscosity μ_t:

$$-\rho\overline{u_i' u_j'}=\mu\left(\frac{\partial U_i}{\partial x_j}+\frac{\partial U_j}{\partial x_i}\right)-\frac{2}{3}\delta_{ij}\rho k \tag{3.10}$$

where δ_{ij} is the Kronecker delta (δ_{ij}=0, when $i \neq j$; and δ_{ij}=1, when $i=j$), and k is the turbulence kinetic energy ($k = \frac{\overline{u_i' u_i'}}{2}$).

The second term on the right-hand-side of Equation (3.10) represents the pressure diffusion caused by turbulence. The purpose for incorporating this term is to preserve equality for the equation when contracted for $i = j = 1$, 2, and 3. These three new equations have the form of $-\rho\overline{u_i' u_j'} = -\frac{2}{3}\rho k$, for i = 1, 2, and 3; and their sum gives -$2\rho k$ on both sides of the equality. The mean-strain rate term is zero for $i = j$ because of the mass continuity and, therefore, the eddy viscosity does not appear in the contracted equation. It is important to note that the eddy viscosity is a property of the flow field that depends on turbulence, while the molecular viscosity is a fluid property. Within the same flow field, the eddy viscosity is usually modeled as a variable parameter.

The scalar fluxes, turbulent heat and concentration fluxes are approximated as additional diffusions caused by turbulence (eddy-diffusivity):

$$-\rho\overline{u_j' T'} = \Gamma_{T,t}\frac{\partial T}{\partial x_j} \tag{3.11}$$

$$-\rho\overline{u_j' c'} = \Gamma_{C,t}\frac{\partial C}{\partial x_j} \tag{3.12}$$

where $\Gamma_{T,t} = \frac{\mu_t}{Pr_t}$, and $\Gamma_{C,t} = \frac{\mu_t}{Sc_t}$ are the turbulent diffusion coefficients for temperature and concentration, respectively; Pr_t is the turbulent Prandtl number, and Sc_t is the turbulent Schmidt number.

The modeling of eddy-viscosity and diffusivity is based on an analogy with laminar flow and molecular transport. Turbulent eddies are represented as molecules, which collide and exchange energy on a microscopic scale. Although the analogy is empirical and questionable (Wilcox, 1993), the performance of the model is fairly reasonable for many practical applications.

With an eddy-viscosity model, the indoor airflow is described by the following time-averaged Navier-Stokes equations for the conservation of mass, momentum, energy, and species conservation:

- Mass continuity equation:

$$\frac{\partial \rho U_i}{\partial x_i} = 0 \tag{3.1}$$

where ρ is the air density, U_i is the mean velocity component in x_i-direction, and x_i is the coordinate (for i=1, 2, 3, x_i corresponds to three perpendicular coordinates)

- Momentum conservation equation:

$$\frac{\partial \rho U_i}{\partial t} + \frac{\partial \rho U_i U_j}{\partial x_j} = -\frac{\partial P}{\partial x_i} + \frac{\partial}{\partial x_j}\left[\mu_{eff}\left(\frac{\partial U_i}{\partial x_j} + \frac{\partial U_j}{\partial x_i}\right)\right] + \rho\beta(T_0 - T)g_i \tag{3.2}$$

where U_j is the mean velocity component in the x_j-direction, p is the mean pressure, μ_{eff} is the effective viscosity, β is the thermal expansion coefficient of air, T_0 is the temperature of a reference point, T is the mean temperature, and g_i is the gravity acceleration in the i-direction.

The last term on the right-hand-side of the equation is the buoyancy term. Note that the turbulence influences are lumped into the effective viscosity as the sum of the turbulent viscosity, μ_t, and laminar viscosity, μ:

$$\mu_{eff} = \mu_t + \mu \tag{3.3}$$

- Energy conservation equation:

To determine the temperature distribution and the buoyancy term in Equation (3.14), the equation for energy conservation must be solved.

$$\frac{\partial \rho T}{\partial t} + \frac{\partial \rho U_j T}{\partial x_j} = \frac{\partial}{\partial x_j}\left(\Gamma_{T,eff}\frac{\partial T}{\partial x_j}\right) + \frac{q}{c_p} \tag{3.4}$$

where $\Gamma_{T,eff}$ is the effective diffusion coefficient for T, q is the thermal source, and c_p is the specific heat.

The effective diffusion coefficient for temperature is proportional to the effective viscosity since the eddy mixing is a source of turbulent diffusivity:

$$\Gamma_{T,eff} = \frac{\mu_{eff}}{Pr_{eff}} = \frac{\mu}{Pr} + \frac{\mu_t}{Pr_t} \tag{3.5}$$

Measurements have shown that Prandtl numbers are nearly constant for many flows and for the entire flow field (Peng 1996). The laminar Prandtl number is Pr=0.71, and the turbulent Prandtl number is Pr_t=0.9.

- Species conservation equation:

$$\frac{\partial \rho C}{\partial t} + \frac{\partial \rho U_j C}{\partial x_j} = \frac{\partial}{\partial x_j}\left(\Gamma_{c,eff}\frac{\partial C}{\partial x_j}\right) + \rho C_s \tag{3.6}$$

where C is the species concentration, $\Gamma_{T,eff}$ is the effective diffusion coefficient for C, and C_s is the species source ($S=\rho C_s$).

The effective diffusion coefficient for concentration is analogous to the effective diffusion coefficient for temperature:

$$\Gamma_{C,eff} = \frac{\mu_{eff}}{Sc_{eff}} = \frac{\mu}{Sc} + \frac{\mu_t}{Sc_t} \tag{3.7}$$

Experiments have shown that the effective diffusion coefficient for concentration is almost the same as the effective viscosity (Peng 1996). Therefore, the laminar Schmidt number Sc is equal to 1.0, and the turbulent Schmidt number Sc_t is equal to 1.0.

Solution of the equations (3.13) – (3.19) provides us the distribution of indoor airflow parameters. This system of equations has only one unknown parameter, turbulent viscosity. The original time-averaged system of equations (3.6) – (3.9) has six unknown Reynolds stresses and three unknown scalar fluxes for each scalar variable. The eddy-viscosity (3.10) and eddy-diffusivity (3.11) – (3.12) assumptions reduced the problem to the eddy (turbulent) viscosity modeling. The additional equation or equations used to calculate the eddy viscosity are called the eddy viscosity turbulence model.

3.3.1 Two-equation Turbulence Modeling

Some complex forms of turbulence modeling require one or two additional transport equations to calculate parameters for the turbulent viscosity. The standard k-ε model (Launder and Spalding 1974) is the most widely used two-equation model in practice, which is able to elucidate the complexities of the indoor turbulent motion with

acceptable accuracy for engineering purposes (Chen and Jiang 1992). The standard k-ε model is chosen as one of the eddy-viscosity turbulence models in the MIT-CFD program.

Since MIT-CFD uses a non-orthogonal coordinate system, the partial differential equations governing steady incompressible flows can be written in the following general form:

$$\frac{\partial}{\partial x_i}\left(C_i\phi - D_{i\phi}\right) = J S_\phi, \qquad i = 1,2,3 \tag{3.8}$$

where the coefficient C_i is related to convection, $D_{i\phi}$ is related to diffusion and S_ϕ is the source terms. $D_{i\phi}$ and S_ϕ are given in Table 3.1 for different dependent variables ϕ. J is the Jacobian of coordinate transformation between the general curvilinear system (x_i) and a reference rectangular system (y_i). Equation (3.20) uses the velocity components V_i, which are along the coordinates y_i instead of along the grid-aligned directions, as shown in Figure 3.1.

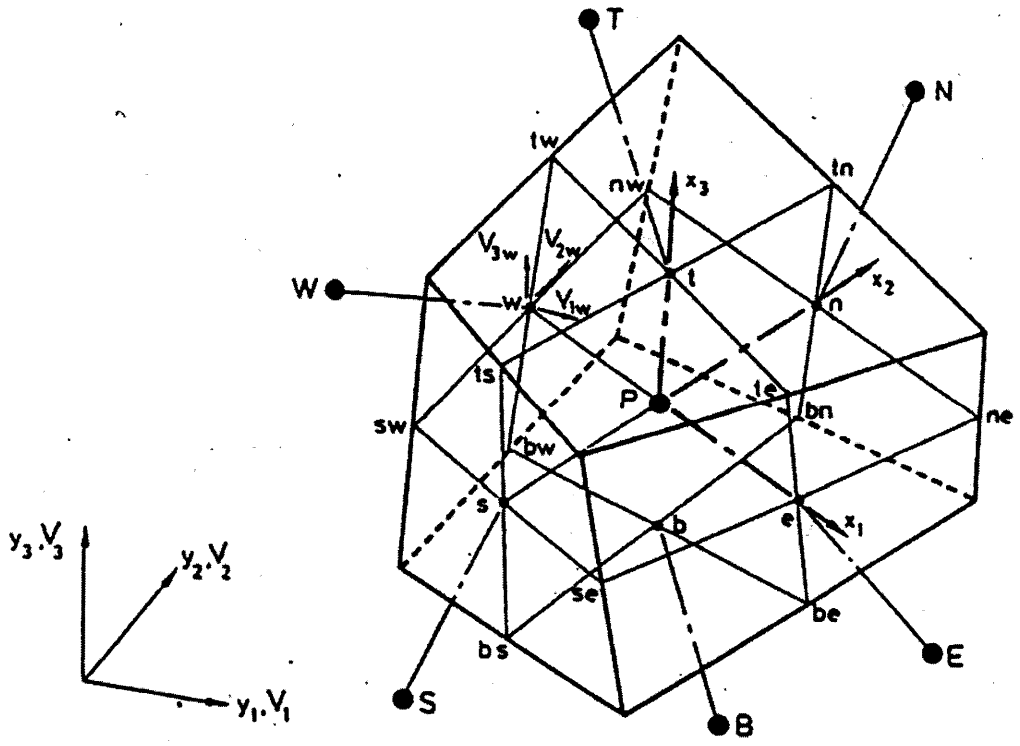

Figure 3.1. A typical control volume centered at node P.

Table 3.1 contains seven conservation equations when $D_{i\phi}$ and S_{ϕ} are specified. The first one is the continuity equation. The next three for $\phi = V_1, V_2, V_3$ are the Navier-Stokes equations for the time-averaged velocity components in three directions. The next two solves turbulent kinetic energy k and its dissipation rate ε. The last equation solves the transport of a scalar quantity S, such as temperature, enthalpy or species concentration. The source terms and the various turbulence model constants are also given in Table 3.1.

As shown in Table 3.1, the turbulent viscosity is calculated from:

$$\mu_t = \rho C_\mu \frac{k^2}{\varepsilon} \tag{3.9}$$

where C_μ =0.09 is the empirical constant. The terms for k and ε transport equations are listed in Table 3.1 as well.

Although the standard k-ε model is popular, it is not universal for all types of indoor airflow. Therefore, many efforts have been directed towards the identification of a suitable model for indoor environment simulation recently.

Chen (1995) evaluated the performance of five k-ε models: the standard k-ε model, a low-Reynolds-number k-ε model, a two-layer k-ε model, a two-scale k-ε model, and a renormalization group (RNG) k-ε model. Those turbulence models were used for the simulation of forced convection, natural convection, and mixed convection room airflows, as well as an impinging jet flow. Those flows are the basic elements of complex indoor airflows. The results were compared to experimental data for validation. Their results showed that both standard k-ε model and the RNG k-ε model were superior, with the RNG k-ε model slightly better to the standard one.

In another study, Muller and Renz (1998) tested the standard k–ε model, a low Reynolds-number k–ε model, and a Reynolds-stress model for the simulation of displacement ventilation. All the models provided similar results, although the low-Reynolds-number model resulted in the best overall agreement. On the other hand, Nielsen (1998) found that the buoyancy term in the low-Reynolds-number k–ε model is the most important factor for displacement ventilation. The damping functions, which are used to modify the standard k–ε model for near-wall laminar and transitional flows, have only small influences on the results. These damping functions are the only difference between the low–Reynolds number k–ε model and the standard k–ε model.

Table 3.1. The standard k – ε turbulent model parameters in the individual equations.

No.	ϕ	$D_{i\phi}$	S_ϕ
1	1	0	0
2	V_1	$\frac{\Gamma_2}{J}\left(B^i_j\frac{\partial V_1}{\partial x_j}+\beta^i_j\omega^j_1\right)$	$-\frac{1}{J}\frac{\partial}{\partial x_j}\left(\beta^j_1 p\right)$
3	V_2	$\frac{\Gamma_3}{J}\left(B^i_j\frac{\partial V_2}{\partial x_j}+\beta^i_j\omega^j_2\right)$	$-\frac{1}{J}\frac{\partial}{\partial x_j}\left(\beta^j_2 p\right)$
4	V_3	$\frac{\Gamma_4}{J}\left(B^i_j\frac{\partial V_3}{\partial x_j}+\beta^i_j\omega^j_3\right)$	$-\frac{1}{J}\frac{\partial}{\partial x_j}\left(\beta^j_3 p\right)$
5	k	$\frac{\Gamma_5}{J}B^i_j\frac{\partial k}{\partial x_j}$	$G-\rho\varepsilon$
6	ε	$\frac{\Gamma_6}{J}B^i_j\frac{\partial \varepsilon}{\partial x_j}$	$\left(C_{1\varepsilon}G-C_{2\varepsilon}\rho\varepsilon\right)\frac{\varepsilon}{k}$
7	S	$\frac{\Gamma_7}{J}B^i_j\frac{\partial S}{\partial x_j}$	S_s

$C_i=\rho\beta^i_j V_j,\ \omega^i_j=\beta^n_j\frac{\partial V_i}{\partial x_n},$

$\beta^i_j=$ cofactor of $\frac{\partial y_j}{\partial x_i}$ in J, $\qquad J=\begin{vmatrix}\frac{\partial y_1}{\partial x_1} & \frac{\partial y_2}{\partial x_1} & \frac{\partial y_3}{\partial x_1}\\ \frac{\partial y_1}{\partial x_2} & \frac{\partial y_2}{\partial x_2} & \frac{\partial y_3}{\partial x_2}\\ \frac{\partial y_1}{\partial x_3} & \frac{\partial y_2}{\partial x_3} & \frac{\partial y_3}{\partial x_3}\end{vmatrix}$

$B^i_j=\beta^i_n\beta^j_n,$

$\Gamma_n=\mu+\frac{\mu_t}{\sigma_n},\quad \mu_t=\rho C_\mu k^2/\varepsilon,$

$G=\frac{\mu_t}{2J^2}\left(\frac{\partial V_i}{\partial x_n}\beta^n_j+\frac{\partial V_j}{\partial x_n}\beta^n_i\right)^2,$

$C_\mu=0.09,\quad C_{1\varepsilon}=1.44,\quad C_{2\varepsilon}=1.92,$

$\sigma_2=\sigma_3=\sigma_4=1,\quad \sigma_5=1,\quad \sigma_6=1.3,\quad \sigma_7=1.$

A general conclusion from the above studies is that the turbulent models wind up differently from one case to the other, even though all the simulated flows are indoor airflows. In general, the standard k–ε model is a relatively stable model that can be easily implemented and has been widely validated to be able to produce reasonably accurate results for many applications. This provides us with the background to exploit the standard k–ε model in MIT–CFD.

3.3.2 Zero-equation Model

With the standard k–ε model, the computation is still time-consuming, if it is applied to study an indoor space with normal size. Since the present investigation intents to couple a CFD program within a multi-zone model, the use of the standard k–ε model may require too much computing resource. Therefore, it is necessary to seek for an avenue to reduce the computing cost. One solution would be to use a simple turbulent model instead of the standard k–ε model that requires solving two additional transport equations as shown in Table 3.1.

Zero–equation turbulence models are the simplest eddy viscosity models. These models have one algebra equation for turbulent viscosity. In analogy to the molecular transport of momentum, Prandtl gave the mixing-length hypothesis (1925), which is the basis for zero-equation models:

$$\mu_t = \rho l_{mix}^2 \left| \frac{dU}{dy} \right| \tag{3.10}$$

where l_{mix} is the mixing length, ρ is the fluid density, and U is the average velocity.

The mixing length is an empirical variable defined as a transverse distance (free path) of small eddies (fluid lumps) over which their original momentums are preserved. The product of the mixing length and the velocity gradient is called mixing velocity, which is also the property of the turbulent flow. Prandtl postulated that the mixing length near solid surfaces is proportional to the distance from the surface. This approximation gives good results only for a certain class of turbulent boundary layers (Wilcox 1993), such as free shear flows (jets, mixing layer, etc.). Calibration of the mixing length is always needed for complex flows.

One of the problems with Prandtl's mixing length theory is that the zero gradient for velocity results in zero turbulent viscosity (Karimipanah 1996). For example, the model gives zero turbulence viscosity in the middle of a pipe that has turbulent flow. Hence, researchers have developed new equations for both mixing velocity and eddy viscosity.

Much effort has been made to extend the applicability of the mixing length model. Van Driest (1956) devised a damping function to include wall-damping effects:

$$l_{mix} = \kappa y\left[1 - e^{\frac{-y^+}{26}}\right] \tag{3.11}$$

where κ (=0.41) is the von Karman constant.

Cebeci and Smith (1974) made the most important modification to the zero-equation model that includes the defect layer, the intermittent phenomena in the boundary layer, surface curvature, and low-Reynolds-number effects, etc. Baldwin and Lomax (1978) proposed a similar two-layer model that does not need to determine the boundary-layer edge in Cebeci-Smith's model.

Both models have been widely applied to many engineering applications (Ameri and Arnone 1994, Nikitopoulos and Michaelides 1995, Liu and Ikehata 1994). Once calibrated, zero-equation models can predict mean flow quantities quite well. While most engineers and scientists today are turning to more sophisticated turbulence models such as two-equation and Reynolds-Stress models, zero-equation models may always have a position in the modeling society because of its simplicity and cost-effectiveness.

In the Prandtl-Kolmogorov assumption, turbulent viscosity is the product of turbulent kinetic energy, k, and turbulent macroscale, l, which is a proper length scale for turbulence interactions:

$$\mu_t = C_v \rho k^{1/2} l \tag{3.12}$$

where $C_v = 0.5478$ is an empirical constant.

The turbulence kinetic energy in equation (3.24) can be expressed with turbulence intensity T_i and mean flow velocity U:

$$T_i = \frac{\sqrt{\overline{u_i'^2}}}{U} = \frac{\sqrt{2k}}{U} \tag{3.13}$$

$$\mu_t = 0.5487\rho \frac{T_i U}{\sqrt{2}} l \tag{3.14}$$

The average turbulence intensity Ti for indoor airflow is assumed to be 10%. This value is a good estimate for the occupied zone in mixing ventilation, yet it can be far from reality near or within the jet region. However, the zero-equation models perform very well for turbulent jets or other boundary layers if properly calibrated (Wilcox 1993).

Chen and Xu (1998) used the assumption of uniform turbulence intensity and derived an algebraic function to express turbulent viscosity as a function of local mean velocity, U, and a length scale, l:

$$\mu_t = 0.03874 \rho U l \tag{3.15}$$

This equation has an empirical constant, a universal value of 0.03874 for all different flows. The length scale, l, is the distance to the closest surface of the enclosure. The model (3.27) is an empirical equation, and has been implemented in MIT-CFD and will be used for the present investigation.

Turbulence should be considered as an engineering approximation rather than scientific law (Ferziger and Peric 1996). Hence, the evaluation of the turbulence model's performance and the justification of its assumptions are performed through its application in solving flow problems. In the present study, both the standard k-ε model and the zero-equation model from Chen and Xu (1998) were used. However, for coupling CFD with CONTAM, only the zero-equation model was used.

3.4 Numerical methods

The above-mentioned differential equations in Table 3.1 and the corresponding turbulence models should be solved numerically. Those partial differential equations are discretized for the domain of the flow field. Several different discretization methods such as finite-element method and finite-volume method may be used, along with advanced grid generation techniques such as unstructured grid and body-fitted coordinates. Since the finite-volume discretization has become the most widely used method owing to less computing time involved, it is also adapted by MIT-CFD together with a non-orthogonal grid system.

The flow field is then discretized into a finite number of cells (control volumes). The program places a computational node at the geometric center of each cell and identifies the grid lines as cell surfaces. Figure 3.1 shows the layout and index of the center points (computational nodes) and corner points (grid nodes) of the control volumes. The indices (i, j, k) of the center points vary from 1 to NI for I-index, from 1 to NJ for j-index, and from 1 to NK for k-index, while those of the corner points start with 2 for each of the i-, j- and k-indices. Besides the triple-index (i, j, k) the program also uses a single-index ii to identify the computational or grid nodes for vectorization. The single-index is related to the triple-index (i, j, k) via:

$$ii = i + (j-1)NI + (k-1)NIJ \tag{3. 16}$$

Thus, if the node P in Figure 3.1 has the triple-index (i, j, k) and the single-index ii, the corresponding indices for the neighboring node N are (i, j+1, k) and ii+NI. This code uses

non-staggered-grid arrangement, namely, the program uses the same control volumes for all the flow variables and all the variables are stored at the computational nodes.

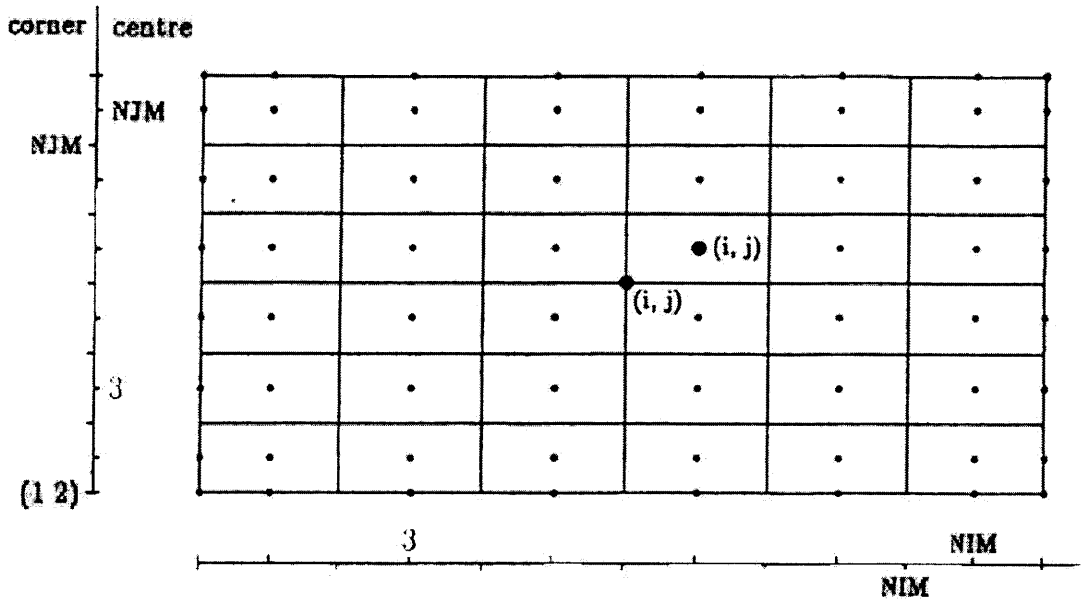

Figure 3. 2. Layout and indexing of cell center and corner points.

3.4.1 Integration of the Governing Equations and Numerical Schemes

The conservation equations can be obtained by integrating Equation (3.20) over a typical control volume centered at P as shown in Figure 3.2.

$$I_e - I_w + I_n - I_s + I_t - I_b = \int_{\Delta V} S_\phi dV \tag{3.17}$$

where I_f represents the total flux of ϕ across the cell-face f (= e, w, n, s, t or b). Each of the surface fluxes I_f contains a convective contribution I_f^C and a diffusive contribution I_f^D, that is

$$I_f = I_f^C + I_f^D \tag{3.18}$$

To solve the Equation (3.29), approximations of convection, diffusion and source terms are required.

- **Approximation of convective terms.** The convective terms in Equation (3.30) can be written as:

$$I_f^C = C_f \phi_f \tag{3.19}$$

where C_f is the mass flux across the cell-face f, and can be calculated for w-, s-, and b-faces as:

$$\begin{aligned} C_w &= \left(\rho b_j^1 V_j\right)_w \\ C_s &= \left(\rho b_j^2 V_j\right)_s \\ C_b &= \left(\rho b_j^3 V_j\right)_b \end{aligned} \tag{3.20}$$

The element ϕ_f is the key to determine both accuracy and stability of numerical solutions, which depends on the numerical schemes applied. The more accurate schemes are often prone to be less stable, and vise versa. In MIT-CFD, five numerical schemes are incorporated for user to make choices according to different problems. They are the upwind scheme (Courant et al. 1952, Patankar, 1980), the standard hybrid differencing (Spalding 1972), third-order unbounded QUICK scheme (Leonard, 1979), second-order bounded SOUCUP (Zhu and Rodi, 1991), and second-order bounded HLPA (Zhu, 1991a). In order to discuss these schemes, let us consider the w-face of the control volume shown in Figure 3.4 and assume, without loss of generality, that $V_w \geq 0$ (V_w is the normal velocity at the w-face). The face value ϕ_w evaluated by each scheme is presented in Table 3.2.

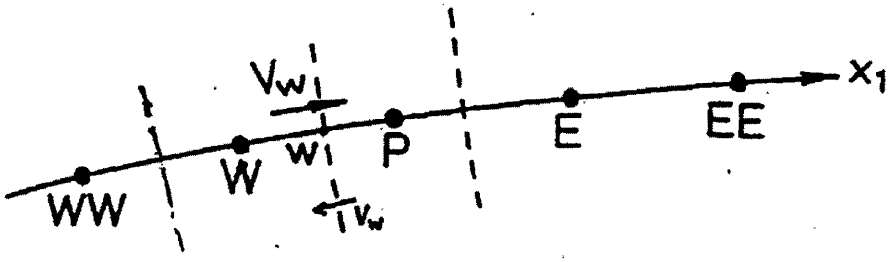

Figure 3.3. Nodes required by convection schemes in x_1-direction.

Hybrid scheme uses either central or upwind differencing according to a cell Peclet number $P_e = \left|C_w / D_w\right|$ (D_w is the diffusive coefficient defined in Equation 3.35); Quick scheme approximates the face value ϕ_w by fitting a parabolic curve through three

nodal values $\phi_P, \phi_w, \text{and} \phi_{ww}$; SOUCUP combines second-order upwind, central and upwind differencing together with the switch from one scheme to another being controlled by an upwind-biased normalized variable, $\hat{\phi}_w = (\phi_w - \phi_{ww})/(\phi_p - \phi_{ww})$; and HLPA is the further implementation using this normalized variable. All the schemes except hybrid scheme are implemented in the MIT-CFD program in a deferred way (Khosla and Rubin 1974). The present study chooses HLPA scheme for numerical simulation throughout, because it generally provides higher numerical stability and faster convergence.

Table 3.2. Numerical schemes implemented in MIT-CFD program.

Scheme	Equation presentation
Upwind	$\phi_w = \phi_W$
Hybrid	$\phi_w = \begin{cases} 0.5(\phi_p + \phi_w) & \text{if } P_e \le 2 \\ \phi_W & \text{otherwise} \end{cases}$
QUICK	$\phi_w = \frac{3}{8}\phi_P + \frac{3}{4}\phi_W - \frac{1}{8}\phi_{WW}$
SOUCUP	$\phi_w = \begin{cases} 1.5\phi_W - 0.5\phi_{WW} & \text{if } 0 < \hat{\phi}_W \le 0.5 \\ 0.5(\phi_P + \phi_w) & \text{if } 0.5 < \hat{\phi}_W < 1 \\ \phi_W & \text{if } \lvert\hat{\phi}_W - 0.5\rvert \ge 0.5 \end{cases}$
HLPA	$\phi_w = \phi_W + \gamma_w(\phi_P - \phi_W)\frac{\phi_W - \phi_{WW}}{\phi_P - \phi_{WW}}, \quad \gamma_w = \begin{cases} 1 & \text{if} \lvert\hat{\phi}_W - 0.5\rvert < 0.5 \\ 0 & \text{otherwise} \end{cases}$

- **Approximation of diffusion terms.** The diffusive flux I_f^D in Equation (3.30) contains two parts:

$$I_f^D = I_f^{DN} + I_f^{DC} \tag{3.21}$$

The first part I_f^{DN} contains only one term that has the first derivative of ϕ in the direction "normal" to the cell-surface f. It can be written, for the w-face for example, as:

$$I_w^{DN} = D_w(\phi_P - \phi_W) \tag{3.22}$$

where

$$D_w = \left[\left(b_1^1 b_1^1 + b_2^1 b_2^1 + b_3^1 b_3^1\right)\Gamma_\phi / \Delta V\right]_w \tag{3.23}$$

The second part I_f^{DC} in Equation (3.33) contains all the other terms. Only normal derivative diffusion flux, I_f^D, is coupled with the convective flux, I_f^C, to calculate the main coefficients of the difference equations; while the cross-derivative diffusion flux, I_f^{DC}, is treated explicitly as a pseudo-source term to avoid the possibility of producing negative coefficients in an implicit treatment.

- **Approximation of source terms.** For all the models used in MIT-CFD, the source terms S_ϕ are linearized as $S_\phi = S_\phi^U + S_\phi^P \phi_P$. Especially for the standard k–ε model, the coefficient S_ϕ^P is defined so that it is always less than or equal to zero for all the conservation equations, and S_ϕ^U always assumes non-negative values for both k- and ε-equations. This enhances the stability of the numerical process and prevents the calculated values of k and ε from becoming negative in low turbulence regions, if standard k–ε model is chosen for simulation.

- **Final form of discretized equations.** Now, the following difference equation results:

$$\left(\sum_{nb} A_{nb} - S_P\right)\phi_P = \sum_{nb} A_{nb}\phi_{nb} + S_U, \quad nb = W, E, S, N, B, T \tag{3.24}$$

The main coefficients A_{nb} that relate the principal unknown ϕ_P to its neighbors ϕ_{nb} contain the combined contribution from both convection and normal diffusion. The physical source term, $S_\phi = S_\phi^U + S_\phi^P \phi_P$, and the cross-derivative diffusion flux I^{DC} are included in the coefficients S^U and S^P. In order to stabilize the iterative solution process, under-relaxation is used in this program.

3.4.2 Solution Procedure

The solution procedure for the system of discretized transport equations is an iterative one because the equations are coupled and the convection terms in momentum equations are non-linear. The pressure field is the most important factor to ensure correctness of calculated velocities. To successfully use the non-staggered grid arrangement, a coupling between the pressure and velocity fields in the discretized momentum and continuity equations must be established. The MIT-CFD program uses

the SIMPLE algorithm (Patankar and Spalding 1972) and the momentum interpolation procedure (Rhie and Chow 1983) to achieve such coupling.

The solution procedure starts with the initial guessed fields for calculated variables (velocity, pressure, turbulent quantities, temperature, and concentration). The sequence in which the calculation is carried out using the standard k-ε model is as follows:

a) Initialize all field values by guess.
b) Solve the V_1, V_2 and V_3-momentum equations using the guessed pressure field.
c) Solve the pressure-correction equation to obtain the pressure-correction at the cell-centers; correct the convective fluxes at the cell-faces, the velocities and pressure at the cell-centers.
d) Solve the k- and ε-equations and update μ_t, if the flow is turbulent.
e) Solve the rest scalar equations, if required.
f) Return to step b with updated field values.

Sequence of the steps b to f is repeated until the convergence criterion is satisfied.

The variables must be solved simultaneously, and the progress towards a solution has to be simultaneous, too. To ensure a stable solution and control the rate of change for calculated variables, under-relaxation is used. Two relaxation techniques are available: linear under-relaxation and false-time steps. Both techniques serve to control the change in variable calculation and increase the numerical stability in MIT-CFD. Finally, the numerical solution should be independent of grid distributions, initial variable distributions, and relaxation techniques.

3.5 Boundary conditions

Boundary conditions are necessary for the mathematical solution of the transport flow equations discussed above. Seven types of most frequently encountered boundary conditions are implemented in MIT-CFD. They are inflow, outflow, symmetry and rigid wall conditions, blockages, sources, and pressure boundaries, respectively.

- **Inflow planes.** At the inflow planes, the values of ϕ (ϕ = V_1, V_2, V_3, k, ε, T, C) are prescribed. There are two types of thermal boundary conditions implemented in MIT-CFD program: either by specifying temperature or by specifying the heat flux. These two thermal conditions apply to the rest types of the boundaries discussed as follows.

- **Outflow planes.** Outlet boundary conditions may be used in conjunction with the inlet boundary conditions (Versteeg and Malalasekera 1995). At the outflow planes, the streamwise gradients of all variables are set to zero, implying a fully developed

flow condition. In addition, the velocities are corrected to ensure the overall mass conservation at the outflow planes.

- **Symmetry planes.** The conditions at a symmetry boundary are: (i) no flow across the boundary and (ii) no scalar flux across the boundary. At the symmetry planes, the normal velocity component and the normal gradients of other variables are set to zero. The convective and normal diffusive fluxes are also set explicitly to zero in this program.

- **Rigid walls and blockages.** For indoor airflow problems, wall and blockages such as furniture, people, and machinery are the most common boundaries. Non-slip condition is an appropriate condition for the velocity components at solid walls, which is used for laminar flows in this program, i.e., the velocity components of the flow are set to those of the walls. The standard wall-functions (Launder and Spalding 1974) are used for turbulent flows. For walls and blockages that are also heat sources/sinks, either first or second thermal condition is applied.

- **Sources.** A user may specify heat sources or contaminants generation, which are independent to the physical geometry. In the discretized governing equations, the boundary conditions as sources appear only in the source terms rather than in the convection terms.

- **Prescribed pressure boundaries.** When the exact details of the flow distribution are unknown but the boundary values of the pressure are available, the constant pressure boundary condition can be used. Typical applications of this boundary condition include external flows around objects, free surface flows, buoyancy-driven flows such as natural ventilation and fires, and also internal flows with multiple outlets (Versteeg and Malalasekera 1995). A typical room in a building is normally associated with multiple openings (such as doors, windows, cracks, orifices, etc.). Pressure boundary condition appears to be important to solve the flow field within such a room. MIT-CFD code is now able to incorporate constant pressure boundary by either total or static pressure that is important for the present study. The pressure correction is set to zero at the nodes when applying the fixed pressure boundary. The pressure is fixed at the nodes just inside the physical boundary. Pressure correction is achieved by taking $S_u = 0.0$, $S_p = -10^{30}$, and the nodal pressure as the required boundary pressure.

3.6 CFD Verification and Validation

The verification and validation of the MIT-CFD program were carried out by adopting a two-prone approach. First, the simulation results are validated by experimental data that are available from the literature for simple thermal, flow, and geometrical boundary conditions. The other is to use inter-model comparison that verifies the simulation results using different models and numerical approaches.

Forced, natural and mixed convection represents the basic elements of room airflows. For simplicity, two-dimensional cases are selected to validate the zero-equation and the standard k–ε model in MIT-CFD. A three-duct-in-series case will be evaluated comparing with the analytical results, which would be further discussed in the next chapter on the coupling issue. A 90-degree planar branch case mentioned in Chapter 2 is used to verify the fixed pressure boundary feature that was developed for the present study. Considering most buildings are rectangular, this investigation uses simple rectangular geometry that mimics typical building or room configurations.

3.6.1 Natural Convection Case

For natural convection, the experimental setup data of Olson et al. (1990) as shown in Figure 3.4 are used. It is a two-dimensional case. The length and depth of the cavity are L= 7.9 m and H= 2.5 m, respectively. The two walls along L are well insulated, and the two walls along H have temperature of 20°C and 12°C, respectively.

Figure 3.5 displays the airflow patterns obtained by the zero-equation model and the standard k-ε model in MIT-CFD program, the Lam-Bremhorst low-Reynolds-number k-ε model (Lam and Bremhorst 1981), and smoke visualization. As expected, the low-Reynolds-number k-ε model can produce the clockwise main flow stream near the surfaces of blockages, and a secondary recirculation (counter-clockwise) within the inner portion of the room. These features, though close to the experimental observation (see Figure 3.5d), are obtained at the expense of large computational resource involved.

Results obtained by the zero-equation and standard k-ε models (Figures 3.5a and 3.5b) reveal that both methods can capture the clockwise main flow stream that is less concentrated near the surfaces compared to the observation. The flow pattern derived from zero-equation model shows a sign of counter-clockwise secondary recirculation near the floor. However, this recirculation is totally absent in the standard k-ε model simulation. While much simpler, the zero-equation model appears to predict a better airflow pattern than that of the standard k-ε model for this particular case.

3.6.2 Forced Convection Case

The forced convection case uses the experimental setup data from Nielsen et al. (1978) shown in Figure 3.6. Reynolds number is 5000 based on the bulk supply velocity and the height of air supply outlet. The air supply outlet is located at the height of h=0.056H, and exhaust inlet h'=0.16H. The length of the room is equal to 3H.

Figure 3.7 compares the airflow patterns by the zero-equation model and the standard k-ε model used in MIT-CFD program. The computed velocity profiles are compared in Figure 3.8 with the experimental data in two vertical sections: x/H=1 and x/H=2 respectively; and two horizontal sections: y/H=0.972 (through the air supply outlet) and y/H=0.028 (through the air exhaust inlet), respectively. The results show that

the standard k-ε model is superior to zero-equation model when dealing with forced convection without the consideration of temperature variation. All four profile curves are close to those of experiment data. However, the results of zero-equation model show strong decay that diffuses the jet-like pattern.

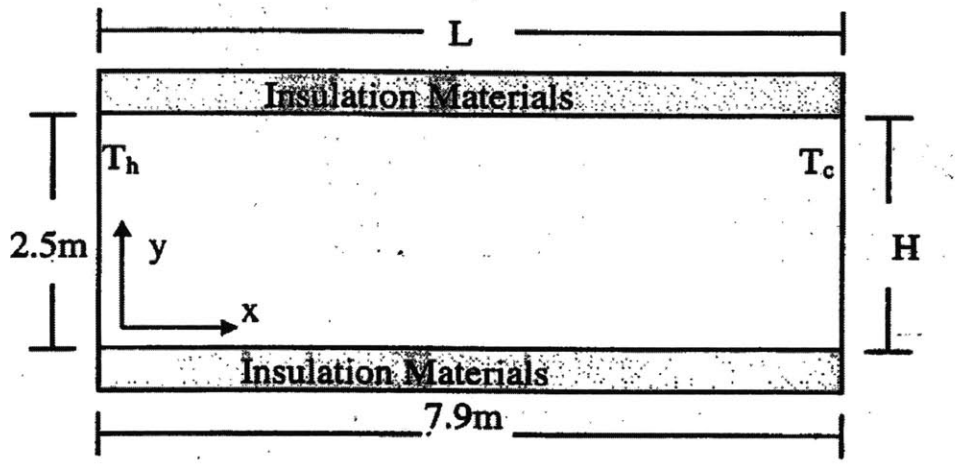

Figure 3.4. Sketch and boundary conditions of the natural convection case.

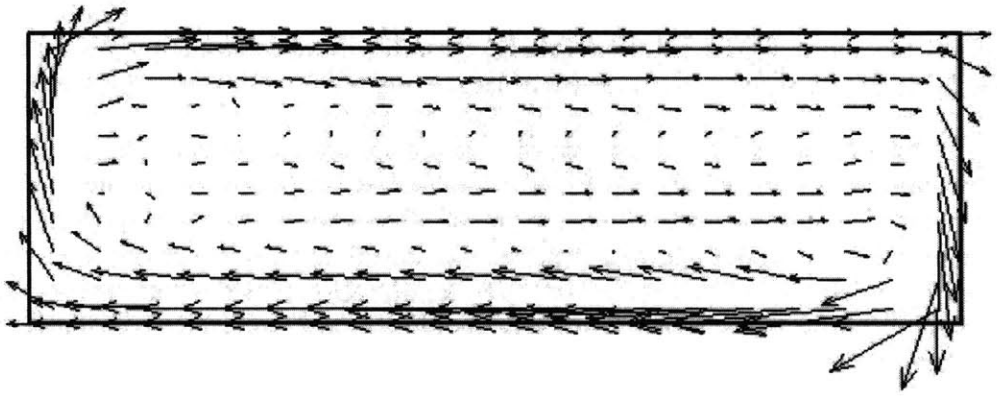

(a)

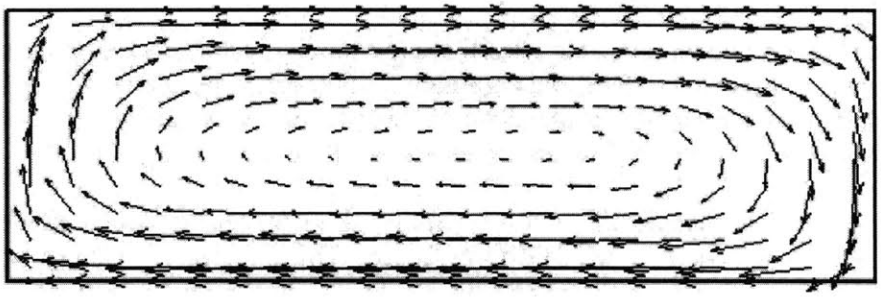

(b)

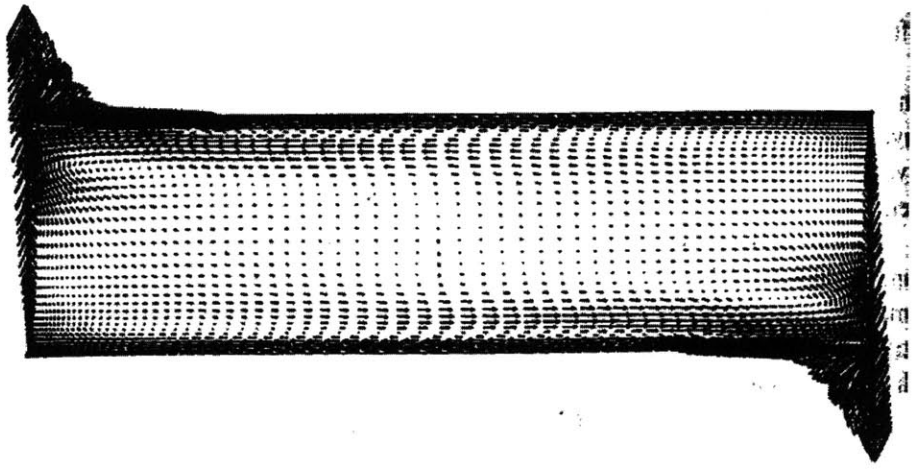

(c)

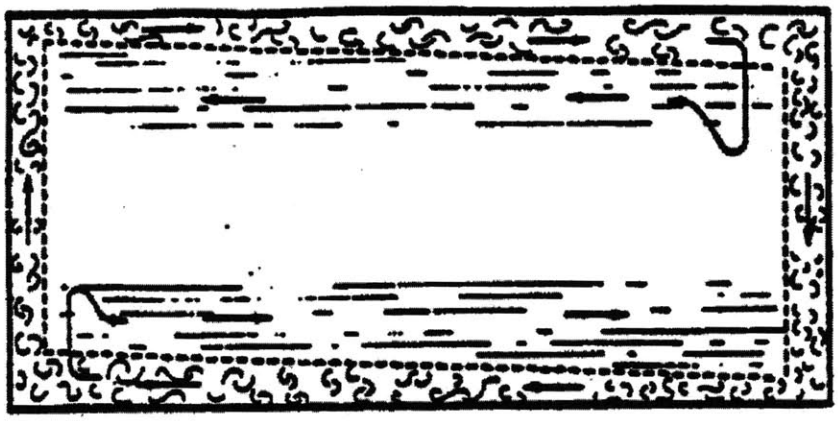

(d)

Figure 3.5. Comparison of the airflow patterns for natural convection: (a) zero-equation model, (b) standard k-ε model, (c) the Lam-Bremhorst low-Reynolds-number k-ε model, (d) smoke visualization

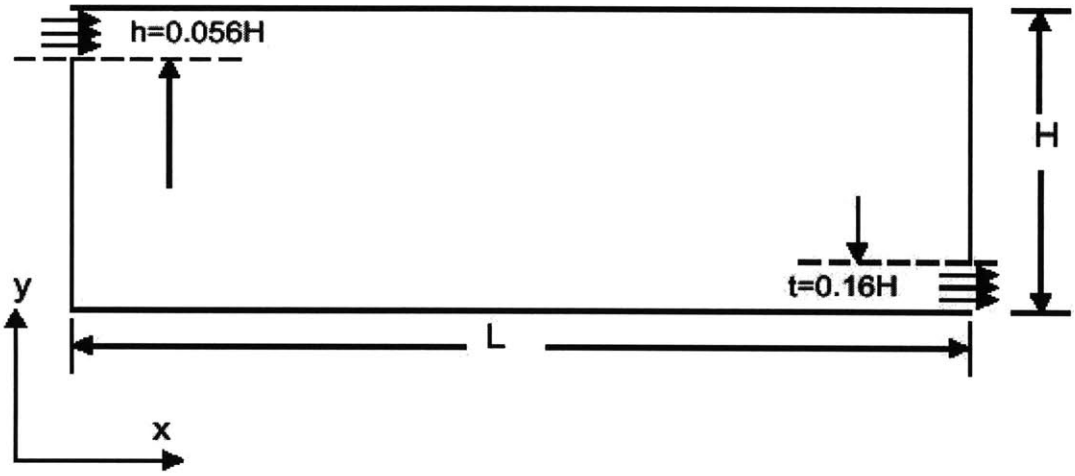

Figure 3.6. The sketch of the forced convection case.

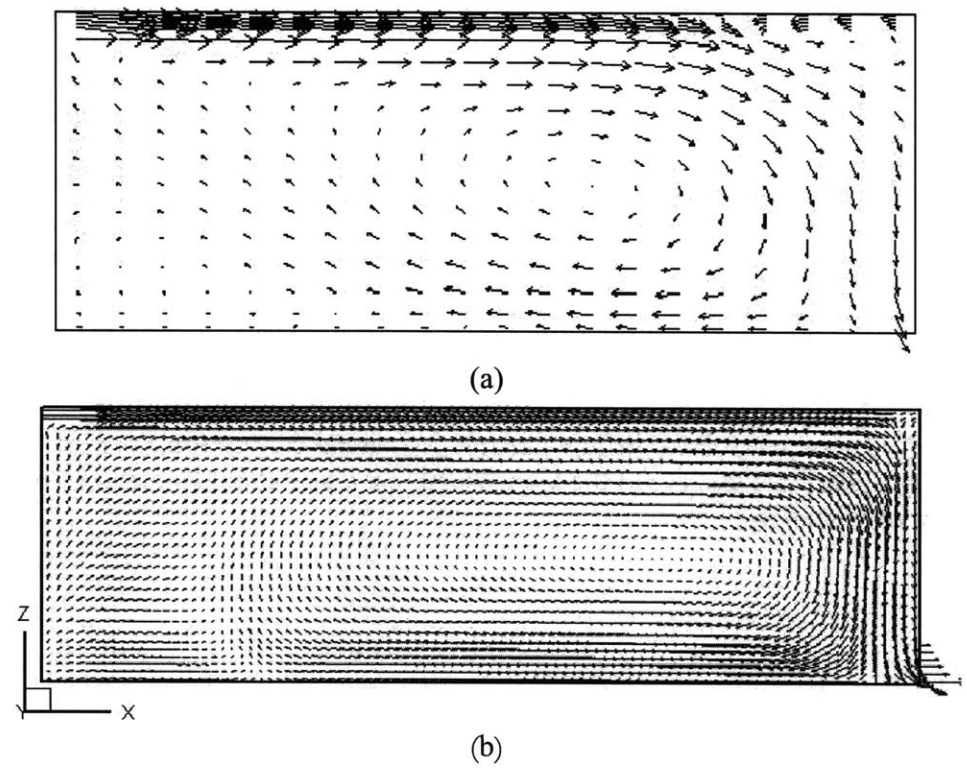

Figure 3.7. Comparison of the airflow patterns for the forced convection: (a) zero-equation model, (b) the standard k-ε model.

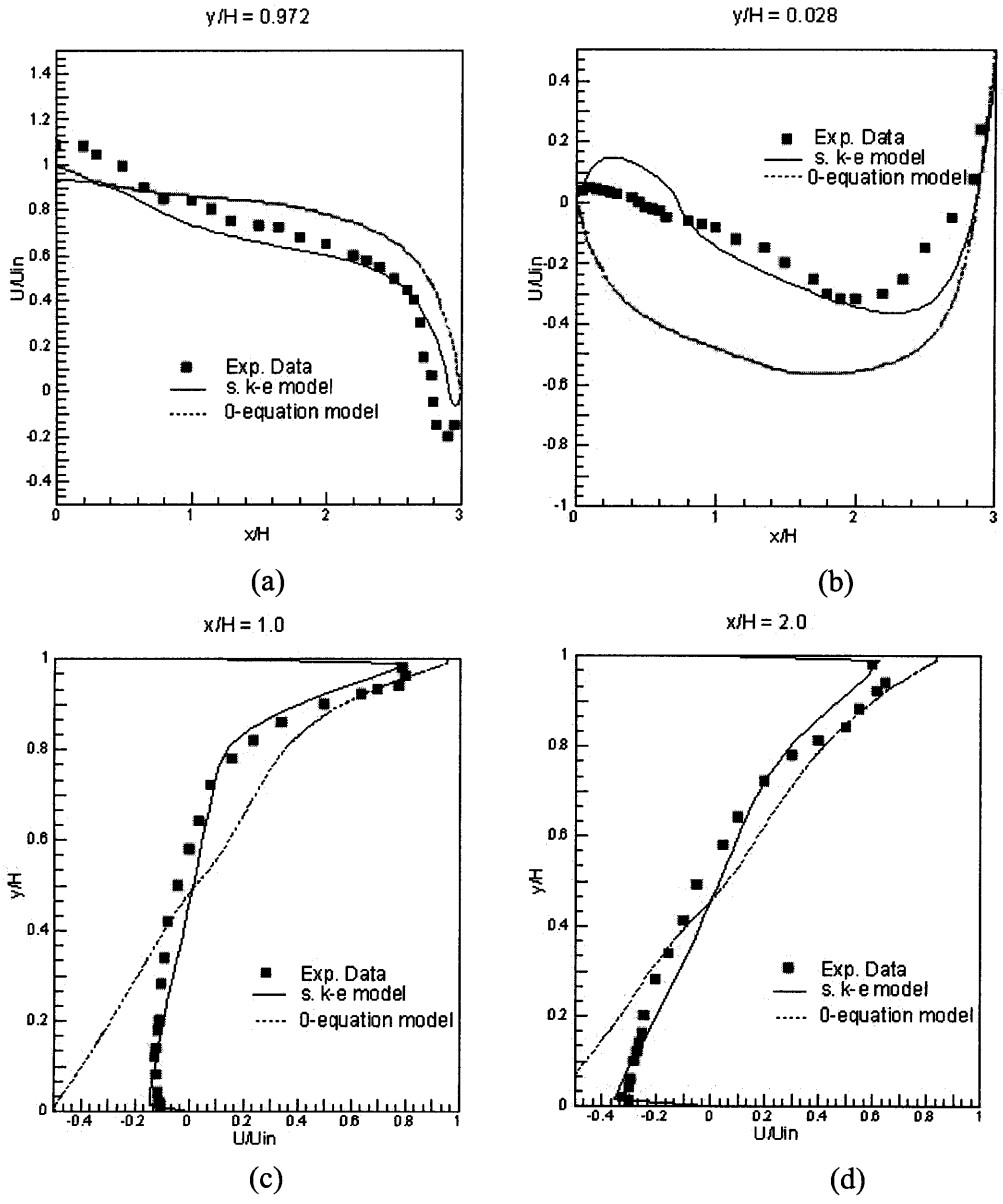

Figure 3.8. Comparison of velocity profiles in different sections of the room with forced convection: (a) at x/H=1, (b) at x/H=2, (c) at y/H=0.972, and (d) at y/H=0.028.

3.6.3 Mixed Convection Case

The mixed convection case uses the experimental data from Schwenke (1975). The case is similar to the forced convection case except that the room length is 4.7H and the height of the air supply outlet h is 0.025H, where H is the room height. The wall on the rightside is heated but the ceiling and the floor are well insulated. Schwenke conducted series of measurements with different Archimedes numbers, Ar ($Ar = \frac{\beta g h_{in} \Delta T_0}{U^2}$), ranging from 0.001 to 0.02.

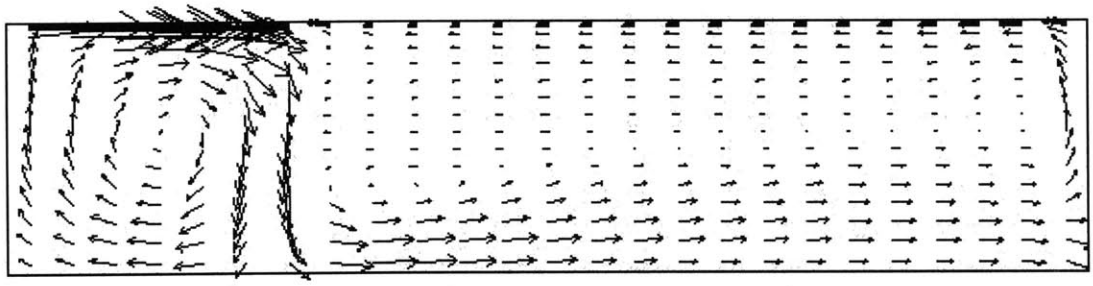

(a)

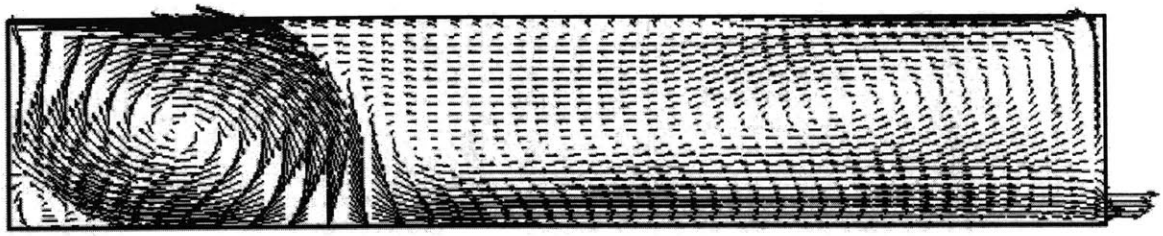

(b)

Figure 3.9. Comparison of the airflow patterns for the mixed convection: (a) the zero-equation model in MIT simplified flow program (Chen and Xu, 1998), (b) the zero-equation model in MIT-CFD.

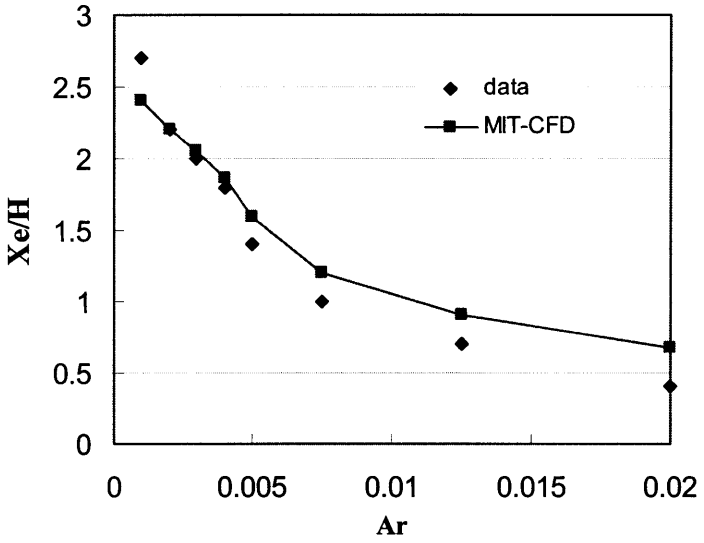

Figure 3.10. Comparison of the penetration length vs. Archimedes number for the room with mixed convection.

Figure 3.9 shows the computed airflow patterns simulated by MIT-CFD program and another MIT simplified flow (Chen and Xu, 1998). The zero-equation model was used in both cases. The two programs produce similar flow patterns with strong forced convection activities on the leftside of the room. Since the MIT simplified flow program has been validated in previous studies, this agreement leads to the conclusion that the MIT-CFD with zero-equation model can produce reasonable results under forced convection condition.

It is found that the airflow pattern is very sensitive to Ar. The computed and experimentally measured penetration depths, X_e, vs. different Ar numbers are displayed in Figure 3.10, where X_e is the horizontal distance of air movement along the ceiling before it falls to the floor. In a low range of Ar, the computed penetration depths are nearly the same as those measured experimentally. This suggests that MIT-CFD program has better performance when forced convection is dominant.

3.6.4 Duct-in-series

This case comprises the airflow through three horizontal parallel-plate ducts connected in series, as illustrated in Figure 3.11. The purpose for studying this case is to check the validity of CFD when it is coupled into the CONTAM. Here we verify the CFD

simulation results by comparing with analytical solution. In the next chapter, the effect of using the coupled program for this particular case will be examined further.

This duct-in-series comprises two 1m ducts and a 3m duct in between (Figure 3.11). Since there is no analytical solution for turbulent flow in such an internal flow, only the laminar situation is evaluated. A uniform stream velocity is exerted at the inlet. The channel therefore has a developing region before the flow is fully developed. Schlichting (1979) proposed an approximate solution for such a flow, which is considered to be the most accurate one so far. Therefore, the results from MIT-CFD are compared to this approximate analytical solution.

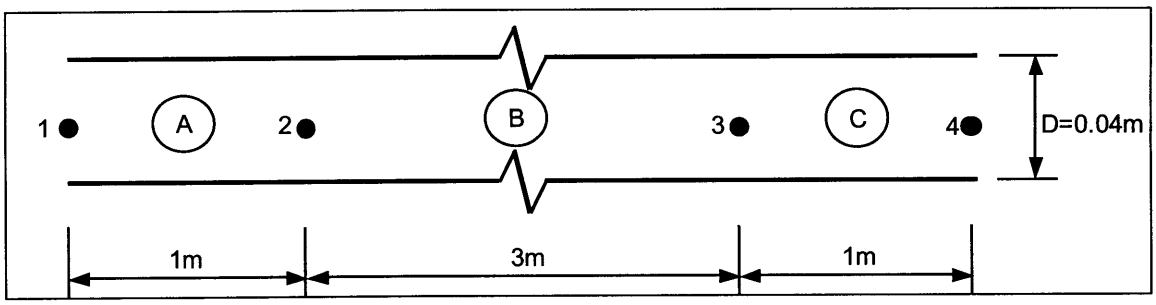

Figure 3.11. Schematics of the three horizontal parallel-plate ducts in series.

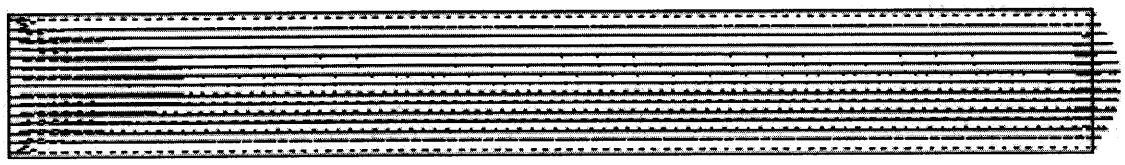

Figure 3.12. Airflow along the 5m-duct.

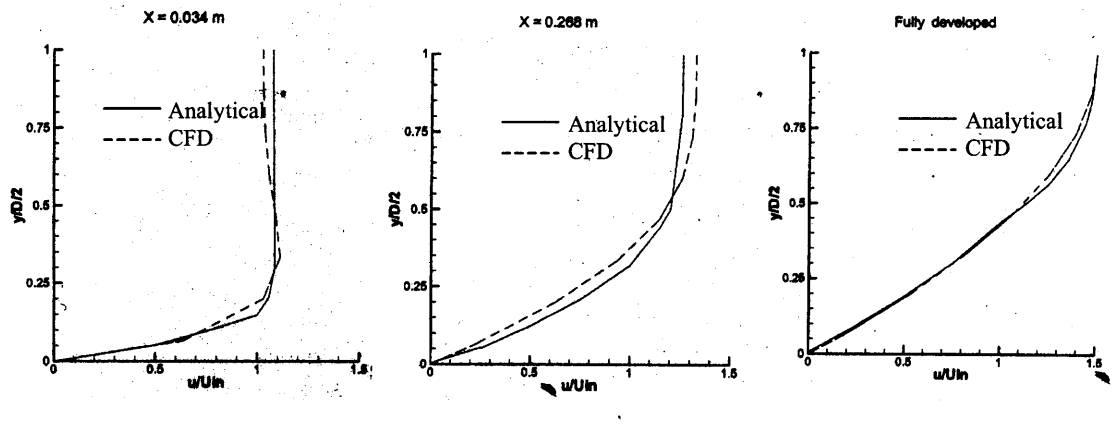

Figure 3.13. Comparison of computational results and analytical results of the duct.

Figure 3.12 shows the airflow pattern along the duct. There is a flow-developing region near the inlet before the flow is fully developed. The CFD results and the analytical results from Schlichting (1979) are compared in Figure 3.13 in terms of normalized width vs. normalized velocity. In fully developed region (which occupies the majority of the duct), the CFD results agree very well with the analytical results (rightmost panel in Figure 3.9). In developing region, reasonable agreements are also evident, although certain disparities between the two set of results are detectable. In general, CFD can provide good results in this particular case, which can be taken as a benchmark case for the future investigation.

3.6.5 A 90-degree Planar Branch Case

The study of indoor environment requires the simulation of airflow in and around buildings. Indoor airflow analysis using CFD normally requires specifying velocities on the openings of the flow domain as boundary conditions. However, in many indoor environment designs, such as natural ventilation designs, the velocities from the open windows and doors are difficult to obtain; instead, the pressure values at those openings are known (Kelkar and Choudhury 2000).

Hence, the MIT-CFD program has been modified to allow either total pressure or static pressure to be specified at the openings as pressure boundary conditions. The static pressure boundary has been verified by comparing the results with numerical data published by Kelkar and Choudhury (2000) and Hayes, et al. (1989).

In order to verify whether MIT-CFD can predict correctly the flow in an enclosure with pressure boundary conditions, the same case of a 90-degree planar branch discussed in section 2.3.3 is investigated. The geometry of the branch is illustrated in Figure 2.20. A uniform grid system with 90×60 control volumes is used for the computation. The main branch and the side branch are of the same width, W.

For simplicity, air is assumed to enter the main branch with a laminar, uniform velocity profile. Although this may induce errors since the flow is not fully developed, the computational results show reasonable agreement with the other two sets of the results published by Kelkar and Choudhury 2000 and Hayes, et al. 1989. Equal static pressures, which are the zero relative pressures, are maintained at the exits of the main and side branches. Based on these conditions, the air splits between the main and side exit branches. A range of Reynolds numbers from 10 to 400 ($Re=WU_c/\nu$, where U_c is the inlet centerline velocity, and ν is the kinematic viscosity) are studied to evaluate the flow sensitivity.

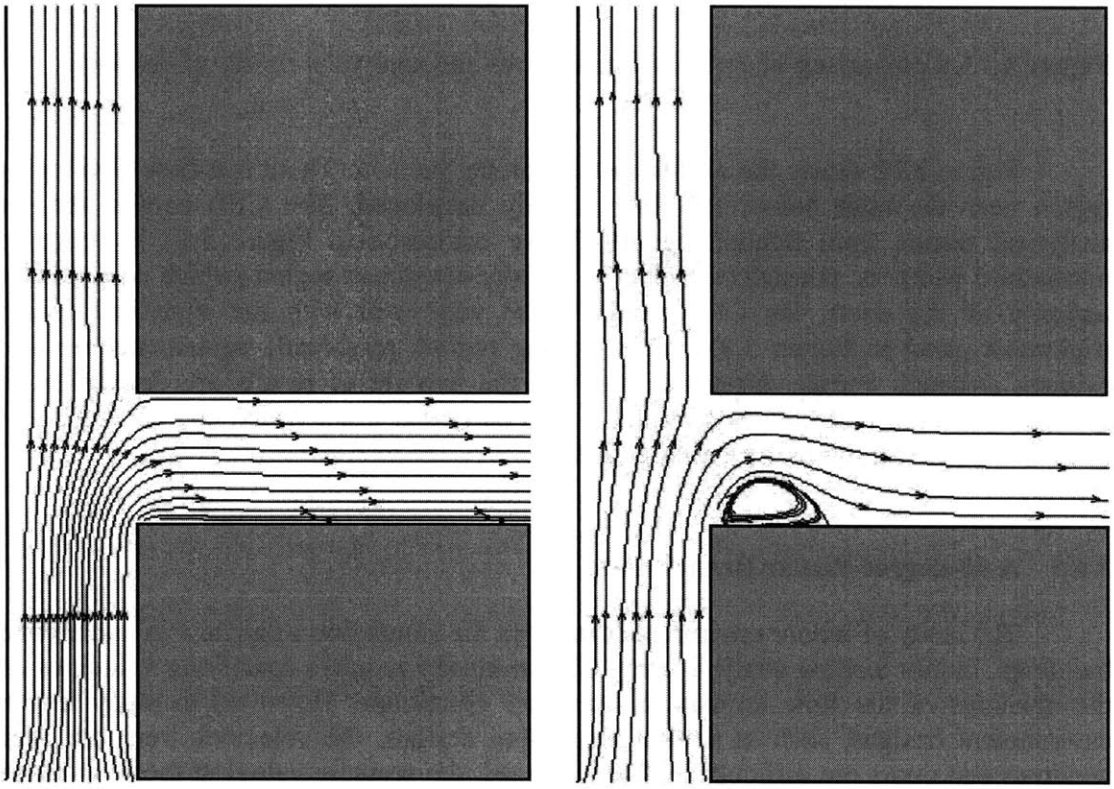

Re=10, MIT-CFD Re=300, MIT-CFD

Figure 3.14. Contours of streamline velocity pattern: (a) Re=10, (b) Re = 300.

Table 3.3. Mass flow rate at the opening under different Reynolds numbers.

Reynolds Number	Fractional Flow rate Φ	Mass Flow Rate at openings (kg/s)			Convergence Criteria	Iterations	Computation Time (s)
		Inlet	Main Outlet	Branch Outlet			
10	0.501	1.82668	0.91501	0.90066	1.0e-5	211	238.2
100	0.787	0.18188	0.14308	0.03857	1.0e-5	255	400.9
200	0.86	0.36367	0.31281	0.05434	1.0e-5	191	194.0
300	0.892	0.54428	0.48558	0.06876	1.0e-5	259	257.9
400	0.908	0.72609	0.65903	0.08572	1.0e-5	272	285.5

Figure 3.14 shows the predicted streamline velocity profile under Re=10 and Re=300. The MIT-CFD program generates similar streamlines as those presented by Kelkar et al. (2000). Flow separation from the lower wall of the side branch occurs at higher Reynolds numbers. The size and extent of flow separation are in good agreement with those of the other study. The effect of increasing Reynolds number on the flow split between the main and the side exit branches is presented in Table 3.3. Under the conditions of equal exit pressures, the fraction of mass flow in the main exit branch to the total flow rate ranges from 0.5 (equal flow split) at creeping flow rates to about 0.9 at Re=400.

When compared the current results with those of the other two studies (Figure 15), there exist similarities and differences (especially for Re=100 to 200). The differences may be largely attributed to the use of the uniform velocity profile in the present study instead of a fully developed, parabolic-shape one. In general, the pressure boundary condition used in our model generates acceptable results.

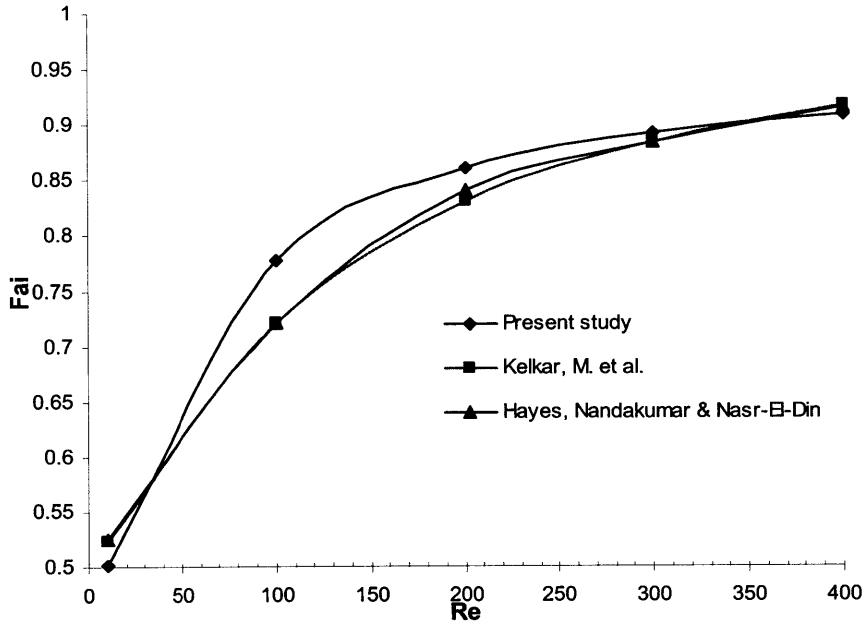

Figure 3.15. Fractional flow rate in main branch as a function of Reynolds number.

3.7 Conclusion Remarks

This chapter gives an overview of mathematical and numerical modeling used in our CFD programs, i.e. the MIT-CFD. A set of experimental cases is chosen to validate the standard k-ε model and the zero-equation model employed in this program. In general, the zero-equation model requires less grid number and computing effort, yet provides similar results as those obtained in experiments, and should be used for further studies. Although CFD requires significant computing effort, it produces informative results with acceptable accuracy. Therefore, MIT-CFD is appropriate to be coupled into the multizone model CONTAM.

CHAPTER 4

COUPLING OF CFD AND CONTAM

4.1 Introduction

The previous chapters described a multizone airflow analysis program – CONTAM and an in-house MIT-CFD program – MIT-CFD, as well as their applications for complementary building simulation. As we can see, both programs have their advantages and limitations.

The limitation of CONTAM lies in the fact of well-mixed assumption. CONTAM cannot represent localized the flow pattern within a room (zone). This makes it impossible to accurately predict flow and temperature field for the purpose of examining contaminant exposure risk and thermal comfort at the certain location inside a room. Sometimes, results from CONTAM simulation cannot well represent real situations, for example, the 90-degree planar branch case discussed in Chapter 2 reflects this limitation.

On the other hand, CFD application also has its inherited limitation because boundary conditions are unknown in many cases. In order to close the equations, user needs to make necessary assumptions on specifying boundary conditions, which pose additional errors in the CFD simulation. A way to lessen the adverse effects of ill-defined boundary conditions is to supply them through a coarse model, such as the CONTAM simulation.

CONTAM is not appropriate for large spaces in a building where CFD play an important role. Therefore, it is desirable to integrate CFD with CONTAM. This chapter mainly presents a preliminary research on the CONTAM/CFD coupling. It demonstrates several possible coupling approaches and emphasizes on the direct coupling of the CONTAM and the MIT-CFD program. The verifications and applications of the coupled program will also be introduced.

4.2 Virtual Coupling by Extracting CFD Information

To perform the CONTAM simulation, weather information, especially wind data, surround the building is required beforehand. This is because the airflow within a naturally ventilated building is essentially driven by wind pressure differences or temperature differences. Wind pressure is a function of wind speed, wind direction, building configuration, and local terrain effects. User must provide such information so that CONTAM simulation can take into account of wind pressure. Therefore how to provide wind pressure information may become a key to the successful simulation. In this section, we present an alternative method that allows CONTAM to perform simulation without pre-known wind pressure information. The method is named as "Virtual Coupling".

4.2.1 Coupling Strategy

The so-called "Virtual Coupling" in context of this thesis refers to a manmade coupling procedure between CFD simulation and CONTAM multizone simulation. Strictly speaking, it is not a real coupling. A simple solid block or hollow shell buildings (Zhai, et al. 2000) represents a complex building without considering the detailed information of inside partitions and other configurations. By accurately specifying the outdoor airflow boundary condition taking into account of windward and leeward airflow directions and magnitudes, CFD simulation can generate a pressure field. The pressure distribution on the building envelope can therefore be extracted and passed into CONTAM as its wind pressure boundary condition so that the CONTAM simulation can be forwarded.

For an unsteady problem, CFD simulates the pressure field as steady problem in time-slice history, and the pressure boundary at each time step is being extracted. The pressure distribution on the building envelope in the time-series is then passed into a special weather file that the CONTAM will take as an input file when simulating unsteady problem.

This coupling scheme involves major effort on CFD modeling side in order to provide CONTAM with steady wind pressure distribution or unsteady weather information. As mentioned earlier, when compared to the extensive labor requirement and time-consuming effort involved in experimental measurements, CFD can provide a much more economic yet viable way to obtain necessary information for the CONTAM to perform simulation.

4.2.2 Problem Definition

In virtual coupling process, there are essentially two separate problems associated with the multizone modeling and the CFD simulation. On CFD side, a simple building geometry that mimics the real building is generated. The prevailing wind information is required in order to set up CFD simulation boundary conditions.

On CONTAM side, the openings in the building are specified during the building configuration. These openings on the building envelope will receive the information calculated by CFD, and the CONTAM simulation can then be forwarded.

This is essentially a one-way interaction coupling since only CFD results can affect the CONTAM simulation in order to improve the CONTAM representation of airflow pattern and ventilation rates.

4.2.3 Case Study—Natural Ventilation for a Shanghai Residential Complex

This study uses a site plan in Shanghai, China to evaluate the CONTAM performance when applying virtual coupling. The evaluated apartment complex, which is

36m in height and consists of 12 stories and 48 apartments, is a part of the developing site that includes many different buildings as shown in Figure 4.1.

The study was first carried out to evaluate decoupled integration methods using CFD to predict indoor airflow pattern with the consideration of the impact of outdoor airflow. Based on the weather data of Shanghai, all the models assume an average wind speed of 3 m/s (at 10m above the ground) that originates from the southeast. To model the wind profile below 10m, an exponential function V=3 m/s × (Height/10 m)$^{0.25}$ is used which incorporates the ground roughness in the boundary layer.

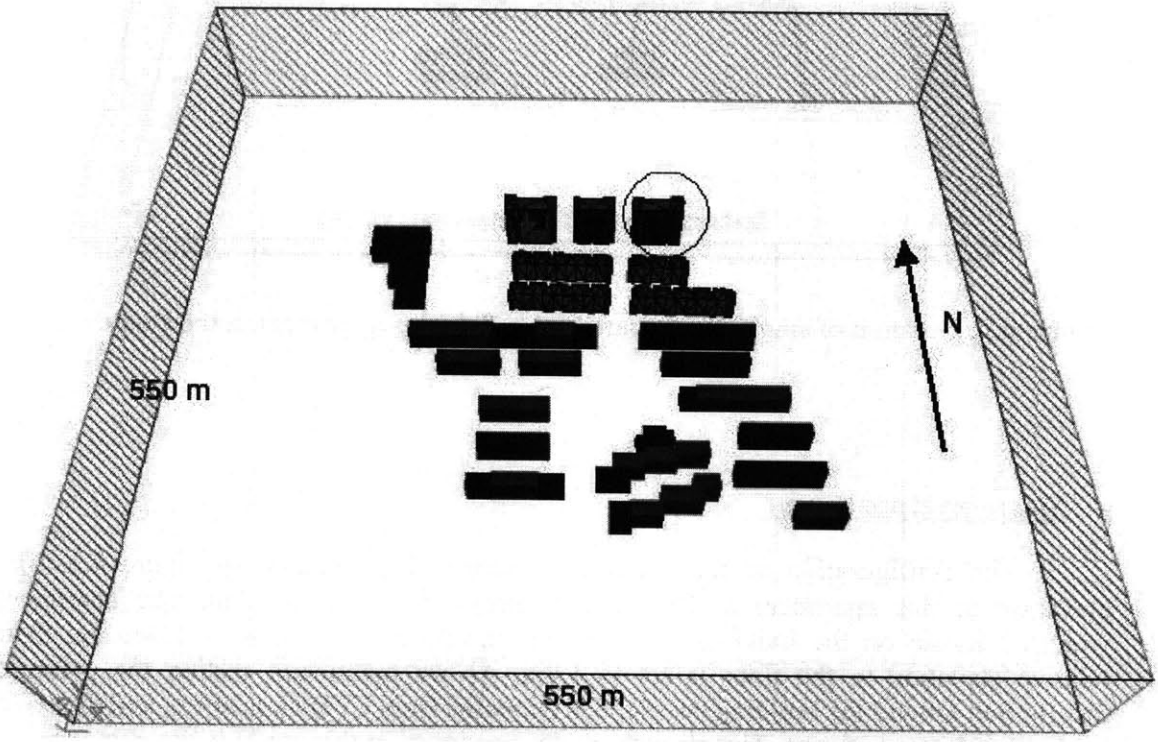

Figure 4.1. Site plan in Shanghai, China; the apartment building studied is circled.

The outdoor flow simulation provides the pressure distribution at the open windows around the building for indoor airflow simulations. Zhai, et al. (2000), conducted CFD simulations for both outdoor and indoor airflow. By performing the outdoor airflow simulations, the averaged relative pressures on each building face were obtained. The task building can be represented in CFD as a solid block or a hollow block that indicates the window locations. The original study compared the pressure distribution obtained from these two different ways. For the present study, the values obtained from the hollow model are used as climate information for CONTAM. Figure 4.2 shows the location of the single-level apartment and the duplex apartment that will be considered in this study.

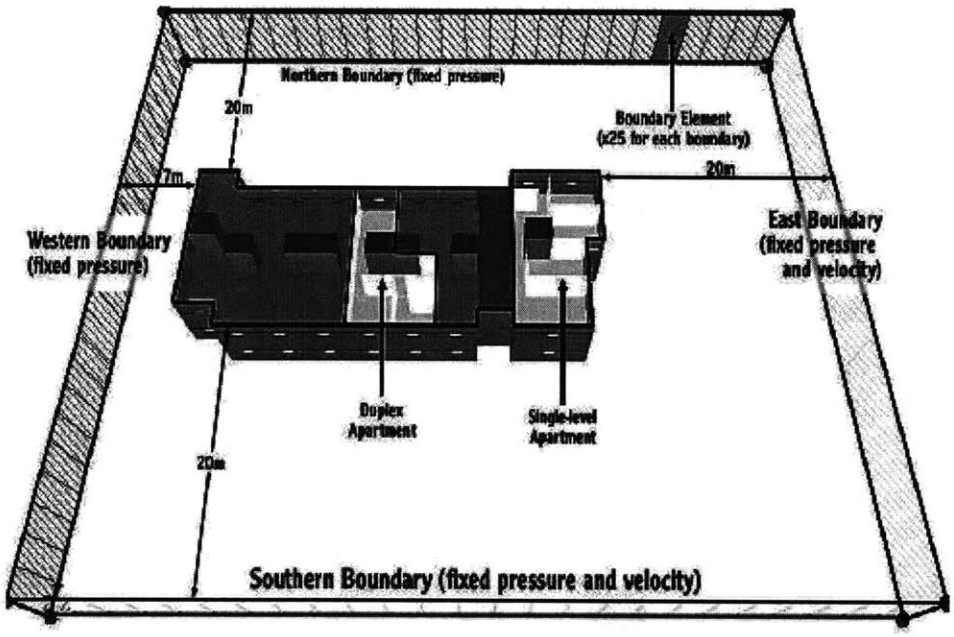

Figure 4.2. Location of single-level apartment and duplex apartment in the study.

- **Single-level apartment**

The configuration of the single-level apartment is shown in Figure 4.3. The elevation of this apartment is 18m and its height is equal to 2.8m. The apartment windows locate on the building envelope are assumed to be 0.5m × 1.0m and their relative elevation to the floor is set to 1.0m. As we mentioned earlier, the pressure distribution around the building envelope is extracted from CFD simulation, and the wind is blowing from southeast. The air path model employed in this study is the one-opening model for a two-way large opening, since all the windows and doors are assumed to be open. Table 4.1 lists the wind pressure across each window derived from CFD.

The airflow pattern in the single-level apartment simulated by CONTAM is shown in Figure 4.4. The result from CFD simulation is also given for comparison. As we can see, CONTAM generates similar general airflow pattern as CFD, except for the room in the upper-right corner where window 6 is located (shown in the circled area in Figure 4.4). The CFD simulation shows that at the window 6, air is flowing from outside (i.e. environment) into the room, whereas the airflow direction is opposite in CONTAM based on the pressure distribution from the CFD simulation of the outdoor airflow field.

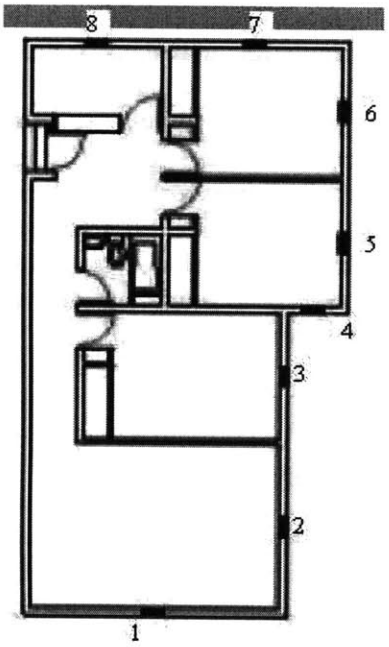

Figure 4.3. Single-level apartment.

Table 4.1. Pressure distribution at each window opening.

Window #	Pressure from CFD (Pa)
1	7.43
2	7.055
3	7.215
4	7.215
5	3.769
6	1.983
7	0.008
8	-6.5

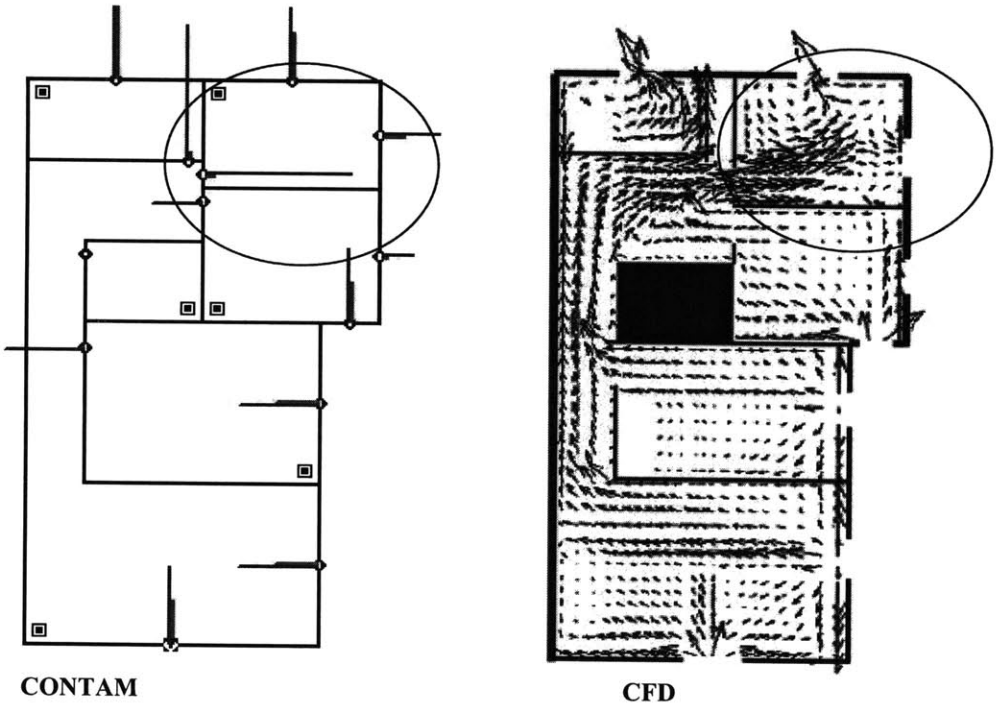

Figure 4.4. Airflow pattern simulated by CONTAM and CFD. Circled room indicates the location where the two simulations are different (see context).

To evaluate the ventilation effectiveness, the air change rate (ACH) of this single-level apartment is computed in the following ways: CFD simulation with heat source; isothermal CFD simulation (i.e. without heat source); CFD simulation considering the impact of outdoor wind; CONTAM simulation using averaged room temperature from CFD results. The comparison of the air change rates resulted from these four different calculations is exhibited in Table 4.2. The air change rate calculated from CONTAM (32.65 ACH) is close to that obtained from CFD simulation (31.84 ACH) without heat sources. This is expected since CONTAM does not include energy balance equation. This again confirms the applicability of CONTAM multizone airflow models as that of CFD in analyzing building airflow, when heat sources are not in consideration.

Table 4.2. Comparison of the air change rates computed from CONTAM and CFD for single-level apartment.

	CFD solving T/Q	CFD w/o solving T/Q	Compact integration	CONTAM using Avg. T from CFD results
Single-level apartment	36.26 ACH	31.84 ACH	36 ACH	32.65 ACH

- **Duplex apartment**

The duplex apartment is located at the same level of the single-floor apartment, which is built in the middle of the building. The layout of this duplex apartment is shown in Figure 4.5. The relative wind pressure (0 Pa for environment as reference) on the north wall is –0.6356 Pa, and the wind pressure on the south wall is 5.882 Pa. The wind is 135° (i.e. coming from South-east relative to North). The windows have the size of 0.5m × 1.0m and are located 1.0m above the floor. However, the kitchen window is located 2.3 m high relative to the floor.

The airflow patterns of this apartment simulated by CONTAM and CFD are displayed in Figure 4.6. At the lower level, CONTAM provides similar airflow pattern as that of CFD. The air change rate predicted from CONTAM is 15 ACH, compared to 18 ACH obtained from CFD simulation (Table 4.3). The difference is about 16.7%, which is fallen into acceptable difference range.

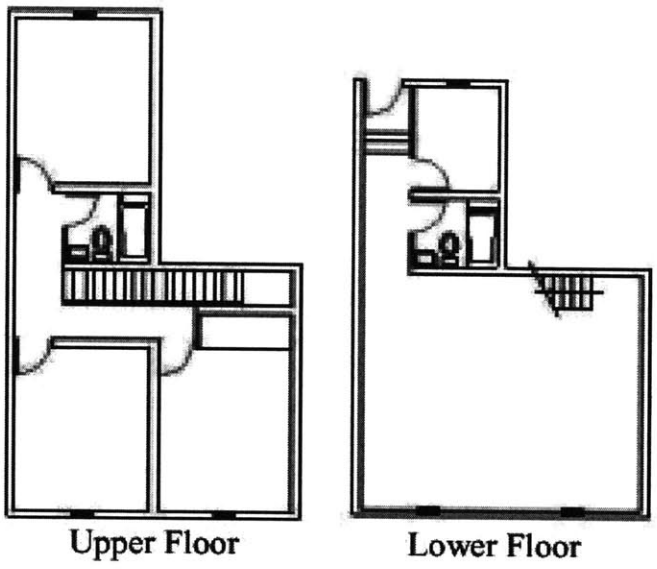

Figure 4.5. The layout of the duplex apartment in Shanghai building complex.

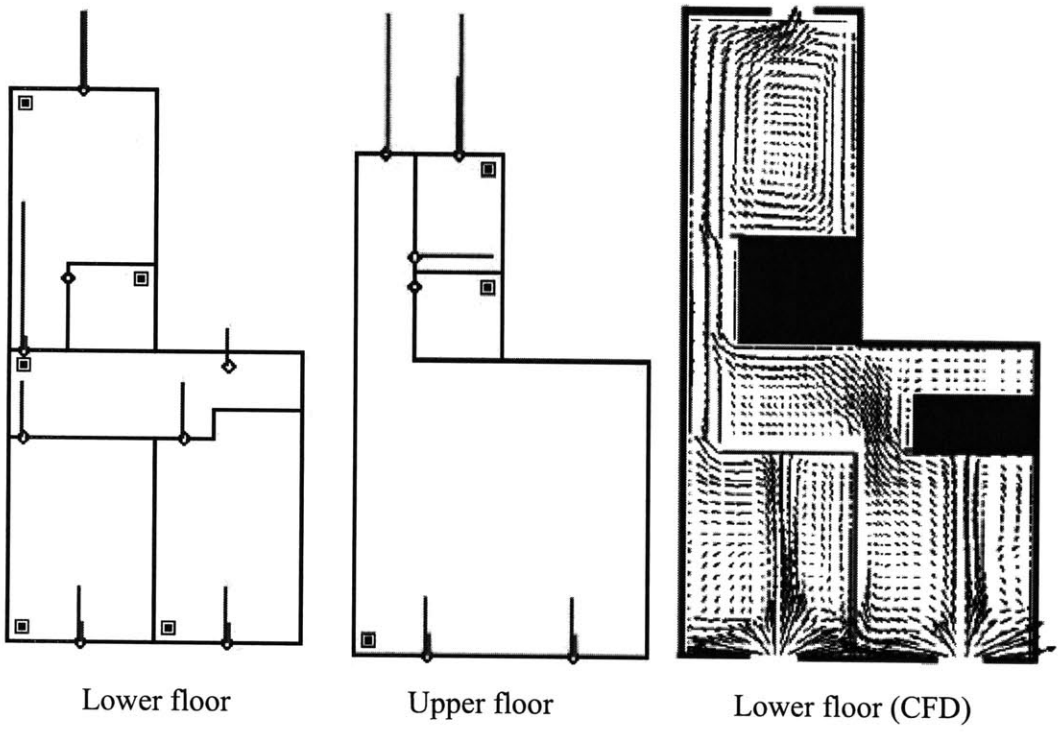

Figure 4.6. The general airflow pattern predicted by CONTAM and CFD.

Table 4.3. Comparison of the air change rates computed from CONTAM and CFD for duplex apartment.

	CFD Compact integration	CONTAM using Avg. T from CFD results
Duplex apartment	18 ACH	15 ACH

Although experimental measurement can provide the most reliable data for simulation, it is usually very expensive in terms of labor and time costs. Apparently, CFD is a viable alternative to experiment. By assuming the most typical wind profile from windward direction, CFD computes the pressure field around the building. The pressure distribution can then be extracted as the climate boundary condition for multizone airflow analysis. In summary, the case studies on Shanghai complex have shown that the virtual coupling of the CONTAM and CFD programs, i.e., the pressure boundary conditions needed by CONTAM are provided by a pre-run CFD model, can produce similar simulation results from CONTAM as compared to those from CFD at a much low cost in terms of computational resource.

4.3 Quasi-dynamic Coupling of CFD into CONTAM

As we discussed in Chapter 2, the 90-degree planar blanch case simulated by CONTAM in Section 2.3.3 indicated that CONTAM is prone to give erroneous results by overlooking the obstacles in the room, such as furniture and occupants. In such cases, CFD provide more reliable information of the airflow field and the air partition through exits. Under such circumstances, one would expect that the CFD results, when being passed directly to CONTAM to update values at the airflow paths, might influence the airflow pattern simulated by CONTAM. This will yield more accuracy. This method is named "Quasi-dynamic Coupling".

4.3.1 Coupling Strategy

Negrao (1995) did a research on the conflation of CFD with a building thermal and mass flow simulation program named ESP-r. As complementary to the thermal coupling, he also discussed the momentum coupling that combines the mass flow equations with CFD momentum equations at inlet and outlet openings. The idea is that the airflow within the zones influences the flow in other parts of the building and vice versa. He pointed out that the common variables at the interface between CFD computational domain and the whole building simulation domain are the mass flow rates and the pressures at the inlet or outlet openings.

In his approach, the mass flow network system and the CFD system are solved separately so that the mass flow network must be decoupled from the CFD domain in

order to be solved. In light of the fundamentals of the ESP-r transient mass flow network and CFD, he treated the airflow entering or leaving the zone where CFD domain was located as sources or sinks of mass obtained from CFD solution, and then used these as known values to solve the remaining flow rates in the mass flow network. The illustration of this approach can be sketched in Figure 4.7 (Negrao, 1995). As shown in Figure 4.7a, a CFD domain replaces the kitchen with equipment. The previous two connections between the lounge and kitchen, and the kitchen and duct system are now substituted by three connections representing the links between the two domains. The nodes A, B and C represent the effect of the CFD cells on the network. As each system solution is performed separately, the mass flow network must be decoupled from the CFD domain. Figure 4.7b shows how the network of Figure 4.7a is detached from the CFD mesh. The vectors at the boundary of the CFD cells connected to the decoupled network represent the airflow entering or leaving the zone, which can be understood as sources and sinks of mass at the A, B and C for mass flow network, as illustrated in Figure 4.7c.

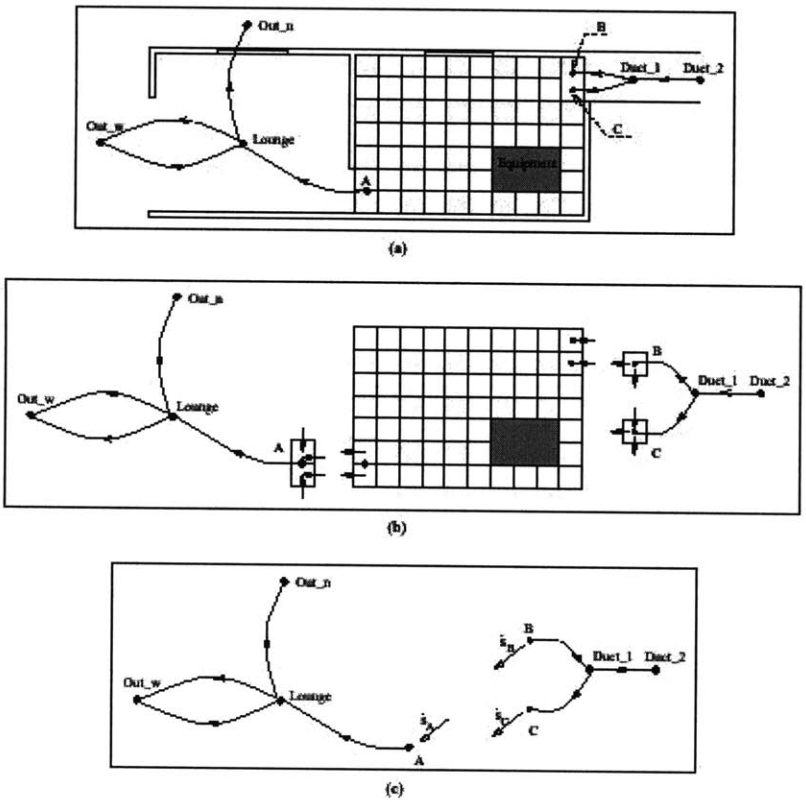

Figure 4.7. Decouple a mass flow network from a CFD domain as presented in Negrao (1995).

However, sources and sinks are not considered in CONTAM, and the flows are evaluated by assuming quasi-steady conditions, i.e. $dm_i/dt = 0$ where m_i is the mass of air in zone i. This leads to:

$$\sum_j F_{j,i} = 0 \tag{4.1}$$

This addresses the need of a different approach for the coupling of CFD with CONTAM.

Quasi-dynamic coupling requires a matching of the mass flow equations of CONTAM with the CFD momentum equations at the inlet and outlet openings. This is achieved by the following: the CFD domain substitutes the zone air node of CONTAM that requires CFD modeling, and the CFD cells at the openings are linked to other zone air nodes in CONTAM domain. A two-way interaction exists between CONTAM and CFD in which the CONTAM supplies the initial boundary conditions for CFD, and the CFD results are fed back into CONTAM so that the CONTAM results for that particular zone are equal to the CFD results. However, there is no mutual influence between CONTAM and CFD once the quasi-dynamic coupling is finished. The coupling process involves two runs for CONTAM (i.e., one run for the initial boundary conditions that are supplied to CFD, and one run for the final results once CFD results are fed back) and one run for CFD. The common variables at the interface between these two domains are mass flow rates and pressures at the inlet or outlet openings. Detailed solution methods are described in the next subsection.

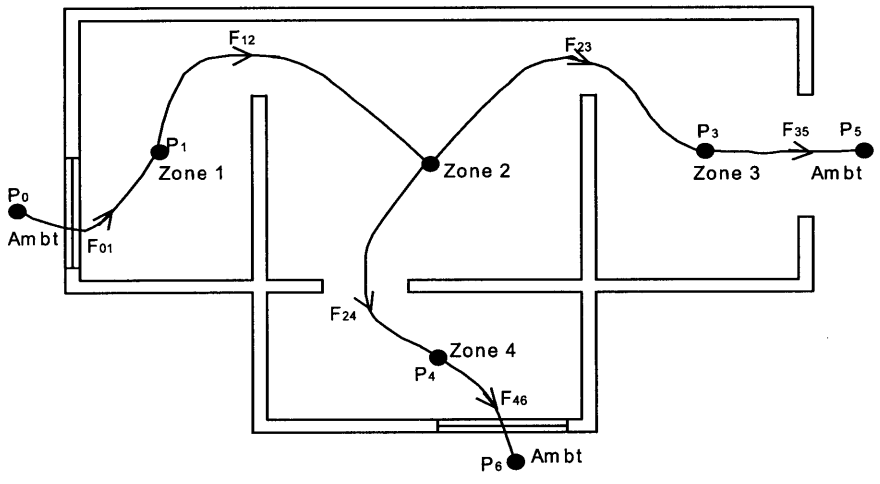

(a)

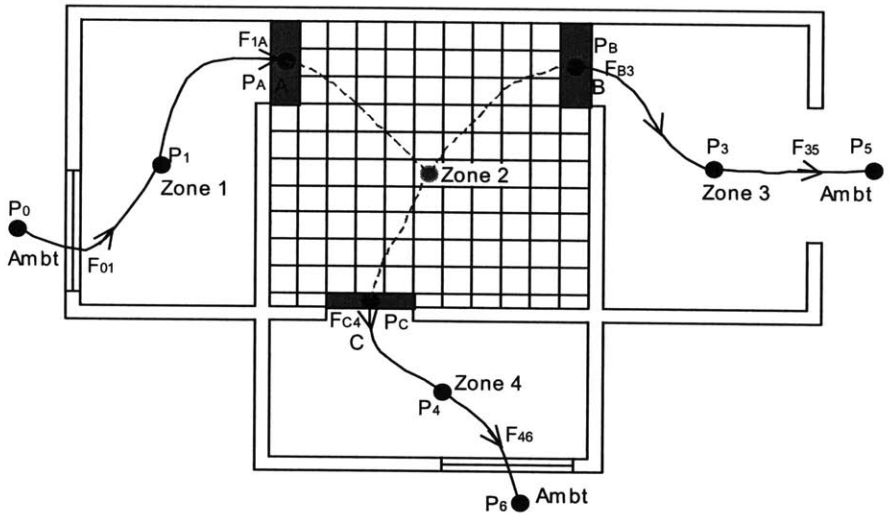

(b)

Figure 4.8. Illustration of the coupling between CFD and CONTAM. (a) network; (b) coupled domain.

4.3.2 Solution Methods

To illustrate the solution process, let us take an example shown in Figure 4.8. Figure 4.8(a) gives a four-zone apartment in CONTAM configuration. Zone 2 is replaced by CFD domain when the quasi-dynamic coupling is being applied, as shown in Figure 4.8 (b). For this particular case, the linkages for coupling are one inlet on the partition wall between zones 1 and 2; and two outlets on the partition walls between zones 2 and 3, and between zones 2 and 4, respectively.

According to the fundamentals discussed in Chapter 2, the flow rate of each airflow path, indicated by F_{ij} (i and j are the neighboring zone numbers) in Figure 4.8, can be expressed by a certain function of the pressure difference along the flow path. Since most infiltration models are based on empirical powerlaw relationship, we therefore choose Equation 2.4 ($F = C(\Delta P)^n$) in calculation.

Thus, the flow rates in Figure 4.8 (a) can be written as:

$$F_{12} = C_{12}(\Delta P)^n = C_{12}(P_1 - P_2)^n,$$

$$F_{23} = C_{23}(\Delta P)^n = C_{23}(P_2 - P_3)^n,$$

$$F_{24} = C_{24}(\Delta P)^n = C_{24}(P_2 - P_4)^n .$$

where P_j is the total pressure of zone j.

In Figure 4.8 (b), zone 2 is replaced by a CFD domain with openings A, B, and C. Since uniform total pressures are assumed in the neighboring zones of the CFD domain, it is reasonable to assume that the total pressures at the openings are just equal to the neighboring zone pressures. i.e:

$$P_A = P_1,$$

$$P_B = P_3,$$

$$P_C = P_4.$$

The solution of the CFD domain is performed assuming the boundary conditions taken from CONTAM. The boundary conditions are the mass flowing to/from the CFD domain through the openings (in this case, A, B and C in Figure 4.8b). They can be specified either through velocity or pressure, or the combination of these two.

Two specific boundary conditions are used to study the quasi-dynamic coupling:

1. Heterogeneous boundary condition: given velocity and direction at inlet A; and static pressure/normal outlet condition at the outlets B and C;

2. Pressure boundary condition: given total pressure boundary condition at both inlet A and outlets B and C.

The velocity type condition is appropriate to those inlet openings where the momentum magnitude can significantly modify the zone airflow pattern and must be known in advance. Usually the effect of the outlet momentum on the zone airflow pattern is not so significant, and therefore static pressure or normal outlet condition can be imposed. The velocities are obtained from the mass flow rates through the openings (airflow through openings A, B and C) divided by the air density and opening areas.

The pressure type boundary condition is applicable to the cases where the inlet momentum changes the flow locally but does not substantially affect the zone airflow pattern, such as a crack whose dimension is much smaller than the size of the cells. In such situation, the pressures calculated by the mass flow network at the neighboring nodes are fixed (P_A, P_B, and P_C in this case) at the CFD cells.

Figure 4.9 explains the step-by-step procedure of this solution process. Again, the four-room apartment shown in Figure 4.8 is used to illustrate this coupling process. At certain time-step (if it is unsteady problem), zone 2 is replaced by a CFD domain with momentum boundary imposed at the inlet A and static pressures at the outlets B and C. The magnitude and direction of the velocity is determined by CONTAM results, F_{12}, and

the inlet size. The static pressures imposed at the outlets are P_B and P_C, which are set to P_3 and P_4, respectively. Upon the given boundary information at the inlet and the two outlets, CFD solves the governing equations for transport variables within the computational domain (Figure 4.8b). Therefore, the new values of airflow rate through the outlets are obtained (the airflow rate at the inlet is set unchanged before and after CFD simulation). In this case, they are F_{B3} and F_{C4}, which are usually different from the values F_{23} and F_{24} calculated from CONTAM multizone model. F_{B3} and F_{C4} then replace F_{23} and F_{24} by assigning new coefficient of the powerlaw relation for the outlets B and C, which are $C_{23}^{new} = \frac{F_{B3}}{F_{23}} C_{23}$ and $C_{24}^{new} = \frac{F_{C4}}{F_{24}} C_{24}$, respectively.

If only these two coefficients are updated in CONTAM while all other flow coefficients of the air paths remain the same, the change of the airflow rate through opening B and C is insignificant compared to the original CONTAM results, which means that CONTAM will never reach the airflow values that equal to CFD results at opening B and C. In order to truly update the airflow rate to conform to the CFD results, we notice that the air paths, 35 and 46, are also influenced by the new values of F_{B3} and F_{C4}. The solution method, therefore, needs to search and identify those two air paths connecting to the ambient environment and assign the new flow coefficients for these two openings, which are correspondingly $C_{35}^{new} = \frac{F_{B3}}{F_{23}} C_{35}$ and $C_{46}^{new} = \frac{F_{C4}}{F_{24}} C_{46}$. Therefore, all the flow coefficients of the openings that relate the outlets in CFD domain are being updated for another CONTAM simulation. By redoing CONTAM simulation, a new set of values for all the airflow paths are obtained. If necessary, CONTAM can then proceed to the next step simulation.

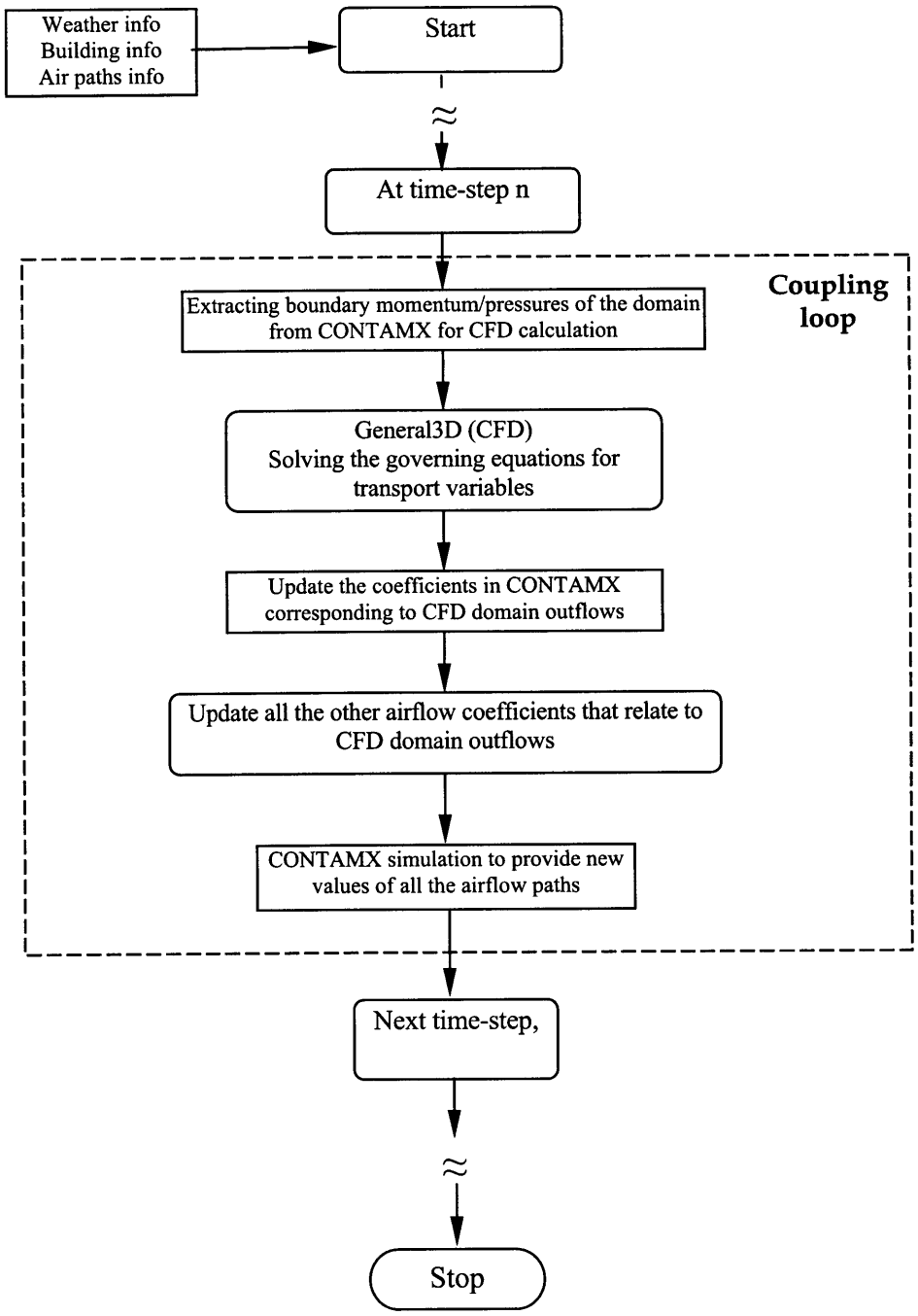

Figure 4.9. Quasi-dynamic coupling flow chart.

4.3.3 Case Studies

In the next several cases, the solution method of quasi-dynamic coupling is applied. The impact of CFD simulation in a critical space on the whole building airflow pattern is investigated.

- **Three ducts in series**

As shown in Figure 4.10, the intermediate duct (3m) B is discretized into numerous small control volumes for CFD simulation. However, the two ducts at both end, A and C, use the CONTAM mass flow network approach. The purpose of this analysis is to check the validity of the CFD system when complied to CONTAM mass flow network, and when the two approaches are considered separately. The results from sole CFD simulation have already been compared with analytical results, which have been discussed in Section 3.6.4 and shown in Figure 3.9. In this section, the whole circuit is investigated by firstly employing a CONTAM mass flow network only, and secondly, the same network but where duct B is modeled by CFD.

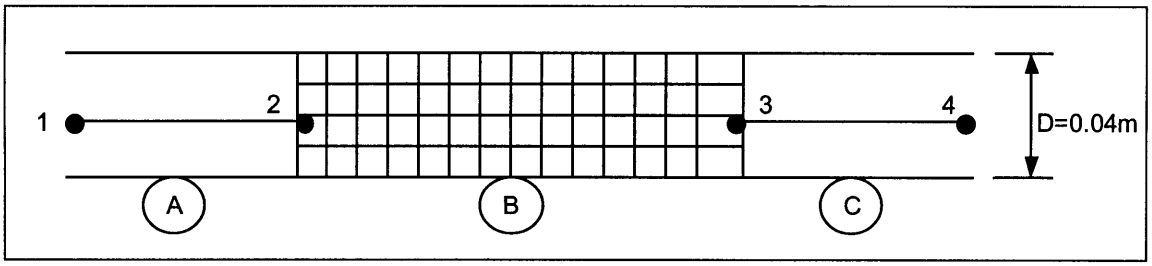

Figure 4.10. Illustration of discretized combined computation domain for 3-duct-in-series.

Given the complexity involved at the entrance region of the duct, the network method treats the airflow as fully developed. The flow is considered isothermal at a constant temperature of 20°C. The mass flow rate and the pressure drop are related by the following power law expression (re-write from Equation 2.4):

$$F = C \times \Delta P^n \tag{4.2}$$

The coefficient C and n can be derived from the analytical solution:

$$C = \frac{\rho D^3}{12\mu L}, \qquad n = 1.0 \tag{4.3}$$

There are two configuration ways to represent these three ducts in CONTAM. As illustrated in Figures 4.11, the ducts are modeled as three zones with four airflow paths at their ends. Based on the analytical solution, the flow coefficients for the air paths are: C_{01}= 10^{10} (meaning no resistance from ambient through airflow path 1), C_{12}=C_{34}=0.3536 for 1m ducts at both sides, and C_{23}=0.11787 for 3m. Compared to the multizone airflow flow network solution with the simulation results from Negrao (1995), the pressure across the air path 1 is 0.51794 Pa in CONTAM, and the pressure at the end is 0 Pa.

Figure 4.12 illustrated another way to present the three-ducts-in-series as a duct flow in CONTAM. The flow coefficients for each section of the duct are 0.3536, 0.11787 and 0.3536, respectively. The resulting pressure difference is 0.51794.

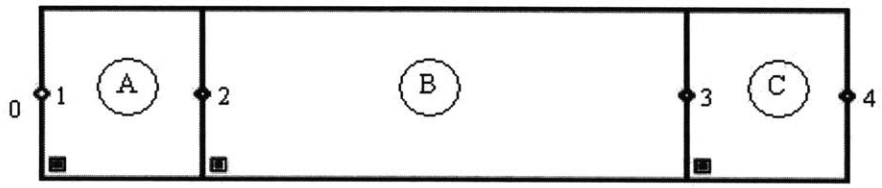

Figure 4.11. CONTAM presentation as airflow paths.

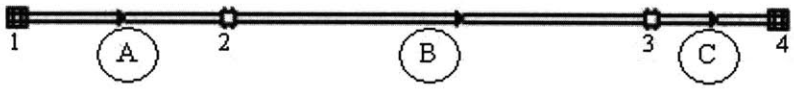

Figure 4.12. CONTAM presentation as ducts.

The mass flow rates through the ducts and the pressures at the nodes 2 and 3 are computed in CONTAM using multizone network approach. The pressure drop in each duct (air path) and the mass flow rate are presented in Table 4.4. The two different presentations of ducts result in almost the same results on pressure drop, which is also very close to the results of ESP-r dps from Negrao (1995). Note the difference in mass flow rate simulated by CONTAM and that by ESP-r is mainly due to the difference in default air density. The difference between these values and the analytical solution are insignificant, because the mass flow equations 4.1 and 4.2 are derived directly from the analytical solution.

Table 4.4. CONTAM mass flow network results compared to ESP-r dps results.

	Mass flow rate (kg/s)	$\Delta p_{1\text{-}2}$ (Pa)	$\Delta p_{2\text{-}3}$ (Pa)	$\Delta p_{3\text{-}4}$ (Pa)
Air Paths	0.036629	0.10359	0.31076	0.10359
Ducts	0.036628	0.10359	0.31075	0.10359
Esp-r dps	0.035643	0.10359	0.31076	0.10359

Next, we coupled the CFD into CONTAM by solving the intermediate duct B using CFD while keeping ducts A and C simulated by the multizone model. According to the airflow rate at the inlet, the uniform velocity of 0.75m/s (corresponding to 0.036629 kg/s) is imposed at the inlet of duct B, and the outflow boundary for fully developed flow is exerted at the outlet. In the combined program, CFD analysis changes the pressure drop in duct B. Different flow models are utilized in this investigation to identify their impact on the final results. The resultant pressure drops along the three ducts are listed in Table 4.5. The results from Negrao (1995) are also listed for comparison.

Table 4.5. Results from the combined approach using different models in CFD-side.

Model	Mass flow rate (kg/s)	$\Delta p_{1\text{-}2}$ (Pa)	$\Delta p_{2\text{-}3}$ (Pa)	$\Delta p_{3\text{-}4}$ (Pa)
No turbulence	0.036629	0.10359	5.36463	0.10359
0-eqn model	0.036628	0.10359	0.06921	0.10359
Standard K-ε	0.036628	0.10359	0.05683	0.10359
Constant Viscosity	0.036628	0.10359	0.89308	0.10359
Esp-r combined approach	0.035836	0.10415	0.84171	0.10415

As can be seen from Table 4.5, different CFD models can result in significant differences in terms of the pressure drop across duct B. If no-turbulence model is employed, the pressure drop along the duct B is much larger than those using turbulence modeling. These complementary results raise the importance for the user in choosing suitable CFD turbulent models for a particular airflow problem.

- **90 degree planar branch case**

This case has been discussed in both Chapter 2 and Chapter 3. We learned that the airflow was split in equal half if a multizone airflow model is used. However, in CFD simulation different Reynolds number employed may result in different airflow split ratio. Only when the Reynolds number is small (between 0 and 10), the airflow partition is nearly half. The higher Reynolds number is in the duct, the more airflow exits through the main outlet. This phenomenon can only be identified by numerical approach, such as

CFD simulation. Therefore, the coupling of CONTAM with CFD is necessary in terms of providing reliable airflow information in such a duct branch.

Figure 4.13 illustrates this 90-degree branch using coupled method. The pressure boundary information is provided in CONTAM. Firstly, by performing CONTAM simulation, the airflow through the main inlet A, the main outlet B, and the branch outlet C is determined, respectively, with half of the total inflow flowing out of both outlet B and C. The pressure imposed at the inlet A (or the airflow through the inlet A) and the pressure at the outlets B and C are used as the boundary condition for the CFD simulation, and the CFD results are then fed back to the CONTAM multizone program using quasi-dynamic method. The new results from the coupled program will be in consistent with the results obtained from CFD-only approach.

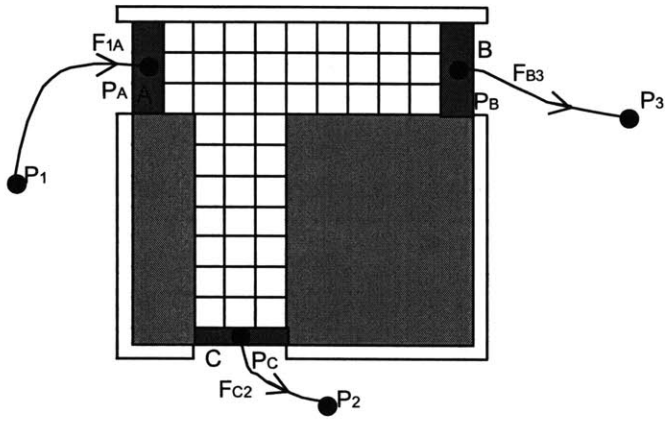

Figure 4.13. Illustration of a 90 degree branch using coupled method.

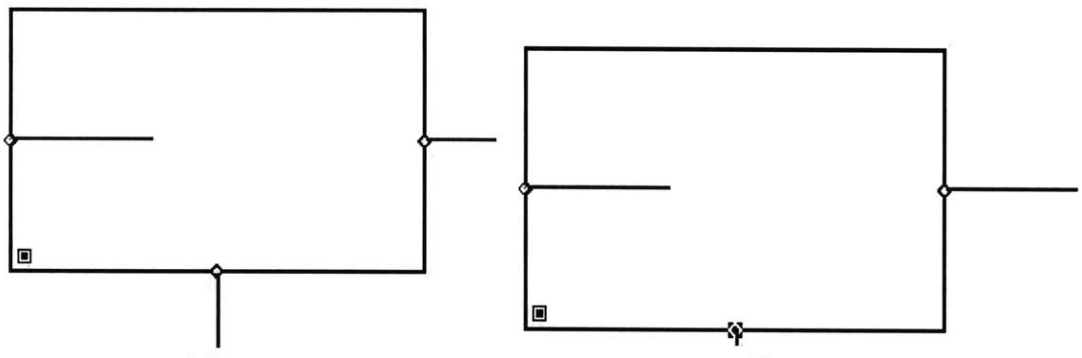

Figure 4.14. 90-degree planar branch case: (a) Airflow pattern before coupling; (b) Airflow pattern after coupling.

Figure 4.14 shows the CONTAM representation of the airflow pattern along the 90-degree planar branch before (Figure 4.14a) and after coupling (Figure 4.14b). Constant mass flow rate, 0.05918 kg/L, is imposed at the air path 1A, and the initial flow coefficient for the air path B2 and C3 is 2.0 kg/L·(Pa)^n, respectively. The CFD side of the coupled program results in different airflow ratio in the two outlets, and the new flow coefficient of the two outlets is therefore computed and passed into CONTAM side of the coupled program. The flow rates of the three openings before and after coupling are listed in Table 4.6 and also presented graphically in Figure 4.15. There is a significant improvement for CONTAM simulation when quasi-dynamic coupling is used. There is no change for the inflow rate since it is fixed during the coupling. However, a significant increase (~72%) for the outflow rate through main exit, and the same significant decrease for the outflow at the other exit, is evident. Also note that the pressure differences are kept unchanged before and after coupling. In brief, the quasi-dynamic coupling adopted here can significantly improve the CONTAM simulation that otherwise cannot be achieved.

Table 4.6. Results of a 90-degree planar branch from by quasi-dynamic coupling.

Airflow Path	Flow rate before coupling (kg/L)	Flow rate after coupling (kg/L)	Original Coefficient kg/L·(Pa)^n	New Coefficient kg/L·(Pa)^n	Pressure difference before (Pa)	Pressure difference after (Pa)
1A	0.005918	0.005918	N/A	N/A	0.000035	0.000035
B2	0.002959	0.005096	2.0	2.582328	0.000004	0.000004
C3	0.002959	0.000822	2.0	0.208337	0.000016	0.000016

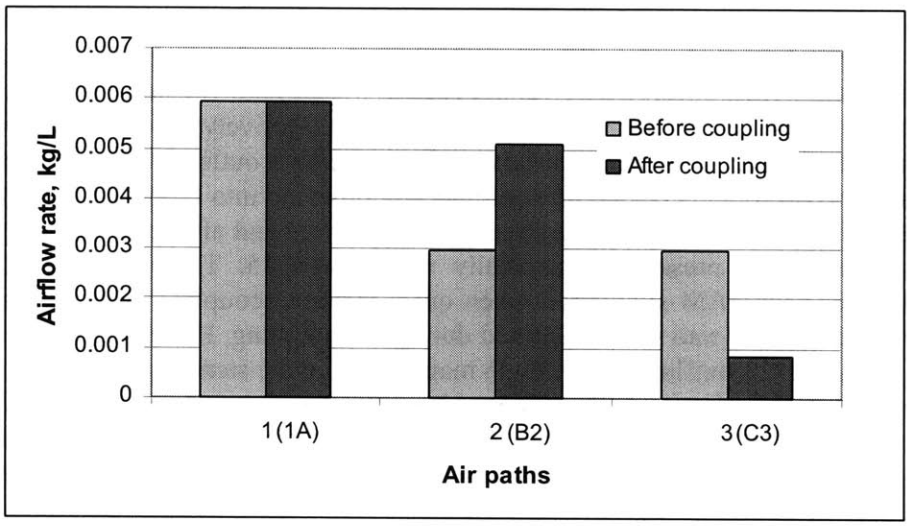

Figure 4.15. Airflow rate through each opening in 90-degree planar branch before and after quasi-dynamic coupling.

- **Modified 90 degree planar branch case 1 (4 zones)**

In order to further explore the solution method of the quasi-dynamic coupling, it is necessary to examine a more complicated case. Based on the above 90-degree planar branch case, a modified case that comprises this branch and three other neighboring zones is set up. As shown in Figure 4.16, there are four rooms with each representing a single zone. The upper middle room (zone 2) has the configuration that is similar to the 90-degree planar branch and is required for detailed flow analysis. Therefore, it is replaced by a CFD domain as illustrated in Figure 4.16. Zone 1 connects with zone 2 through opening A. Opening B connects zone 2 and zone 3, and Opening C connects zone 2 and zone 4. Zone 1, zone 2 and zone 3 each has one opening that connects to the ambient surroundings, respectively. Initially, the opening 01 has wind pressure of 0.36 Pa and a flow coefficient of 0.01 kg/L·$(Pa)^n$. The opening 35 has 0 Pa wind pressure and a flow coefficient of 0.02 kg/L·$(Pa)^n$, while the opening 46 has 0 Pa wind pressure and a flow coefficient of 0.04 kg/L·$(Pa)^n$. The flow coefficient for the openings A, B and C are set to be the same, which is 1 kg/L·$(Pa)^n$. In addition, the flow exponential rate for all the air paths is designed to have the same value 0.5.

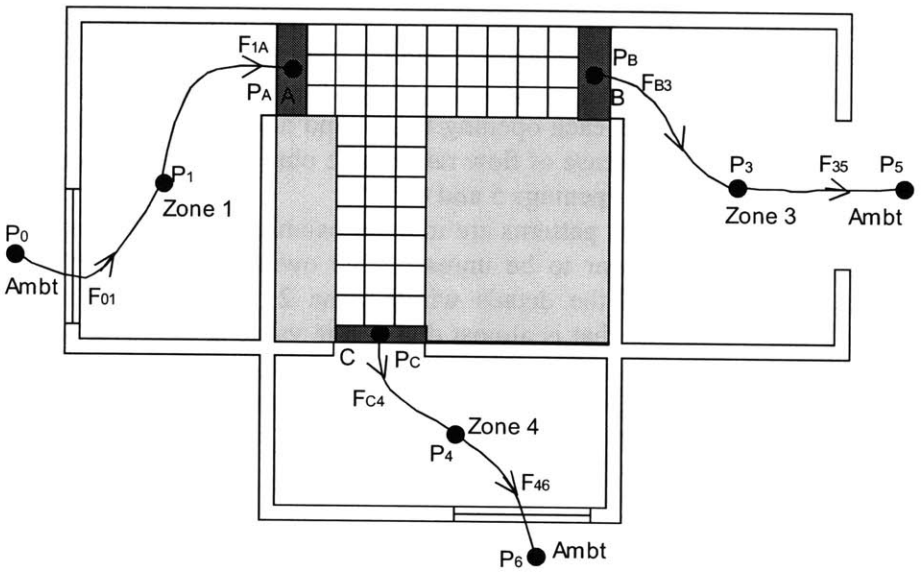

Figure 4.16. 4-zone configuration modified from 90-degree planar branch case.

The impact of using the coupled program on airflow inside the building is visually presented in CONTAMW sketchpad, where 4.17a represents the airflow pattern before coupling and 4.17b refers to the airflow pattern after coupling. As can be seen, the airflow split at the outlets of the upper middle room changes significantly, which also influences the airflow in the adjacent rooms.

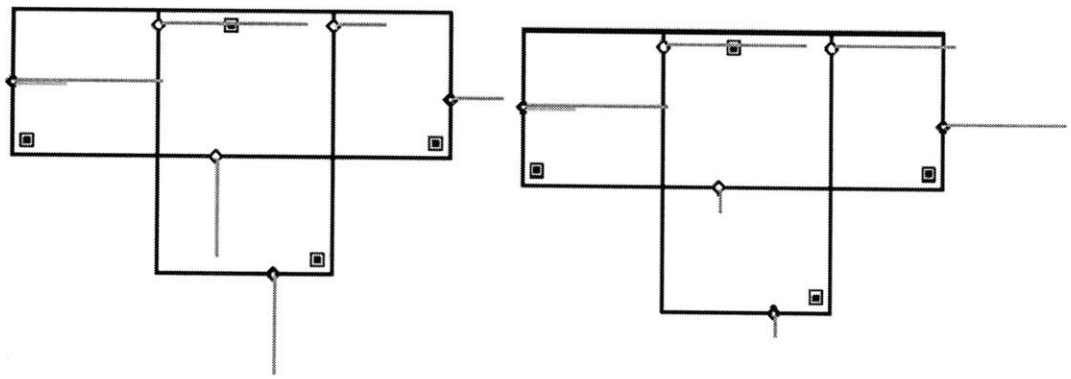

(a) (b)

Figure 4.17. Modified 90-degree planar branch case 1 (4 zones): (a) Airflow pattern before coupling; (b) Airflow pattern after coupling.

The detailed results computed by CONTAM only and by the coupled program are displayed in Table 4.7. Although the pressure difference across each opening does not change before and after coupling, new coefficient in the powerlaw relation for each opening has been derived based on the CFD simulation results. Thereafter, a new value of airflow through each opening is obtained by CONTAM multizone airflow network model. The change of the airflow through each opening before and after coupling is also listed in Figure 4.18, where a 158.3% increase of flow rate can be observed at openings 2 and 4, and a 79.2% decrease is evident at openings 5 and 6.

Before coupling, although the flow patterns are in mass balance, the flow rates at the four above-mentioned openings appear to be unreasonable owing to the fact that CONTAM cannot take into account of the details within zone 2. For example, the secondary exit opening 5 has a flow rate that is almost double the value at the main exit opening 2, which also leads to erroneous airflow through downstream rooms at openings 3 and 6. However, the coupled program produces a much consistent and improved result that reflects the contributions from CFD.

Table 4.7. Results of the modified 90-degree planar branch case 1 (4 zones) by quasi-dynamic coupling.

	Airflow Path	Flow rate before coupling (kg/L)	Flow rate after coupling (kg/L)	Original Coefficient kg/L·(Pa)^n	New Coefficient kg/L·(Pa)^n	Pressure difference before (Pa)	Pressure difference after (Pa)
1	1A	0.005918	0.005918	1.0	1.0	0.000035	0.000035
2	B3	0.001973	0.005096	1.0	2.582328	0.000004	0.000004
3	01	0.005918	0.005918	0.01	0.01	0.350225	0.350225
4	35	0.001973	0.005096	0.02	0.051647	0.009736	0.009736
5	C4	0.003945	0.000822	1.0	0.208337	0.000016	0.000016
6	46	0.003945	0.000822	0.04	0.008333	0.009725	0.009725

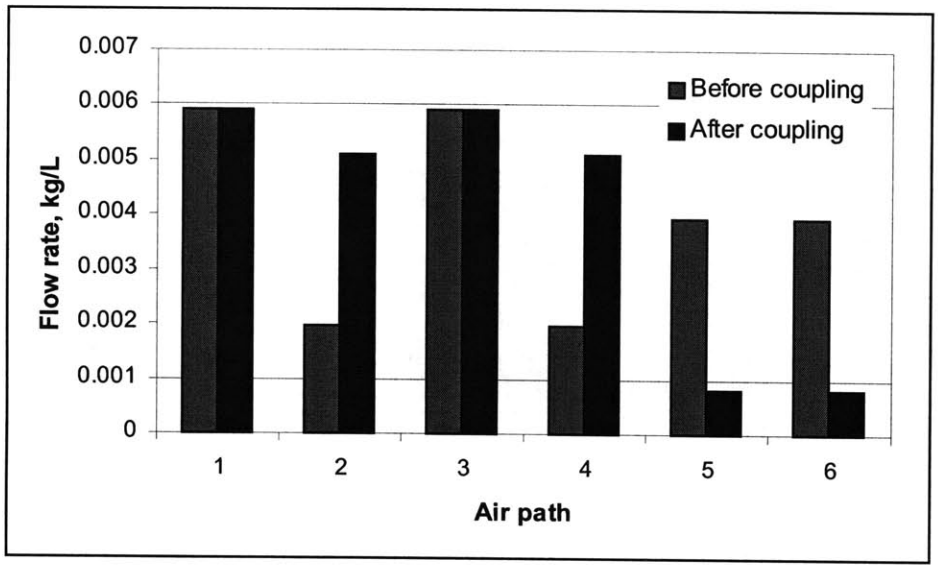

Figure 4.18. Airflow rate through each opening in modified 90-degree planar branch case 1 (4 zones) before and after quasi-dynamic coupling.

- **Modified 90 degree planar branch case 2 (6 zones)**

When the 90-degree planar branch case is further extended by adding more complexity (i.e., adding one room to connect rooms 3 and 4, and adding another room in adjacent to rooms 3 and 6), such as the building configuration shown in Figure 4.19, a convention for the search algorithm must be developed. Taking this 6-zone building as our example, it would be easy for the search engine to find out that the outflow F_{36} is influenced by the inflow F_{B3}, and the outflow F_{46} is influenced by the inflow F_{C4}. However, the outflow F_{67} is influenced by both the inflows F_{36} and F_{46}. Ideally, the search algorithm should automatically judge and chose the one that has predominant influence on flow F_{67}. Nonetheless, the current search algorithm will update the flow coefficient for flow F_{67} twice according to both F_{47} and F_{46}. If building configuration is further complicated, the search algorithm follows the same rule for the outflow openings that are influenced by multiple inflow openings.

To further examine the coupled program, we study this 6-zone apartment using quasi-dynamic strategy. The air path information for zones 1-4 is the same as the previous 4-zone case. The air path 36 has a flow coefficient of 1 kg/L·(Pa)^n, and the flow coefficients for openings 46, 57 and 67 are all to be 0.01 kg/L·(Pa)^n, respectively. Again, the flow exponential rate for all the airflow paths is kept constant that is equal to 0.5.

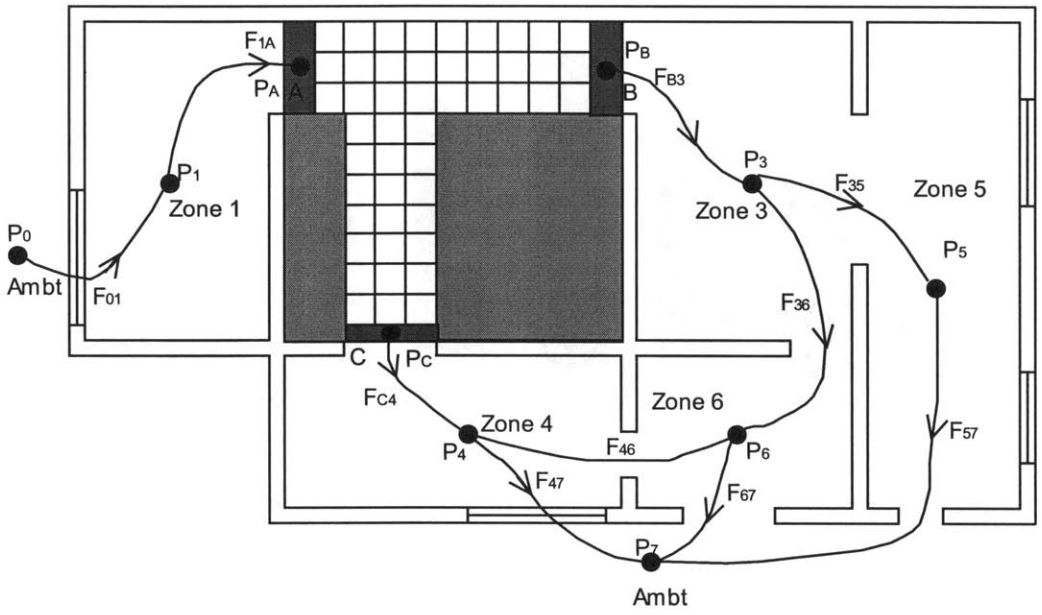

Figure 4.19. 6-zone configuration modified from 90-degree planar branch case.

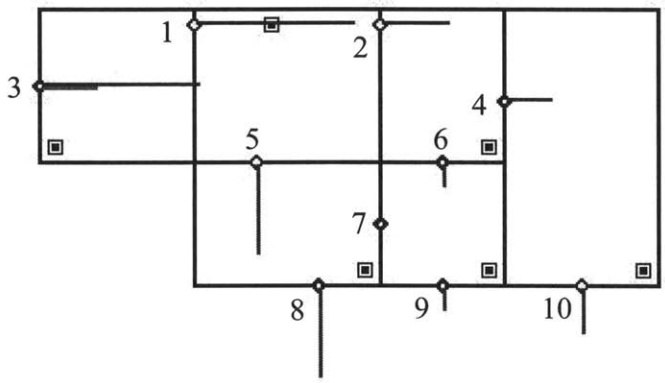

(a)

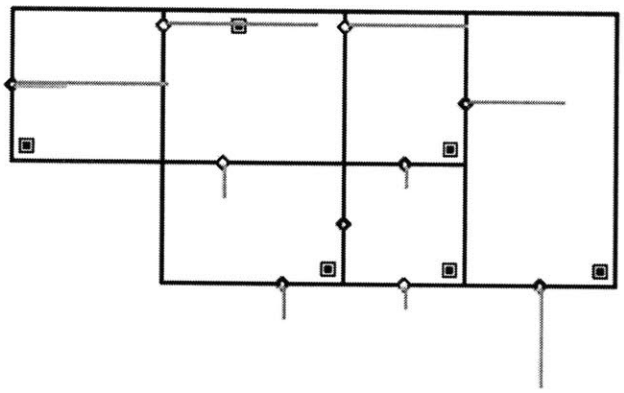

(b)

Figure 4.20. Modified 90-degree planar branch case 2 (6 zones): (a) Airflow pattern before coupling (numbers in the figure indicate the path identification); (b) Airflow pattern after coupling.

The general airflow patterns before and after coupling represented by CONTAMW are shown in Figure 4.20. The detailed information of changes in airflow rates and flow coefficients are listed in Table 4.8. Figure 4.21 visually presents the differences of the airflow rates before and after coupling for all the ten airflow paths. As can be seen, the un-coupled CONTAM generates erroneous airflow pattern, while the coupled program can significantly improve the result by taking into account of the detailed structure within zone 2 by CFD simulation. This results considerable changes for the airflow rates (either increase or decrease accordingly) that are affected. Openings 4, 10, 2, and 7 are among the ones that have significant positive airflow rate changes, while openings 5 and 8 are the two paths that have negative airflow rate changes. These coupling results also validate the path-searching algorithm that is employed for this study.

Table 4.8. Results of the modified 90-degree planar branch case 2 (6 zones) by quasi-dynamic coupling.

	Airflow Path	Flow rate before coupling	Flow rate after coupling	Airflow % change	Original Coeff.	New Coeff.	Pressure difference before (after)
1	1A	0.005915	0.005883	-0.5%	1.0	1.0	0.000035
2	B3	0.001927	0.003127	+62.3%	1.0	2.643487	0.000007
3	01	0.005915	0.005883	-0.5%	0.01	0.01	0.352755
4	35	0.000898	0.001910	+112.7%	0.02	0.052870	0.007200
5	C4	0.003988	0.002756	-30.9%	1.0	0.205868	0.000011
6	36	0.001029	0.001217	+18.3%	1.0	2.643487	0.000001
7	46	0.000026	0.000039	+50%	0.01	0.002058	0.000004
8	47	0.004013	0.002796	-30.3%	0.04	0.008237	0.007198
9	67	0.001004	0.001178	+17.3%	0.01	0.005442	0.007202
10	57	0.000898	0.001910	+112.7%	0.01	0.026435	0.000003

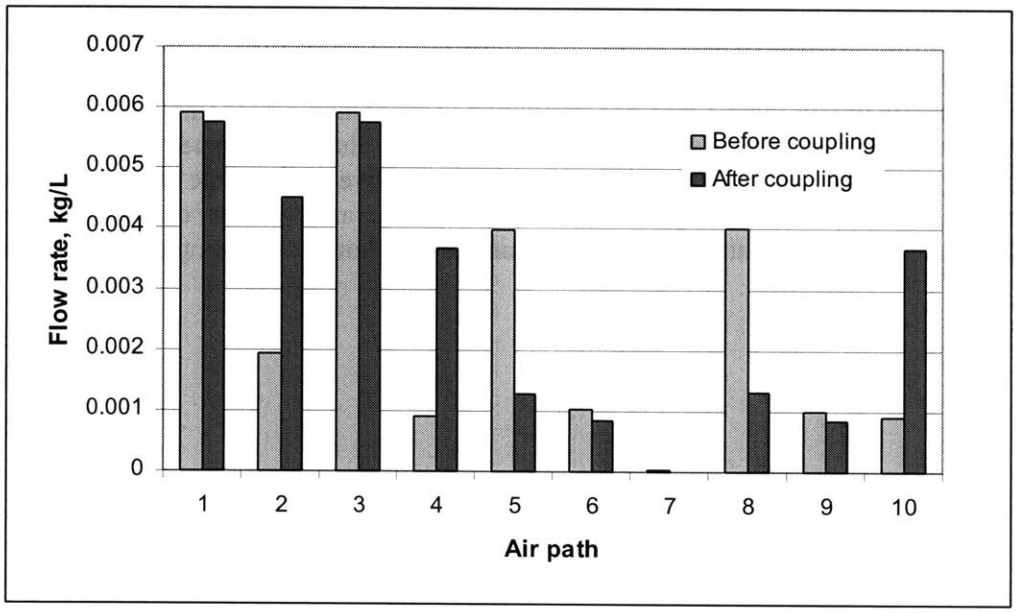

Figure 4.21. Airflow rate through each opening in modified 90-degree planar branch case 2 (6 zones) before and after quasi-dynamic coupling.

4.4 Dynamic Coupling of CFD into CONTAM

In the previous section, quasi-dynamic coupling has been discussed. It assumes that CFD produces the "true" airflow pattern and therefore can completely substitute the values of their corresponding air paths in CONTAM. This coupling strategy, though a two-way interaction to a certain degree, requires no active interaction between CONTAM and CFD. However, CFD results may also be questionable as we discussed earlier (for example, when different closure models for the turbulence are used). This leads to the limitation when applying the quasi-dynamic coupling. Under most circumstances, CONTAM should in principle be fed back to CFD constantly, not only for the initial step as in quasi-dynamic coupling. To achieve such active two-way interaction between CFD and CONTAM, a dynamic coupling strategy has to be developed.

4.4.1 Coupling Strategy

Similar to quasi-dynamic coupling, dynamic coupling is also based on Equation 4.1, i.e., the flow rates at all openings should be in mass balance. The inlet and outlet openings are the interface for combining the mass flow equation of CONTAM with the CFD momentum equations. Just as quasi-dynamic coupling, the CFD domain substitutes a particular zone air node, and the CFD cells at the openings are linked to other zone air nodes. The dynamic coupling requires a mutual feedback between the CONTAM and CFD simulations. One may expect that the final results of such coupling are only partially replaced by CFD simulation so that the impact of CONTAM on the final results is also taken into account. In order to include mutual influence between multizone airflow results and CFD results, a special solution method is developed in the following section.

4.4.2 Solution Methods

Iteration between CONTAM and CFD is necessary at each time-step (if the problem is unsteady) till a mutually consistent solution is achieved. The flow chart for dynamic coupling is shown in Figure 4.22. The mutually consistent solution cannot be obtained until the convergence criterion is met, which means that the maximum flow rate difference between CFD and CONTAM results should be less than the defined convergence criterion.

The coupling loop begins with CONTAM modeling for one time step after the input data (i.e., building, air paths, or weather information) has been adequately supplied. CONTAM calculates zone pressure (*Pi*) and airflow rates (*Fi*) of the air paths as the output. Such information is then used to specify the boundary conditions for the room (zone) that will be simulated by the MIT-CFD. Except for the information at the interface that will be passed from CONTAM simulation results, all the other information for that particular CFD domain is given in CFD input file before CFD simulation. Next, the CFD model will be executed until its own convergence criteria have been met. CFD-calculated airflow rates for the openings will be averaged, which are indicated by $\bar{f}i$ in the flow chart

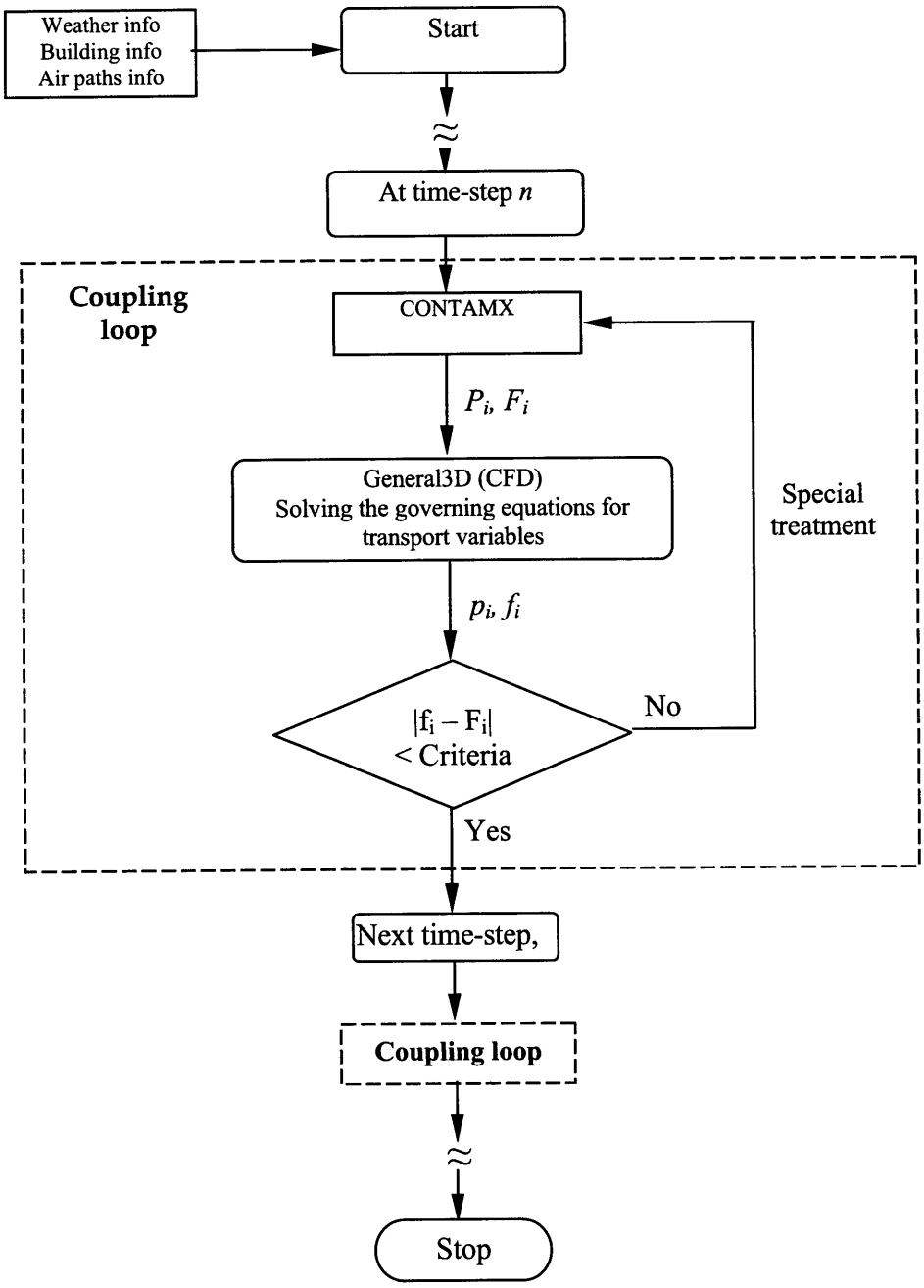

Figure 4.22. Dynamic coupling flow chart. Capital letters denote the results from CONTAM (*P* and *F*), while small letters indicate the results from CFD; Subscript *i* represents the identification number of air path; *n* is the time-step.

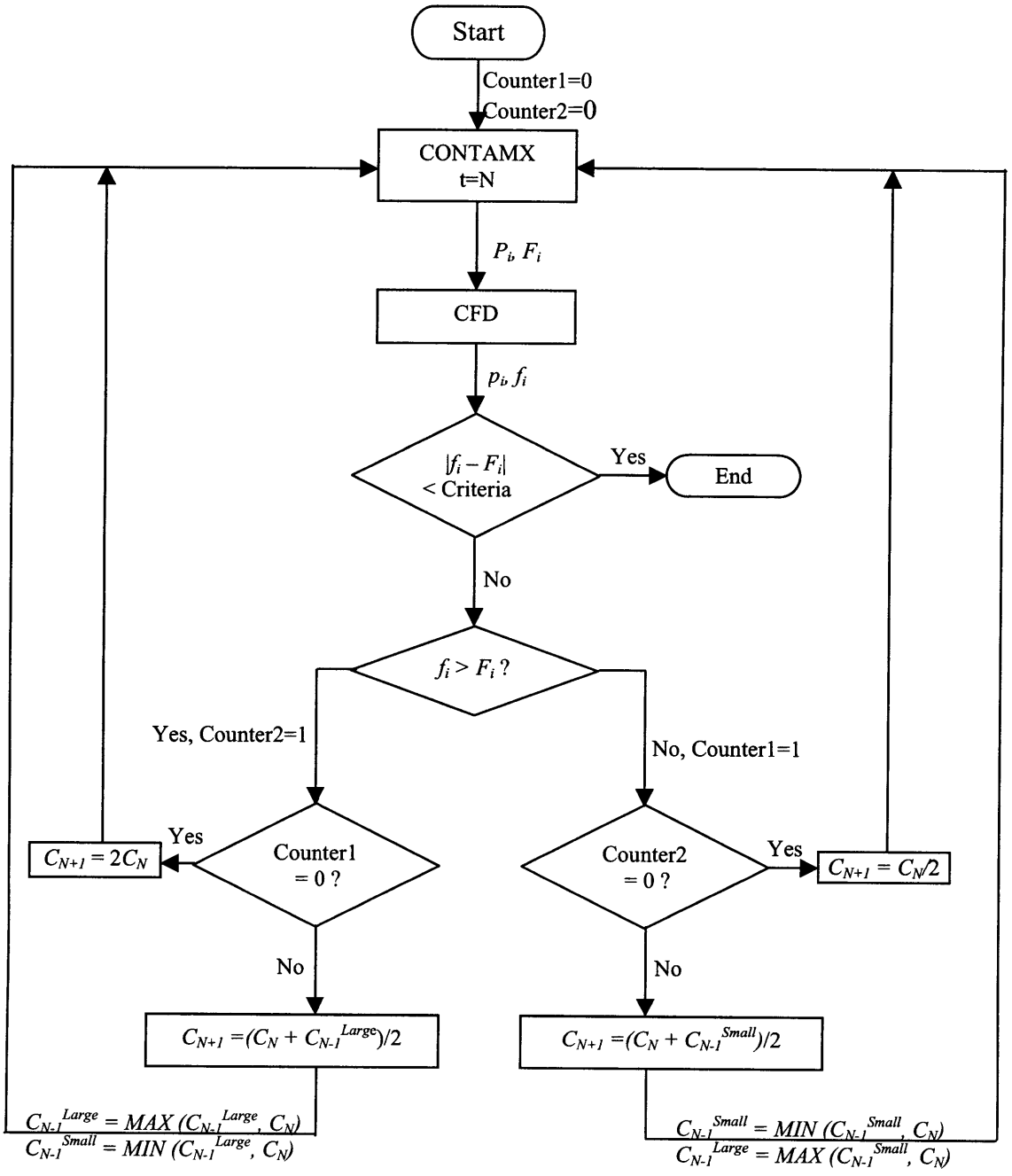

Figure 4.23. Special procedure in dynamic coupling seeking new coefficients of powerlaw relation that will minimize the airflow rate difference of CONTAM and CFD simulations.

shown in Figure 4.22. A comparison is then made to evaluate whether the difference between the *fi* and *Fi* is smaller than the convergence criterion set by user. The iteration between CONTAM and MIT-CFD will continue until this convergence criterion is met.

If the criterion for the coupled program is not met, a special procedure is introduced in order to seek new coefficients of powerlaw relation that are employed for the next CONTAM simulation to minimize the airflow rate differences. This method searches over a given interval known to contain the optimal coefficient that makes the flow rates from CONTAM and CFD converge. By successively halves/doubles/averages that interval restricting the search within it, the optimal coefficient can then be found. Figure 4.23 illustrated such a procedure employed in the present study. Two counters are used to coordinate the coefficient updating and are set to zero initially. If the CFD result, f_i, is larger than the previous CONTAM simulation result, F_i, Counter2 is set to 1. Then the program judges whether Counter1 is equal to zero. If yes, the air path flow coefficient is doubled before a new CONTAM run (The rationale behind this is to force the CONTAM airflow, F_i, in this case, to be increased so that it will be closer to CFD result, f_i). With the new flow coefficient of the air path, CONTAM computes a set of new air path values and feed the boundary pressure and momentum information to CFD for another new CFD run. If f_i is still larger than F_i, the procedure repeats until the first time when f_i is less than F_i. Now, Counter1 is set to be 1, and the program judges whether Counter2 is equal to zero. Since Counter2 has already been assigned to be 1 at the beginning of the iteration, the new flow coefficient is set to be the mean value of the current flow coefficient and the smaller flow coefficient from the previous run (Again, the purpose of this is tying to force F_i to be closer to f_i). This mean value of flow coefficient is then used for another CONTAM run.

Another way around, if the first-time CFD result, f_i, is less than CONTAM result, F_i, Counter1 is assigned to be 1. The program then judges whether Counter2 is equal to zero. If yes, the flow coefficient for the air path is assigned to be half of the original flow coefficient, which will be used for CONTAM to perform another simulation. The iteration will continue until f_i is larger than F_i. For the first time both Counter1 and Counter2 are equal to 1, the mean value of the airflow path coefficient and the previous larger air path flow coefficient will be calculated and passed to CONTAM to perform another round of simulation. Iteration between CONTAM and CFD simulation will continue until the prescribed convergence criterion is met. The final results from the coupled CFD and CONTAM simulation are thus achieved.

4.4.3 Numerical Stability

Since the iteration is involved in dynamic coupling process, the stability of this coupling scheme should be examined. In the case studies that will be discussed in the next section, less than 10 iterations between CONTAM and CFD are needed before the convergence criterion is met indicating that the scheme is quite stable. The method introduced in Figure 4.23 can ensure the criterion be finally met for all the cases.

4.4.4 Case Studies

In order to examine the applicability of the dynamic coupling scheme, the same two modified 90-degree planar branch cases as discussed in Section 4.3.3 will be studied for the convenience of comparison.

- **Modified 90 degree planar branch case 1 (4 zone)**

The configuration of this case is shown in Figure 4.16. The impact of using the dynamically coupled program on the airflow inside the building is visually presented in CONTAMW sketchpad, where 4.24a represents the airflow pattern before dynamic coupling; and 4.24b refers to the airflow pattern after dynamic coupling. In Table 4.9, the detailed airflow results computed by CONTAM only and by the dynamic coupling are presented. A comparison of the airflow rate without coupling, with quasi-dynamic coupling, and with dynamic coupling is shown in Figure 4.25. As expected, the flow pattern in dynamic coupling is somewhat in between those from un-coupled and quasi-dynamic coupling, and is closer to the latter. The dynamic coupling corrects the erroneous airflow partition between the two exits of the room 2 and those at the air paths downstream. The dynamic feedback from CONTAM into CFD is also effective in allowing the possibility of inaccurate CFD simulation to be weighted less.

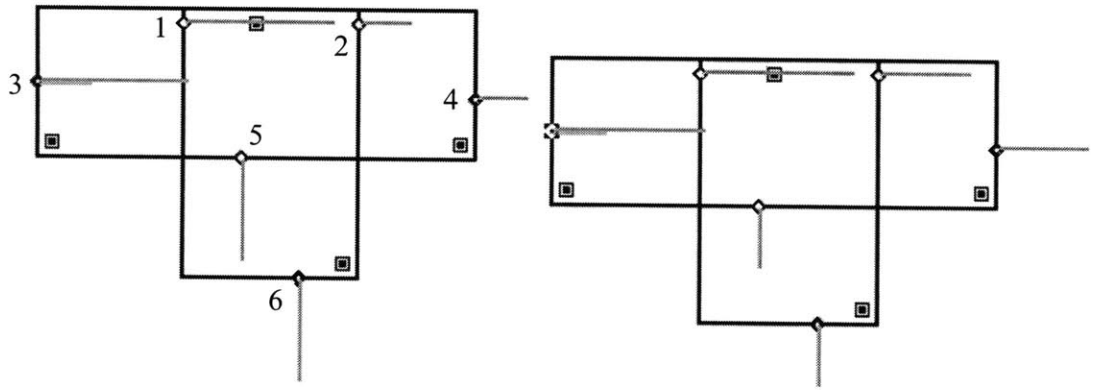

Figure 4.24. Dynamical coupling – modified 90-degree planar branch case 1 (4 zones): (a) airflow pattern before coupling. Air path identification numbers are also indicated; (b) airflow pattern after coupling.

Table 4.9. Results of the modified 90-degree planar branch case 1 (4 zones) by dynamic coupling.

	Airflow Path	Flow rate before coupling (kg/L)	Flow rate after coupling (kg/L)	Original Coefficient kg/L·(Pa)^n	New Coefficient kg/L·(Pa)^n	Pressure difference before (Pa)	Pressure difference after (Pa)
1	1A	0.005918	0.005918	1.0	1.0	0.000035	0.000035
2	B3	0.001973	0.003576	1.0	1.812468	0.000004	0.000004
3	01	0.005918	0.005918	0.01	0.01	0.350225	0.350225
4	35	0.001973	0.003576	0.02	0.036249	0.009736	0.009736
5	C4	0.003945	0.002342	1.0	0.593663	0.000016	0.000016
6	46	0.003945	0.002342	0.04	0.023747	0.009725	0.009725

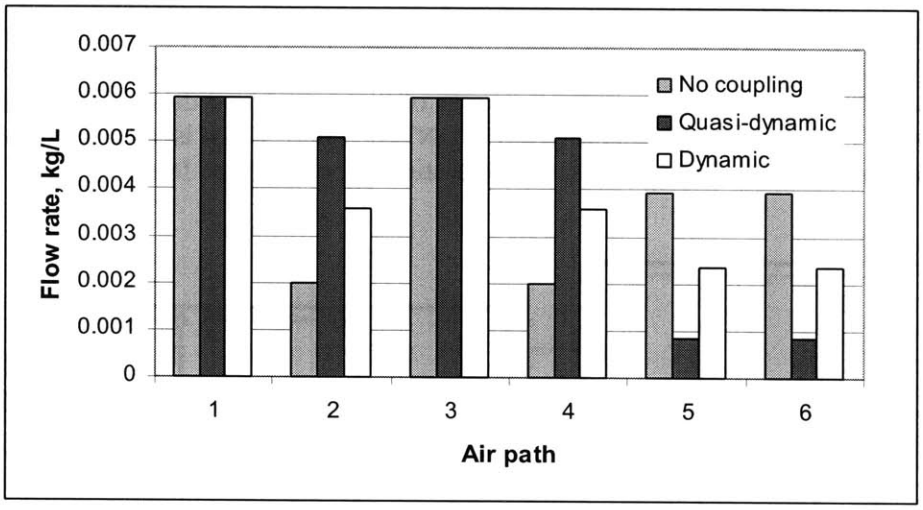

Figure 4.25. Airflow rate through each opening in modified 90-degree planar branch case 1 (4 zones) before and after quasi-dynamic and dynamic coupling.

- **Modified 90 degree planar branch case 2 (6 zones)**

To further examine the dynamic coupling scheme, the more complicated 6-zone apartment case is also studied. The configuration is shown in Figure 4.19. The general airflow pattern in this building before and after dynamic coupling is represented by CONTAMW sketchpad as shown in Figure 4.26. The detailed information of the airflow rates and the flow coefficients before and after coupling is listed in Table 4.10. Figure 4.27 visually presents the differences of the airflow rate without coupling, with quasi-dynamic coupling, and with dynamic coupling.

In this case, significant differences in airflow patterns exist not only between the dynamic coupling and the un-coupled cases, but also between the dynamic coupling and the quasi-dynamic coupling cases. The flow rates in dynamic coupling not only correct the erroneous flow partition through the major and secondary exits, but also indicate a large portion of air exits through the main exit corridor (i.e., through air paths 2, 4, and 10) that is even larger than that of quasi-dynamic coupling. Although the latter results may need to be verified by experimental measurement, it shows that the results can never be achieved either through un-coupled CONTAM or through CFD simulation individually, addressing the importance of the dynamic coupling.

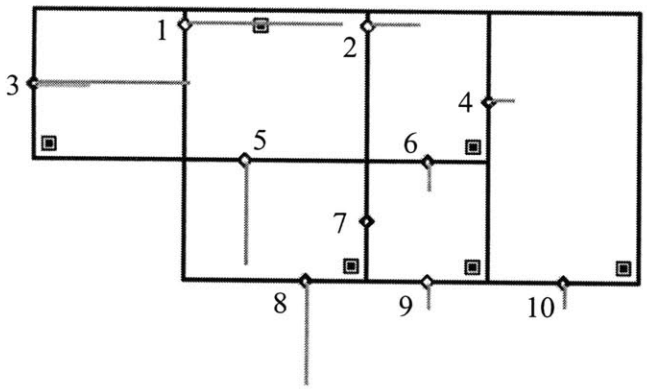

(a)

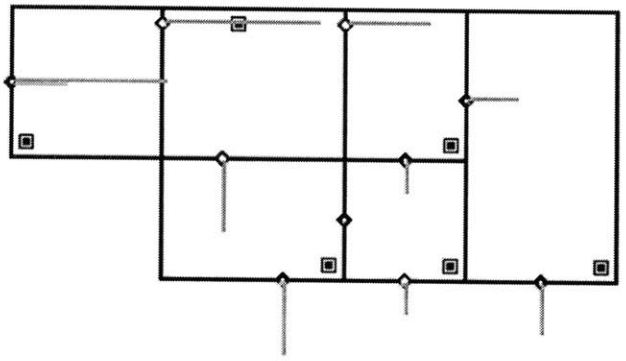

(b)

Figure 4.26. Dynamic coupling – modified 90-degree planar branch case 2 (6 zones): (a) airflow pattern before coupling. Air path identification numbers are also indicated; (b) airflow pattern after coupling.

Table 4.10. Results of the modified 90-degree planar branch case 2 (6 zones) by dynamic coupling.

No.	Airflow Path	Flow rate before coupling	Flow rate after coupling	Original Coefficient	New Coefficient	Pressure difference before	Pressure difference after
1	1A	0.005915	0.005751	1.0	1.0	0.000035	0.000035
2	B3	0.001927	0.004523	1.0	2.643487	0.000007	0.000007
3	01	0.005915	0.005753	0.01	0.01	0.352755	0.352755
4	35	0.000898	0.003671	0.02	0.052870	0.007200	0.007200
5	C4	0.003988	0.001272	1.0	0.205868	0.000011	0.000011
6	36	0.001029	0.000852	1.0	2.643487	0.000001	0.000001
7	46	0.000026	0.000008	0.01	0.002058	0.000004	0.000004
8	47	0.004013	0.001295	0.04	0.008237	0.007198	0.007198
9	67	0.001004	0.000844	0.01	0.005442	0.007202	0.007202
10	57	0.000898	0.003671	0.01	0.026435	0.000003	0.000003

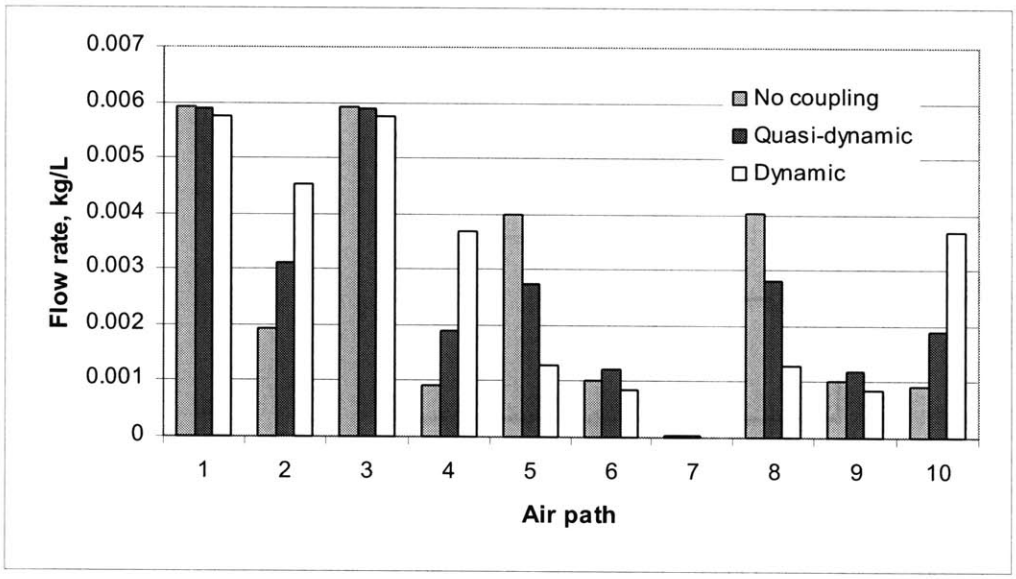

Figure 4.27. Airflow rate through each opening in modified 90-degree planar branch case 2 (6 zones) before and after quasi-dynamic coupling and dynamic coupling.

- **Modified forced convection case**

In order to achieve reasonable results, it is important that boundary information should be exchanged properly between CONTAM and CFD. Under current coupling stage, CFD decides whether momentum or pressure boundary information is used for the simulation. Such information is provided by CONTAM and may also affect later CONTAM simulation when CFD results are being fed back. If momentum information is needed for CFD simulation, the mass flow rate calculated by CONTAM is converted to uniform normal velocity across the opening as the velocity boundary condition for CFD. After CFD computation, the sum of the mass flow rate across each cell of the opening is averaged and passed back to CONTAM to update the flow coefficient in the power law expression. The assumption of uniform normal velocity across the opening may introduce additional error. This case study is to examine the validity of such an assumption.

Here we study a three-dimensional forced-convection case modified from the original experiment conducted by Nielson, et al. (1979), which has been widely used by many researchers for validation studies of their numerical simulation programs. The original experiment used a scale model to simulate indoor airflow. The size of the model is W/H = 1.0, L/H = 3.0. The inlet and outlet heights are h_{in}/H = 0.056 and h_{out}/H=0.16, respectively. The widths of the inlet and outlet are the same as those of the model. Based on the inlet height, the flow Reynolds number was set to 5000.

Modified by Musser (2000), the computational model was maintained in the original geometry, which was a single isothermal chamber with 9 m long, 3 m wide, and 3 m high. However, the room was further divided in half by a partition wall with an opening on it as illustrated in Figure 4.28. There is an air inlet (h_{in} = 0.168 m) located on the top of the west wall and a forced outlet (h_{out}=0.48 m) added to the lower west wall in Room 1. The remaining supply air passes through the opening to Room 2, and the air exits Room 2 through a passive outlet on the lower east wall that has the same size as the forced outlet (Figure 29). The opening connecting the rooms is 1 m wide. Five different opening heights were used for simulation: 0.09 m, 0.25 m, 0.59 m, 1.14 m, and 2.24 m.

The present investigation focused on the prediction of airflow by the coupled program. The opening heights of 0.09 m, 0.59 m and 2.24 m are used. There are two cases being studied with the dynamic coupling that is applied to either the first room or the second room. When the first room is being coupled, the inlet and forced outlet mass flow rates calculated from CONTAM will be passed into CFD domain through updated inlet velocity; the passive outlet boundary in CFD domain uses the specified pressure (static pressure) calculated from CONTAM, which is the pressure in Room 2. The computational results of the passive outlet mass flow rate would be passed back into CONTAM for next run. When the second room is being coupled, the inlet mass flow rate calculated from CONTAM will be converted to be uniform velocity and passed into CFD. Static pressure, which is the ambient pressure (in this case, it is equal to zero) will be used for the passive outlet. For both cases, only one iteration is required between CONTAM and CFD.

The results calculated by the coupled program are presented in Figures 4.30, 4.31 and 4.32 for the partition opening of 0.09m, 0.9m and 2.24m, respectively. For each figure, the first three diagrams show the results when Room 2 being coupled, and the rest three diagrams show the results when Room 1 is being coupled.

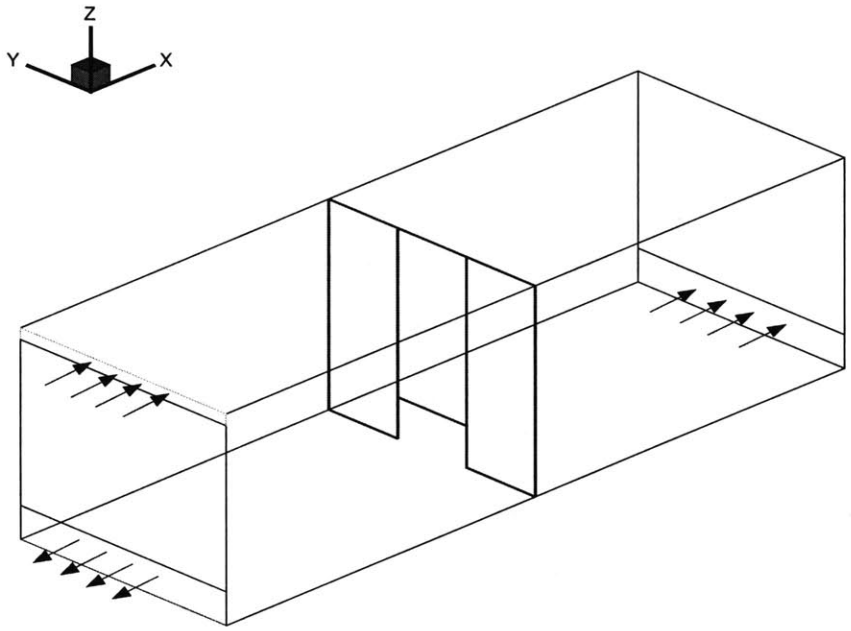

Figure 4.28. Three-dimensional presentation of the modified forced convection case.

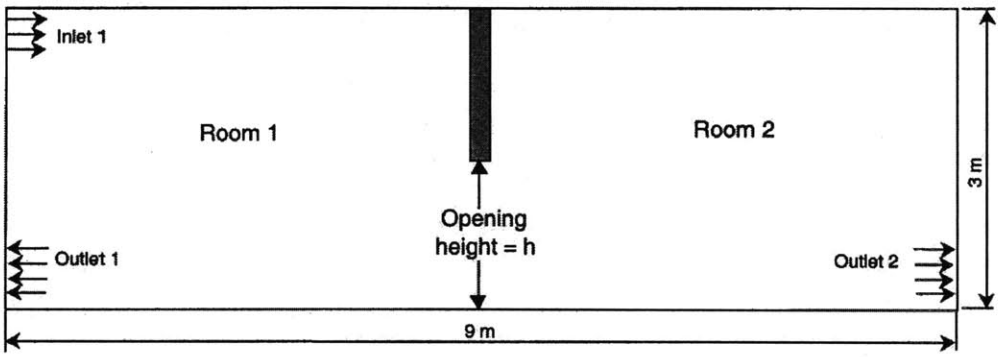

Figure 4.29. Modified forced convection case – room geometry (Musser, 2001).

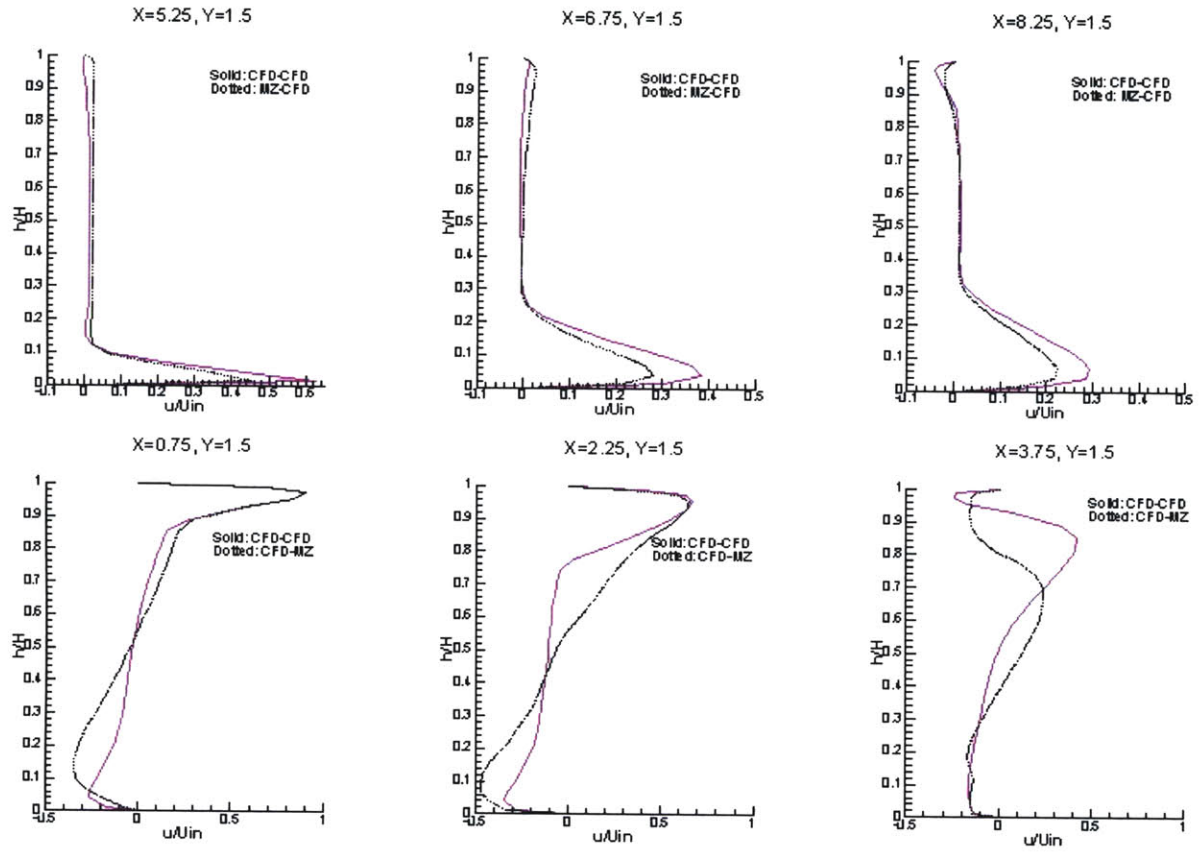

Figure 4.30. Non-dimensional velocity profile for room 1 and 2 by using CFD simulation only and by using the coupled program (CFD + CONTAM), opening height = 0.09m. The upper three panels show the results where room 2 is being coupled; the lower three panels are the results when room 1 is being coupled.

Figure 4.30 illustrates the impact of coupling when a very small opening is located between the two zones. As one can see, larger discrepancy occurs when Room 1 is being coupled. Because the opening located in the middle of theses two rooms is fairly small (0.09m), a passive outlet with specified pressure boundary may not be a suitable assumption for this scenario. On the other hand, when Room 2 is being coupled, an assumption of forced flow with uniform inlet velocity is appropriate. The results from the coupled program and those from CFD-only simulation show reasonable agreement, although the coupled program under-estimates the airflow in the lower region of Room 2, where the outlet openings are located.

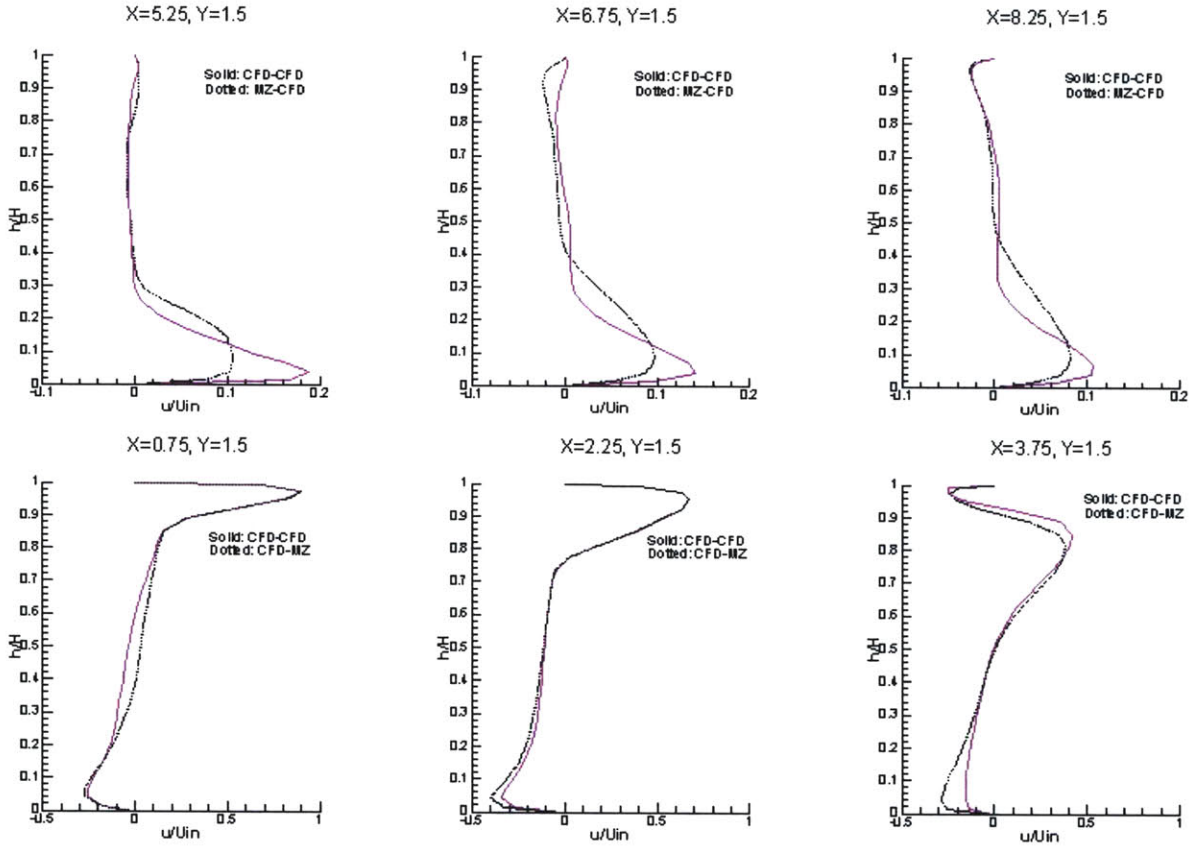

Figure 4.31. Non-dimensional velocity profile for Room 1 and 2 by using CFD simulation only and by using the coupled program (CFD + CONTAM), opening height = 0.59m. The upper three panels show the results where room 2 is being coupled; the lower three panels are the results when room 1 is being coupled.

Figure 4.31 shows the results computed when the opening between Room 1 and Room 2 has the height of 0.59m. Reasonable agreement of the computed results can be observed in Room 1, which indicates that a passive outlet with specified pressure value of Room 2 from CONTAM is appropriate under this circumstance. When Room 2 is the domain for calculation using the coupled program, some discrepancy is found in the lower part of Room 2. The coupled program under-estimates the airflow rate in this region. However, the velocity profiles still show a general agreement.

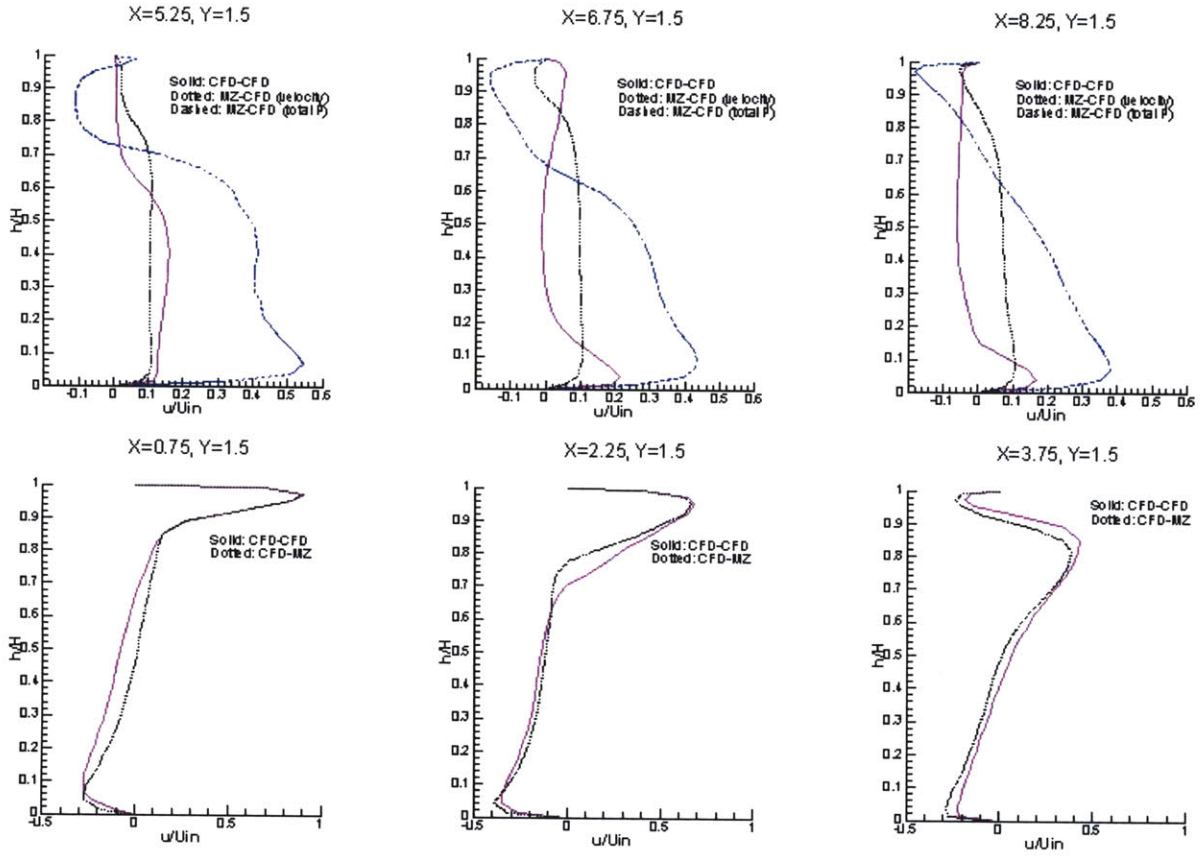

Figure 4.32. Non-dimensional velocity profile for Room 1 and 2 by using CFD simulation only and by using the coupled program (CFD + CONTAM), opening height = 2.24m. The upper three panels show the results where room 2 is being coupled; the lower three panels are the results when room 1 is being coupled.

Figure 4.32 presents the results when the opening between two rooms is very large, i.e., having a height of 2.24m. Two different coupling strategies are used when Room 2 is being coupled: an uniform velocity at the inlet opening and a specified total pressure boundary conditions. The total pressure value is obtained from multizone airflow analysis, which is the total pressure of Room 1. When room 1 is being coupled, the velocity profiles simulated by CFD-only and by coupled program show a good agreement. When Room 2 is being coupled, larger discrepancy is found for both uniform velocity inlet and the pressure boundary conditions. From this particular case, it suggests that the uniform velocity inlet boundary is superior to the specified pressure boundary even when the opening is large.

In general, the momentum boundary condition appears to be appropriate for the inlet flow, whereas the static pressure boundary condition is suitable for the outlets.

4.5 Discussion and Conclusion Remarks

In this chapter, the potential of airflow analysis using the coupled program were assessed in three hierarchical strategies. In the first scheme – virtual coupling, the scheme involves major effort on CFD modeling side because the CFD domain is much larger than that of CONTAM in order to offer more accurate boundary conditions for CONTAM, when such boundary conditions are usually unavailable or hard-to-obtain from experimental measurements. A single-floor apartment and a duplex apartment in a Shanghai complex were used for the case studies applying this coupling strategy. Boundary information for all the windows was provided by CFD simulations conducted by Zhai, et al. (2000). The ventilation rate of each apartment was calculated by CONTAM, which was compared to the results from original CFD results. The air change rates calculated by virtual coupling are in reasonable agreements with the results from CFD-only study, which provides a platform for future application using such a coupling strategy. The virtual coupling strategy is useful when CFD results in a large scale are available or the computational resource involved by CFD is acceptable.

For the other two coupling strategies (quasi-dynamic and dynamic coupling), CFD domain is usually much smaller than the CONTAM domain, which can take into account of the detailed structure with a particular zone node.

Quasi-dynamic coupling is achieved by providing the boundary conditions from an initial CONTAM run to the CFD domain that substitutes a zone node of CONTAM, and CFD results are then fed back to CONTAM for its next run. A pre-assumption is that CFD can produce the "true" flow pattern and CONTAM results should be changed accordingly. A three-duct-in-series case, a 90-degree planar branch case, and two multizone cases modified from the 90-degree planar branch were studied using this coupling strategy. The results show that the quasi-dynamic coupling can significantly alter the airflow pattern that is inaccurate in the CONTAM-only simulation. However, this coupling strategy can only reflect a two-way interaction to a certain degree since no active interaction is involved between CONTAM and CFD. Another limitation is that the results are heavily biased towards CFD simulation, yet the latter may be inaccurate due to its own shortcomings.

A dynamic coupling strategy is designed to realize the active two-way interaction between CFD and CONTAM, and partially offset the biases in the quasi-dynamic coupling. A solution method that dynamically changes the coefficient in the powerlaw relation has been developed in order to automatically search for the optimal coefficients that may force the airflow rates from both CONTAM and CFD to converge. The same two multizone cases modified from the 90-degree planar branch were used to validate the coupling strategy. For the 4-zone case, the dynamic coupling corrects the erroneous airflow partition, and the dynamic feedback from CONTAM into CFD is also effective in the sense that the possible inaccurate CFD simulation can be weighted less. For the 6-zone case, significant differences in airflow pattern exist among the un-coupled CONTAM, quasi-dynamic coupling, and dynamic coupling simulations. The difference

between the dynamic and quasi-dynamic coupling for this particular case raised an interesting phenomenon (i.e., the exit airflow rates are even larger than those from quasi-dynamic coupling) that warrants further investigation, especially from experimental measurements.

A three-dimensional two-zone case modified from Nielson's case (1979) was also applied for the coupling to justify different boundary specification. The coupling results suggest that the coupling using the uniform velocity boundary for inlets and the specified pressure boundary for outlets is the most appropriate when dealing with small opening. When inlet opening is large, such assumptions may result in significant discrepancy. However, the use of uniform velocity for inlet is still superior to the use of specified pressure boundary. Therefore, cautious must be taken to choose proper boundary conditions for the coupled program.

In addition, even though the multizone airflow network approach can provide results similar to the coupled method in some cases, the coupled method can provide detailed information, such as velocity and temperature distribution in the room that studied.

Several limitations of the dynamic coupling need to be brought into attention here. When applying this strategy to the AIVC three-floor case discussed in Chapter 2, no convergent results can be found. A step-by-step examination indicates that this is due to the inherit inability for the CONTAM codes to change the sign of the coefficient in powerlaw relation, since the airflow directions simulated by CONTAM and CFD are opposite at the first interaction. Major code changes must be made to take into consideration of this anomaly. The bisection search algorithm developed here may not be the most efficient one. Other search engine can be more effective under certain circumstance. Further, the co-variation between C and n in the powerlaw relation may also be taken into account.

CHAPTER 5

CONCLUSIONS AND FUTURE WORK

5.1 Conclusions

This chapter presents the main results and conclusions from the research done in this thesis. The present work is a contribution to the development of building airflow analysis. It attempts to represent complex reality with a higher degree of integrity by coupling a multizone airflow model (CONTAM) with a CFD program (MIT-CFD).

The objective of this thesis was to develop methodologies that can be used to couple CONTAM and MIT-CFD for indoor environmental design. The methodologies should ideally keep both programs relatively independent to each other yet provide user both general and detailed information on indoor environment parameters such as the distributions of air velocity, air temperature and contaminant concentration. These parameters are essential to determine indoor air quality, thermal comfort, and energy consumption for the design of energy-efficient and healthy indoor environment.

Before developing the coupling approaches, both CONTAM and MIT-CFD were evaluated for its validity and applicability. The inter-model comparison on AIVC three-floor building case verified that the CONTAM is an appropriate multizone airflow analysis tool. However, the practice in predicting the personal exposure of a French house indicated that there exists significant discrepancy between the results obtained by the CONTAM and by the extensive CFD simulations. Moreover, CONTAM simulation resulted in equal airflow split through the main and the side outlet branches in a 90-degree planar duct branch, while both experimental and numerical studies showed that the higher the Reynolds number, the more the air flows through the main branch outlet. Therefore, a coupled approach by which CFD simulates the critical room and CONTAM remains to simulate the other part of the whole building would be necessary to provide both general airflow information and the detailed airflow information in a critical region within a building.

The MIT-CFD program has been adapted for coupling by adding an option of specified pressure boundary condition. This program was validated extensively by comparing with experimental data. In order to demonstrate its applicability in indoor airflow analysis, three cases – natural convection, forced convection and mixed convection – were studied. For further work on developing coupling approach, additional two duct cases – a three-duct-in-series and a 90-degree planar branch – were studied. The results were verified comparing to analytical solution or other numerical solutions. Although CFD requires significant computing effort, it can produce informative results with acceptable accuracy. Therefore, MIT-CFD is appropriate to be coupled into the multizone model CONTAM.

The purpose of developing coupling techniques is to take advantages from both multizone model and CFD, and lessen their specific shortfalls. The coupling techniques can be implemented in the following two ways:

- The unknown pressure boundary information of the whole building for CONTAM can be provided by CFD simulation in a large scale;

- The CFD boundary conditions can be supplied by CONTAM simulation and the inability of CONTAM to predict airflow property gradients within a single space can be replaced by CFD simulation.

The first technique, named "virtual coupling," was applied to two apartment cases in a Shanghai complex. One apartment has a single floor and the other one is a duplex. CFD treated the building complex as a blockage or a hollow blockage, and the pressure distribution around the building was determined by CFD simulation. Such pressure boundary information is quite important for CONTAM to determine general ventilation rates and airflow pattern. The pressure boundary information was extracted from CFD simulation and passed into CONTAM. The CONTAM results for the ventilation rates of these two apartments were compared to CFD-only simulation. The ventilation rate for the single floor apartment obtained by this approach is similar to that from CFD simulation without considering energy equation. Although the ventilation rate for the duplex apartment is lower than that of CFD simulation, it is still within acceptable range. Therefore, it is a viable way to use CFD simulation to provide climate information for a whole building CONTAM simulation. The virtual coupling technique is useful when CFD results in a large scale are available or the computational resource involved by CFD is acceptable.

The second technique implemented in the present study involves the use of CONTAM simulation results supplying boundary information for CFD to simulate a particular room. Usually, the room is a large space or a critical region in the whole building. Two coupling strategies were devised: quasi-dynamic coupling and dynamic coupling, with different degrees of complexity and sophistication. The first approach elaborates a simple method where CFD simulation results for the coupled zone are passed directly into CONTAM multizone model. The application of this method should rely on the fact that CFD simulation results for the particular zone are truly reliable. No iteration is needed between CFD and CONTAM. The final CONTAM results should reflect CFD results directly. From the several case studies presented in this thesis, quasi-dynamic coupling results in very different airflow distribution in room and through the openings. In the three-ducts-in-series case, the middle duct replaced by CFD domain results in significant difference of pressure drop along the duct from that of CONTAM depending on different turbulent model employed. In the 90-degree planar branch case and its two modified multi-room cases, the largest differences in airflow rates across the openings reflect a significant influence due to the coupling. The results show that the quasi-dynamic coupling can significantly alter the airflow pattern that is inaccurate in the CONTAM-only simulation. However, this coupling strategy can only reflect a two-way interaction to a certain degree since no active interaction involved between CONTAM

and CFD. Another limitation is that the results are heavily biased towards CFD simulation, yet the latter may be inaccurate due to its own shortcomings.

For most cases, CFD results and CONTAM results should be mutually influenced. This led to the investigation on dynamic coupling. Just as its name implies, dynamic coupling allows an active two-way coupling, which takes into account of both CFD and CONTAM simulation results. A bisection scheme is developed in order to facilitate an automatic search for optimal powerlaw coefficients that may force the airflow rates from both CONTAM and CFD to converge. The same two multizone cases modified from the 90-degree planar branch were used to validate the coupling strategy. For the 4-zone case, the dynamic coupling corrects the erroneous airflow partition and the dynamic feedback from CONTAM into CFD is also effective in the sense that the possible inaccurate CFD simulation can be weighted less. For the 6-zone case, significant differences in airflow pattern exist among the un-coupled CONTAM, quasi-dynamic coupling, and dynamic coupling simulation.

The results from these case studies underscore the importance of using coupled program to perform indoor air quality analysis. By identifying the critical region, CFD simulation can provide this single confinement detailed information of air velocity, temperature and contaminant distribution, while improved general airflow information can be provided by CONTAM multizone airflow analysis model at the same time. The importance of such coupling scheme can be clearly seen from the results that compared. The convergence of the combined flow network and CFD domain is readily to obtain by using the numerical scheme that is introduced in Chapter 4.

The flow computed from the multizone flow network approach can be imposed in two different ways within CFD domain: a known pressure at the boundary cells or a known momentum at the interface of the opening cells. The modified force convection case examined the applicability of using these two different boundary conditions. The results suggest that momentum boundary for inlet and specified pressure boundary for outlet is the best combination, especially when the opening is small. This is verified by comparing the results with CFD-only simulation. For the large opening case, the results by using momentum boundary and by pressure boundary are compared. It shows that even for large opening, uniform velocity assumption is still superior to the specified pressure boundary. Hence, the author suggests using uniform velocity for inlets and specified pressure for outlets for dynamic coupling.

5.2 Future work

Although the coupled approaches have demonstrated their potentials in indoor air quality analysis, the developed coupling approach still have much room for further improvement and validation before they can be fully employed.

First of all, the coupling techniques need to be improved in order to be able to deal with inconsistent airflow direction between CONTAM results and CFD results. The

current code can only deal with simple case, where the airflow directions from CONTAM and from CFD simulations are the same. However, in some cases, especially when there are multiple openings located in the coupled domain and pressure boundary conditions are used for all the openings, the airflow directions from CFD simulation may different from those of CONTAM results. A delegate case would be the AIVC three-floor building case, which has a stairwell that connects to the other rooms and the ambient through five openings. In this case, pressure boundary condition for each opening can be obtained from CONTAM simulation. When these boundary conditions are passed into CFD, it generates quite different airflow distribution. Major alteration in the CONTAM code is needed to include such situations.

Secondly, further numerical studies are required to examine the current coupling methodology for further improvement. Most cases that are illustrated in this thesis are simple in order to clarify the fundamental strategies employed at current stage. For example, the bisection search algorithm developed here may not be the most efficient one. Other search engine can be more effective under certain circumstance. Further, the co-variation between C and n in the powerlaw relation may also be taken into account.

Thirdly, a validation of the coupled program should be done by using experimental method to assess the reliability of the coupled program. In this thesis, there are no experimental data for validation. An immediate case would be the 6-room modified 90-degree planar branch case in dynamic coupling.

Moreover, the current coupled program performs the CONTAM and CFD simulations one after another. For dynamic coupling, iteration between CFD simulation and CONTAM is required to reach the convergence. In this process, nearly all the computing time was consumed by CFD simulation, which makes the coupling very inefficient. A way to couple both iterations may be further developed to yield a more economic allocation of the computing resources.

Lastly, the current coupled program only deals with powerlaw airflow relationship and analyzes the airflow without contaminant influence. Methods need to be developed to apply to all kinds of airflow paths and to include contaminant gradients.

The recommended further validations and research should provide insight in different airflows from the studied ones and strengthen the reliability of the dynamic simulation using the coupling approach.

REFERENCES

AIVC, 1999. "Applicable models for air infiltration and ventilation calculation," AIVC Technical Note, no. 51

Ameri, A.A. and Arnone, A. 1994. "Prediction of turbine blade pass heat transfer using a zero and a two-equation turbulence model," *ASME Proceedings of the International Gas Turbine and Aeroengine Congress and Exposition*. Paper 94-GT-122, June 13-16, Hugus, Neth ASME, New York, pp. 1-8.

ASHRAE 1997. *ASHRAE Handbook – 1997 Fundamentals*, Atlanta GA

ASHRAE. 1999. "Ventilation for acceptable indoor air quality," *ANSI/ASHRAE Standard 62 - 1999*, ASHRAE, Atlanta.

Axley, J. 2000. "Zonal models using loop equations and surface drag cell-to-cell flow relations," *ROOMVENT'2000*, pp. 235-240

Baldwin, B.S., and Lomax, H. 1978. "Thin-layer approximation and algebraic models for separated turbulent flows," *AIAA Paper*, Huntsville, AL, pp. 78-257.

Baker, P.H., Charples, S., Ward, I.C. 1987. "Air flow through cracks," *Building and Environment*, Pergamon, 22(4): 293-304

Cebeci, T. and Smith, A.M.O. 1974, "Analysis of turbulent boundary layers," *Ser. In Appl. Math & Meth*, XV, Academic Press, 1974.

Chen, Q. 1995. "Comparison of different k-$\sum$ models for indoor airflow computation," *Numerical Heat Transfer*, Part B, Fundamentals, 28: 353-369.

Chen, Q. and Jiang, Z. 1996. "Simulation of a complex air diffuser with CFD technique," *Proc. of ROOMVENT '96*, Vol. 1, pp. 227-234.

Chen, Q. and Xu, W. 1998. "A zero-equation turbulence model for indoor airflow simulation," *Energy and Buildings*, Vol. 28, pp. 137 – 144.

Conte, S.D., de Boor, C. 1972. *Elementary Numerical Analysis*, McGraw-Hill, New York, NY.

Courant, R., Isaacson, E., and Rees, M. 1952. "On the solution of non-linear hyperbolic differential equations by finite differences," *Comm. Pure Appl. Math.*, vol.5, pp. 243

Deardorff, J.W. 1970. "A numerical study of three-dimensional turbulent channel flow at large Reynolds numbers," *Journal of Fluid Mechanics*, Vol. 42: 453-480.

de Montureux, C., François, C., Lapenu, L.
"Catalogue de logements-types."
Provided by EDF. 1996.

Dhatt, G., Touzot, G., Catin, G. 1984. *The Finite Element Method Displayed*, John Wiley & Sons, New York.

Ellis, M.W. and Mathews, E.H. 2002. "Needs and trends in building and HVAC system design tools," *Building and Environment*, vol. 37, pp. 461 – 470

Emmerich, S. J. 2001. "Validation of multizone IAQ modeling of residential-scale buildings: a review," *ASHRAE Transactions*, vol. 102, Pt. 2

Esmen, T. 1985. "The status of indoor air pollution," *Environmental Health Perspectives*, Vol. 62, pp. 259-265.

Etheridge, D., Sandberg, M. *Building Ventilation Theory and Measurement*. John Wiley & Sons: New York, 1996.

Ferziger, J.H., and Peric, M. 1996. "Computational methods for fluid dynamics," *Springer-Verlag*, New York.

Feustel, H.E., Dieris, J. 1992. "A survey of airflow models for multizone structures," *Energy and buildings,* vol. 18. Amsterdam: Elsevier Sequoia.

Fisk, W. 2000. "Health and productivity gains from better indoor environments and their relationship with building energy efficiency," *Annu. Rev. Energy Environ.* 25:537-66

Furbringer, J., Roulet, C., and Borchiellini R (eds) 1996. "Evaluation of COMIS: final report," IEA Annex 23.

Haghighat, F., Li, Y., Megri, A. C. 2001. "Development and validation of a zonal model—Poma," *Building and Environment*, vol. 36, pp. 1039-1047

Hays, R. E., Nandakumar, K., Nasr-El-Din, H. 1989. *Computers & Fluids*, vol. 17, no. 4, pp. 537-553

Herrlin, M.K. 1992. "Air-flow studies in multizone buildings – models and applications," Royal Institute of Technology.

Howarth, A.T. 1985. "The prediction of air temperature variations in naturally ventilated room with convective heating," *Building Services Engineering Research and Technology*, vol. 64, pp. 169-175

Huang, J. 2001. "Modeling contaminant exposure in a French house", Final report.

Inard, C., Bouia, H., Dalicieux, P. 1996. "Prediction of air temperature distribution in buildings with a zonal model," *Energy and Buildings*, vol. 24, pp. 125-132

Inard, C., Buty, D. 1991. "Simulation of thermal coupling between a radiator and a room with zonal models," *Proceeding of 12th AIVC conference*, vol. 2, Ottawa, Canada, 1991, p. 125-131

Inard, C., Depecker, P., Roux, J. 1997. "Un modèle simplifié pour la prédiction du champ de temperature dans les bâtiments," *Rev Cén Therm*, vol. 36, pp. 113-123

Karimipanah, T. 1996. "Turbulent jets in confined spaces," *Ph.D. Dissertation*, Center for Built Environment, Royal Institute of Technology, Galve, Sweden.

Kelka, K.M., and Choudhury D. 2000. "Numerical method for the prediction of incompressible flow and heat transfer in domains with specified pressure boundary conditions," *Numerical Heat Transfer*, Part B, 38:15-36.

Launder, B. E., and Spalding, D. B. 1974. "The numerical computation of turbulent flows," *Compt. Meths. Appl. Mech. Eng.,* Vol. 3, pp. 269 – 289.

Lebrun J. 1970. "Exigences physiologiques et modalities physiques de la climatisation par source statique concentrée", PhD thesis, University of Liège, 1970, pp.270

Lebrun J. 1994. "Simulation of HVAC systems," *Renewable Energy*, 5(2): 1151-1158

Leonard, B. P. 1979. "A stable and accurate convective modeling procedure based on quadratic interpolation," *Comput. Meths. Appl. Mech. Eng.,* Vol. 19, pp. 59 – 98.

Liu, H., and Ikehata, M. 1994. "Computation of free surface waves around an arbitrary body by a Navier-Stokes solver using pseudocompressibility technique," *Int. J. Numerical Methods in Fluids*, 19(5): 395-413

Molhave, L. 1982. "Indoor air pollution due to organic gases and vapors of solvents in building materials," *Environment International*, Vol. 8, pp. 117-127.

Musy, M., Wurtz, E., Winkelmann, F., Allard, F. 2001. "Generation of a zonal model to simulate natural convection in a room with a radiative/convective heater," *Building and Environment*, vol. 36, pp. 589-596

Muller, D., and U. Renz. 1998. "Measurements and prediction of room airflow patterns using different turbulence models," *Proc. of ROOMVENT '98*, Vol.1, pp.109 -116.

Musser, A. 2001. "An analysis of combined CFD and multizone IAQ model assembly issues", *ASHRAE Transactions,* vol. pp .

Nero, A.V. 1988. "Controlling indoor air pollution," *Scientific Americ*an, Vol. 258, pp. 42-48.

Nielsen, P.V. 1998. "The selection of turbulence models for prediction of room airflow," *ASHRAE Trans.*, 104(1): SF-98-10-1.

Nielsen, P.V., Restivo, A., and Whitelaw, J.H. 1978. "The velocity characteristics of ventilated rooms," *J. of Fluid Engineerin*g, 100: 291-298.

Nikitopoulos, D.E., and Michaelides, E.E. 1995. "Phenomenological model for dispersed bubbly flow in pipes," *AIChE Journa*l, 41(1): 12-22.

NIST. 2000. "CONTAMW 1.0 User Manual," NIST, 2000

Olson, D. A., Glicksman L.R., and Ferm. H.M. 1990. "Steady-state natural convection in empty and partitioned enclosures at high Rayleigh numbers," *ASME J. Heat Transfer,* 112: 640-647.

Partankar, S. V. 1980. "Numerical Heat Transfer and Fluid Flows", Taylor & Francis, 1980

Patanka, S.V., and Spalding, D. B. 1972. "A calculation procedure for heat, mass and momentum transfer in three-dimensional parabolic flows," *Int. J. of Heat and Mass Transfer*, Vol. 15, pp. 1778 – 1806.

Pelletret, R. Y. and Keilholz, W. P. 1997. "COMIS 3.0 – a new simulation environment for multizone air flow and pollutant transport modeling," *Building Simulation '97 – fifth international IBPSA Conference*, Prague, IBPSA

Peng, X. 1996. "Modeling of indoor thermal conditions for comfort control in buildings," *Ph.D. Dissertatio*n, Delft University of Technology, Delft, The Netherlands.

Persily, A., and Linteris, G. 1983. "A comparison of measured and predicted infiltration rates," *ASHRAE Transactions*, 89(2B): 183-200

Prandtl, L. 1925. "Uber die ausgebildete Turbulenz," *ZAM*M, 5: 136-139.

Rhie, C. M., and Chow, W. L. 1983. "Numerical study of the turbulent flow past an airfoil with trailing edge separation," *AIAA J.,* Vol. 21, pp.1525 – 1532.

Rodriguez, E. A., Alvarez, S., Coronel, J. F. 1994. "Modeling stratification patterns in detailed building simulation codes," *Proceedings of European Conference on Energy Performance and Indoor Climate in Buildings*, Lyon, France, 1994

Shaelin, A., Dorer V., et al. 1993. "Improvement of multizone model predictions by detailed flow path values from CFD calculation," *ASHRAE Transactions*, 93-7-4, pp. 709-720

Smagorinsky, J. 1963. "General circulation experiments with the primitive equations, I. The basic experiment," *Monthly Weather Rev.,* Vol. 91, pp.99 – 164

Spalding, D. B. 1972. "A novel finite-difference formulation for differential expressions involving both first and second derivatives," *Int. J. Num. Meth. Eng.,* Vol. 4, pp. 551-559.

Spengler J.D., Chen Q. 2000. "Indoor air quality factors in designing a healthy building," Draft, to be published.

Stone, H. L. 1968. "Iterative solution of implicit approximation of multidimensional partial differential equations," *SIAM J. on Num. Analysis*, Vol. 5, pp. 530 – 558.

Stuart Dols, W., Walton, G., Denton, K. 1997. "CONTAMW1.0 user manual," Gaithersburg, MD, NIST

Togari, S., Arai, Y., Miura, K. 1993. "A simplified model for predicting vertical temperature distribution in a large space," *ASHRAE Transactions 1993,* vol. 99, pp. 84-99

Upham, R. 1997. "A validation study of the airflow and contaminant migration computer model CONTAM as applied to tall buildings," M.S. thesis, The Pennsylvania State University.

Versteeg, H. K., Malalasekera, W. 1995. "An introduction to computational fluid dynamics," Prentice Hall, 1995.

Walton, G.N. 1989. "Airflow network models for element-based building airflow modeling," *ASHRAE Transactions,* 89-6-5, pp. 611-620

Wilcox, D.C. 1993. "Turbulence modeling for CFD," *DCW industries, Inc.*

Wurtz, E., Nataf, J. 1994. "Balidation des modèles zonaux décrits par l'environnement orienté objet SPARK," *Proc. European Conf. Energy Performance and Indoor Climate in Buildings,* Lyon, France, 1994, pp. 785-790

Wurtz, E., Nataf, J., Winkelmann, F. 1999. "Two- and three-dimensional natural and mixed convection simulation using modular zonal models in buildings," *International Journal of Heat and Mass Transfer*, vol. 42, pp. 923-940

Zhai, Z., Hamilton, S.D., et al. "Integration of indoor and outdoor airflow study for natural ventilation design using CFD," *Proceedings 21st AIVC Annual Conference. "Innovations in Ventilation Technology,"* 26-29 September 2000, paper 13

Zhu, J. 1991. "A low diffusive and oscillation-free convection scheme," *Cormmun. Appl. Num. Meths.*, Vol. 7, pp. 225 – 232.

Zhu, J. and Rodi, W. 1991. "A low dispersion and bounded convection scheme," *Comput. Meths. Appl. Mech. Eng.*, Vol. 92, pp. 88 – 96.